12-2013

Crack Growth Behavior Under Creep-Fatigue Conditions Using Compact and Double Edge Notch Tension-Compression Specimens

Santosh B. Narasimha Chary
University of Arkansas, Fayetteville

Crack Growth Behavior Under Creep-Fatigue Conditions Using Compact and Double Edge Notch Tension-Compression Specimens

Crack Growth Behavior Under Creep-Fatigue Conditions Using Compact and Double Edge Notch Tension-Compression Specimens

A dissertation submitted in partial fulfillment
of the requirements for the degree of
Doctor of Philosophy in Mechanical Engineering

By

Santosh Balaji Narasimha Chary
Anna University
Bachelor of Engineering in Mechanical Engineering, 2005
Oklahoma State University
Master of Science in Mechanical Engineering, 2007

December 2013
University of Arkansas

This dissertation is approved for recommendation to the Graduate Council.

_____
Dr. Ashok Saxena
Dissertation Director

_____
Dr. James C. Newman, Jr.
Committee Member

_____
Dr. Sunder Ramasubbu
Committee Member

_____
Dr. Joseph J. Rencis
Committee Member

_____
Dr. Douglas E. Spearot
Committee Member

_____
Dr. Min Zou
Committee Member

ABSTRACT

The American Society for Testing and Materials (ASTM) has recently developed a new standard for creep-fatigue crack growth testing, E 2760-10, that supports testing compact specimens, C(T), under load controlled conditions. C(T) specimens are commonly used for fatigue and creep-fatigue crack growth testing under constant-load-amplitude conditions. The use of these specimens is limited to positive load ratios. They are also limited in the amount of crack growth data that can be developed at high stress intensity values due to accumulation of plastic and/or creep strains leading to ratcheting in the specimen. Testing under displacement control can potentially address these shortcomings of the load-controlled tests for which the C(T) geometry is unsuitable.

A double edge notch tension-compression, DEN(T-C), specimen to perform displacement controlled creep-fatigue crack growth testing is developed and optimized with the help of finite element and boundary element analyses. Accurate expressions for estimating the fracture mechanics crack tip parameters such as the stress intensity parameter, K, the crack mouth opening displacement ($CMOD$), and the load-line displacement (LLD) are developed over a wide range of crack sizes for the DEN(T-C) specimen. A new compliance relationship for use in experimental testing has been developed by using the compliance form available in ASTM E-647 standard. Experimentally determined compliance value compared well with the new relation for C15 steel (AISI 1015) and P91 steel tested at room and elevated temperature conditions respectively. Fatigue crack growth rate data generated using the DEN(T-C) specimens on the two metallic materials are in good agreement with the data generated using standard compact specimens; thus validating the stress-intensity factor and the compliance equation for the double

edge notch tension-compression specimen. The testing has shown that the DEN(T-C) specimen is prone to crack asymmetry issues. Through inspection of fatigue surfaces, it has been found that that better alignment control procedures are needed to ensure symmetric crack fronts for the DEN(T-C) specimen.

Creep-fatigue crack growth tests were conducted on 9Cr-1Mo (P91) steels at 625°C with various hold times. These tests were conducted using C(T) specimens under constant load amplitude conditions (tension-tension) and DEN(T-C) specimens under displacement like conditions (tension-compression). Crack growth data generated under creep-fatigue conditions using standard C(T) specimens correlated well with crack growth data generated using DEN(T-C) specimens. The crack growth rates per cycle increased significantly with increase in hold time when crack growth data were plotted with the cyclic stress intensity parameter, ΔK. A transient behavior in the initial portion of da/dN versus ΔK plots were observed for the hold time tests, as reported previously by several other researchers. It is shown for the C(T) specimens that the creep-fatigue interactions during crack growth for various hold times are represented better by the $(C_t)_{avg}$ parameter implying that the P91 steel behaves in a creep-ductile manner. Significant differences (factors of 2 to 5) were observed between the calculated values of $(C_t)_{avg}$ and those based on measured values of force-line deflection. It is also shown that there is a high risk of obtaining invalid data in longer hold time tests under force-control conditions.

The usefulness of DEN(T-C) specimens for crack growth studies under displacement controlled conditions to combat ratcheting problems in tests conducted under load conditions is established. The tests conditions for the round-robin program on creep-fatigue crack growth testing in support of ASTM E-2760 are finalized. Further developments needed in creep-fatigue crack growth testing are also presented.

ACKNOWLEDGEMENTS

With sincere gratitude, I would like to thank my mentor and advisor, Prof. Ashok Saxena, for his beneficence, of which this thesis is only a small part. Prof. Joseph Rencis, Dean, College of Engineering, Tennessee Tech University (former Head of the Mechanical Engineering Department at the University of Arkansas) was instrumental in my decision to begin my doctoral studies. I am indebted for his help and friendship during my formative years in the school.

I have been extremely fortunate to have worked with several leading researchers in the field of Fracture Mechanics. American Society of Testing Materials (ASTM), through my mentor was instrumental in providing me the platform to perform such collaborative research. Hence, I would like to acknowledge ASTM and the committee E08 on Fatigue and Fracture. In this regard, I would like to thank Prof. James C. Newman, Jr. of Mississippi State University for all the technical discussion and help with analysis. His knowledge, dedication, enthusiasm and professionalism toward his work and toward students are inspirational. I hope to continue these discussions with him in the future. Appreciation is also extended in this regard to Dr. R. Sunder of BiSS Research, ITW. I have spent a great deal of time drawing from his wisdom and learning from his professionalism. With their insight and guidance, I learned how to conduct numerical and experimental fracture mechanics related work. Dr. Andrew Rosenberger, AFRL is thanked for the good conversations during the various meetings.

It is time to acknowledge all my former colleagues and employers; Bob Ott, Dennis Jackson and Kalyan Bhamidi at Caterpillar Inc., Shane Dohermann, Chris Davis, Rich Wolf and all the R&D colleagues at Hawk Corporation., Phillip Gravett, Sachin Shinde and other colleagues at Siemens Energy, Inc. for their friendship and several stimulating discussions. In

particular, I would like to thank Phil for being a great mentor, enhancing my fracture mechanics skills and also being very supportive in my endeavors. I have been profoundly impacted by his guiding hand.

These were largely made possible by my teachers at my current and former universities. Hence, I would like to thank Professors C.E.Price, Jay Hanan, Jim Smay and late Ranga Komanduri at the Oklahoma State University; Professors Doug Spearot (for his help with Material Science), Rick Couvillion (for his help with Heat Transfer), I. C. Jong, Joseph Rencis (for their help with Mechanics) and Ashok Saxena (for imparting the Fracture Mechanics knowledge) at the University of Arkansas. Prof. Min Zou, Prof. Doug Spearot, reading members of my committee, and all the faculty members at the Oklahoma State University and University of Arkansas are thanked for their support as well.

Jerry Boice and his test support personnel at Westmoreland Testing and Research and Dr. R. Sunder and his test support personnel at BiSS Research, ITW, are gratefully acknowledged for their assistance in the testing program without which this project would never been complete. Jeff Knox in the machine shop, Kathy Jones and Kristy Fink in the Dean's office at the College of Engineering deserve a special appreciation for all their help and support with logistics.

A special thanks to Shawn Coleman for help with programming and research discussions. Former and current members of Mechanical Properties Research Labs including, Sau Wee Koh, Rahul Rajgarhia, Jeff Evans and Valliapa Kalyanasundaram are thanked for their consistent help during the course of this work. I would also like to thank Electric Power Research Institute, Charlotte for providing the test material for this program. Financial support from the Irma F. and Raymond C. Giffels' Chair in Engineering and the ASTM International Graduate Scholarship are

also profoundly appreciated. The eventual success of this project is dedicated to Prof. Ashok Saxena for his lifelong contribution in the area of time dependent fracture mechanics and to late Dr. Bilal Dogan, formerly of EPRI, who provided much inspiration, support and ideas for this work.

Finally, my deepest gratitude goes to my family and friends, especially my father, for his vision and encouragement; mother, for her patience; and brother, for his support.

DEDICATION

Dedicated to the whole range:

Poet's dream ……. TO…….. Philosopher's vision

and the middle path which is gradual and ideal

TABLE OF CONTENTS

LIST OF FIGURES

LIST OF TABLES

LIST OF SYMBOLS

a	Crack length
A	Secondary creep (power law creep) coefficient
B	Specimen thickness
B_N	Net thickness for side-grooved specimens
C_t	Time-dependent fracture mechanics parameter
$(C_t)_{avg}$	Time average value of C_t
$(da/dN)_{cycle}$	Cycle-dependent crack growth rate
$(da/dN)_{time}$	Time-dependent crack growth rate
$(da/dt)_{avg}$	Average time rate of crack growth
E	Young's modulus
F	K - calibration function
F'	Derivate of F with respect to a/W
H	Specimen height
K	Stress intensity parameter
n	Secondary creep exponent
N	Number of fatigue cycles
P	Applied load
r_c	Creep zone size
$\dot{r_c}$	Angular functions on which the creep zone size depends
R	Load ratio
t_r, t_h, t_d	Rise time, hold time and decay time in loading waveforms

V_c	Load-line deflection due to creep
$\dot{V}_c$	Load-line deflection rate
W	Specimen width
α	Scaling factor in the analytical expression for C_t
β	Scaling factor
ΔJ	Total value of J -integral
ΔK	Stress intensity factor range under fatigue loading
ΔP	Applied load range
ΔV_c	Load-line deflection change during hold due to creep
$\varepsilon, \dot{\varepsilon}$	Strain and strain rate respectively
σ_{cy}	Cyclic yield strength

LIST OF ABBREVIATIONS

ASME	American Society of Mechanical Engineers
AISI	American Iron and Steel Institute
ASTM	American Society for Testing and Materials
BiSS	Bangalore Integrated System Solutions
BEA	Boundary Element Analysis
C-F	Creep-fatigue
C-FCG	Creep-fatigue crack growth
CMOD	Crack Mouth Opening Displacement
CPCA	Compression Pre-cracking Constant Amplitude
C(T)	Compact Specimen
DEN(T)	Double Edge Notch Tension
DEN(T-C)	Double Edge Notch Tension-Compression
EC	Extensive Creep
EPFM	Elastic-Plastic Fracture Mechanics
EPRI	Electric Power Research Institute
FEA	Finite Element Analysis
LEFM	Linear Elastic Fracture Mechanics
LLD	Load Line Displacement
LMP	Larson Miller Parameter
LVDT	Linear variable differential transformer
M(T)	Middle Crack Tension

ORNL	Oak Ridge National Laboratory
RR	Round-robin
SEN(B)	Single Edge Notch Bending
SEN(T)	Single Edge Notch Tension
SSC	Small Scale Creep
TC	Transition Creep
TDFM	Time Dependent Fracture Mechanics
TTP	Time-temperature parameter
UA	University of Arkansas
USC	Ultra-supercritical
UTS	Ultimate tensile strength
YS	Yield strength

CHAPTER 1

Introduction

1.1 Motivation for Research

Higher energy conversion efficiencies are achieved by an increase in the operating temperature of power-plant components such as steam headers, steam turbines, gas turbines, and nuclear reactors [1]. The operating cycle for these components typically consists of a startup phase followed by continuous high temperature operation under sustained load and eventually shutdown; thus, creep-fatigue damage considerations become a major concern in the design and operation of these components to ensure structural integrity [2]. Figure 1.1 shows the section of the steam header with high stress locations (marked) and the load/stress versus time history experienced at these locations during one complete cycle. These duty cycles typically involve combination of transient stress, period of sustained stress and high temperatures. Thus, creep deformation can occur during both the loading portion of the cycle and at the sustained load period [3].

Service condition is simulated in the laboratory by using different loading waveforms as shown in the figure 1.2. Elastic, plastic and creep deformation at the crack tip is achieved by the use of such wave shapes at elevated temperature [4]. Creep deformation can take place at the crack tip during the hold time as well as during the loading portion of the cycle in a trapezoidal loading waveform. Creep deformation results in stress redistribution causing changes in elastic strains [2]. The extent of creep deformation at the crack tip during loading depends on the rate of loading and is generally accompanied by elastic and plastic deformation. Part of the accumulated creep strains are reversed due to cyclic plasticity during the unloading portion of the cycle.

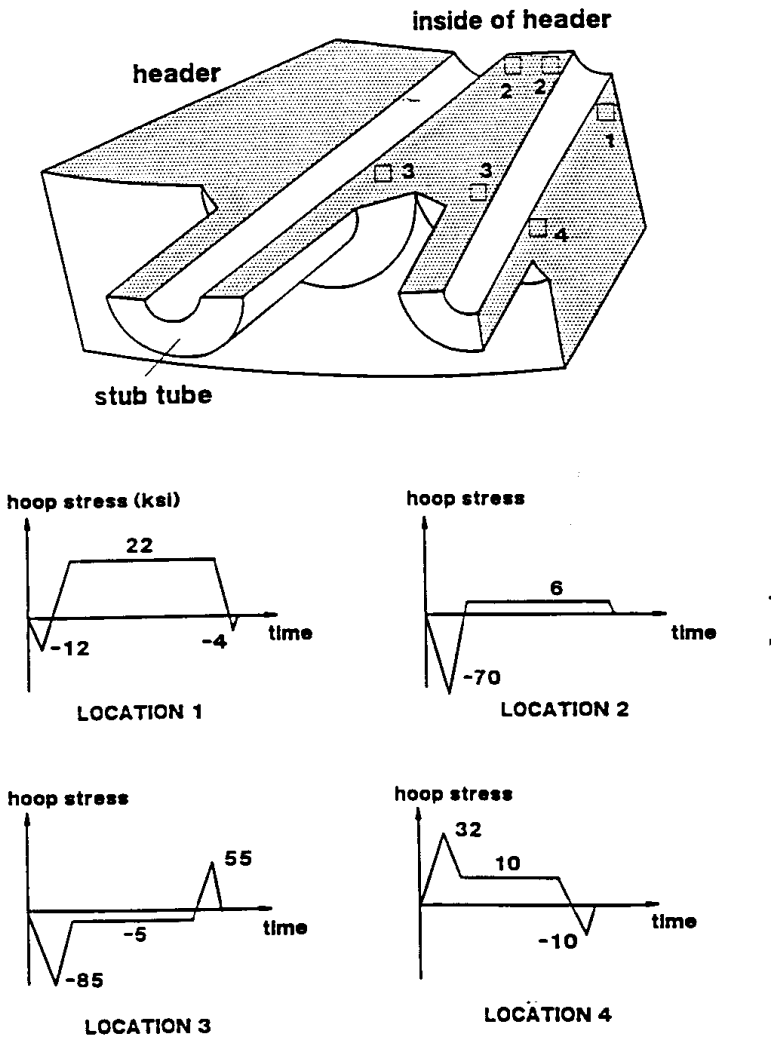

Figure 1.1. Schematic representation of the stress versus time histories at critical location in a steam header [3].

Fracture mechanics approaches have been previously used to characterize creep-fatigue crack growth behavior in materials. All these studies [5,6,7] performed on creep-ductile power plant materials using C(T) specimens demonstrated that $(C_t)_{avg}$ to be the most effective crack tip parameter in correlating creep-fatigue crack growth rates in such materials. The American Society for Testing and Materials (ASTM) has recently developed a new standard for creep-fatigue crack growth (C-FCG) testing, ASTM E2760-10 [8]. It is primarily concerned with testing pre-cracked compact specimens, C(T), subjected to uniaxial tensile cyclic forces in load

control mode to determine the creep-fatigue crack growth properties of nominally homogeneous materials. There has been considerable research on C-FCG behavior using load controlled conditions [1-7] due to the relative simplicity of the experiments. Currently, the C-FCG standard ASTM E2760-10 specifies testing only C(T) specimen under load controlled conditions. These tests are limited in the extent of creep-fatigue crack growth data that can be developed due to ratcheting of the specimen, especially in creep-ductile materials.

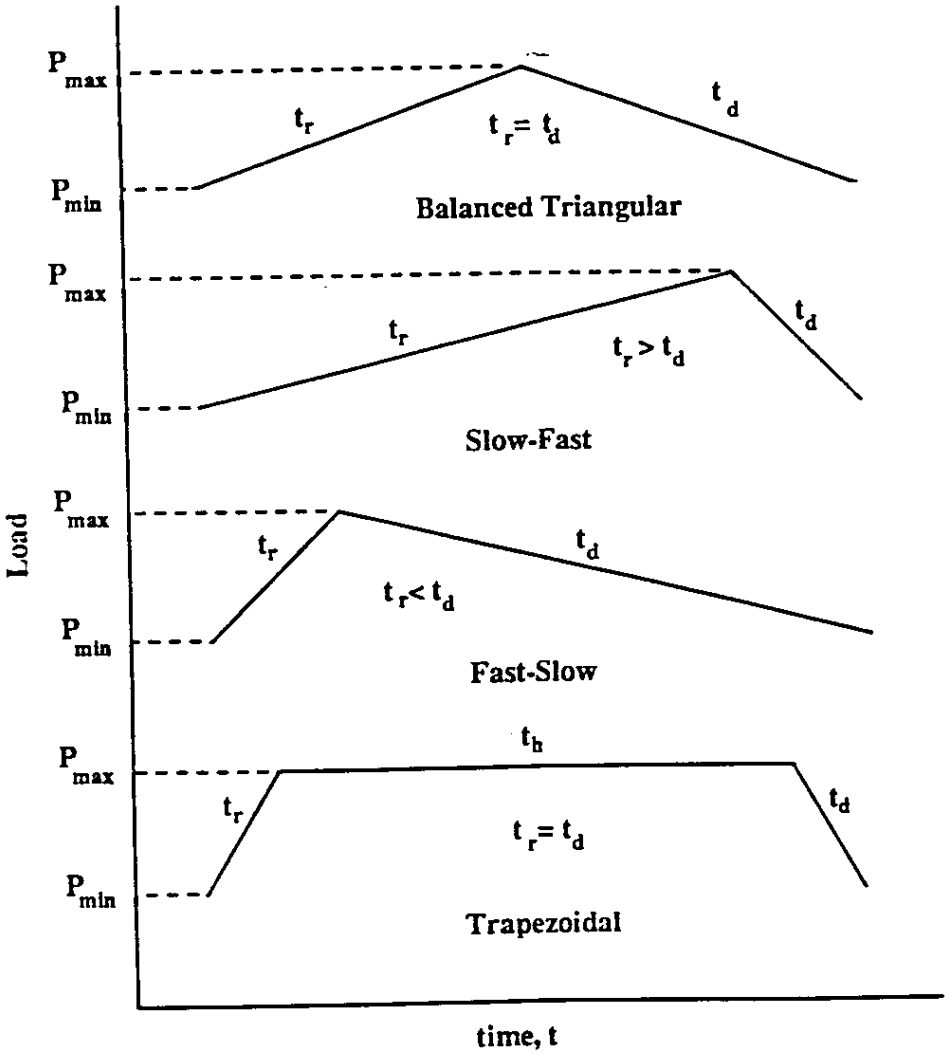

Figure 1.2. Various types of loading waveforms typically employed in creep-fatigue experiments [2].

Of particular interest to the thesis research is the crack growth behavior of 9Cr-1Mo steel under creep-fatigue conditions. The steel is designated by the American Society for Testing and Materials (ASTM) as grade T91/P91 steel. The prefixes in this designation correspond to tubing and piping applications, respectively. The P91 steel is commonly used in structural components such as steam headers, superheater and reheater tubes in ultra-super critical power plants. Such components typically operate at high steam pressures and temperatures under a combination of cyclic loading conditions with long hold periods under sustained stress. Increasing the maximum operating temperature of these steels up to 625-650°C is desirable to increase the energy efficiency of USC power plants, as discussed earlier [9,10]. Hence, one of the goals of the thesis research is to characterize the creep-fatigue interactions in this class of steels at the critical temperature, 625°C, and to achieve a thorough understanding of the crack growth behavior using pre-cracked compact specimens subjected to uniaxial tensile cyclic forces in load control mode.

Figure 1.3 shows the various test specimen geometries used in fracture mechanics testing. Compact specimens, C(T), are commonly used for crack growth testing under load-controlled, fatigue, creep and creep-fatigue conditions; for example, see ASTM Standards E647, E1457 and E2760 [8,11,12]. The advantages of C(T) specimens, relative to other geometries such as the middle crack tension specimen, M(T), and single edge notch bend, SEN(B) specimen and others such as double-edge-notch tension DEN(T), include a large specimen area available between $0.2 \leq a/W \leq 0.7$ to grow the cracks; relatively low machine loads to apply high values of the stress intensity factor, K; and relatively small volumes of material needed to machine C(T) specimens. On the other hand, the use of C(T) specimens is limited to tension-tension cyclic loading conditions [1] which is a limitation for testing low strength materials or testing at elevated temperatures when creep deformation occurs at relatively low K values leading to ratcheting of

the specimen. Ratcheting is the accumulation of permanent deformation (plastic and/or creep strains) with every load cycle. If the specimen displacement at the load-line due to plastic and/or creep strains during loading can be reversed by switching the mode to displacement control during unloading, ratcheting of the specimen can be avoided and more crack extension data can be extracted from each test. Other specimen geometries such as the M(T) specimens are used for generating fatigue crack growth data under negative load ratios. Even though these specimens are suitable for compressive loading, they are known to have lower constraints, thus requiring larger un-cracked ligaments for generating crack growth data under nonlinear plastic, creep and creep-fatigue conditions.

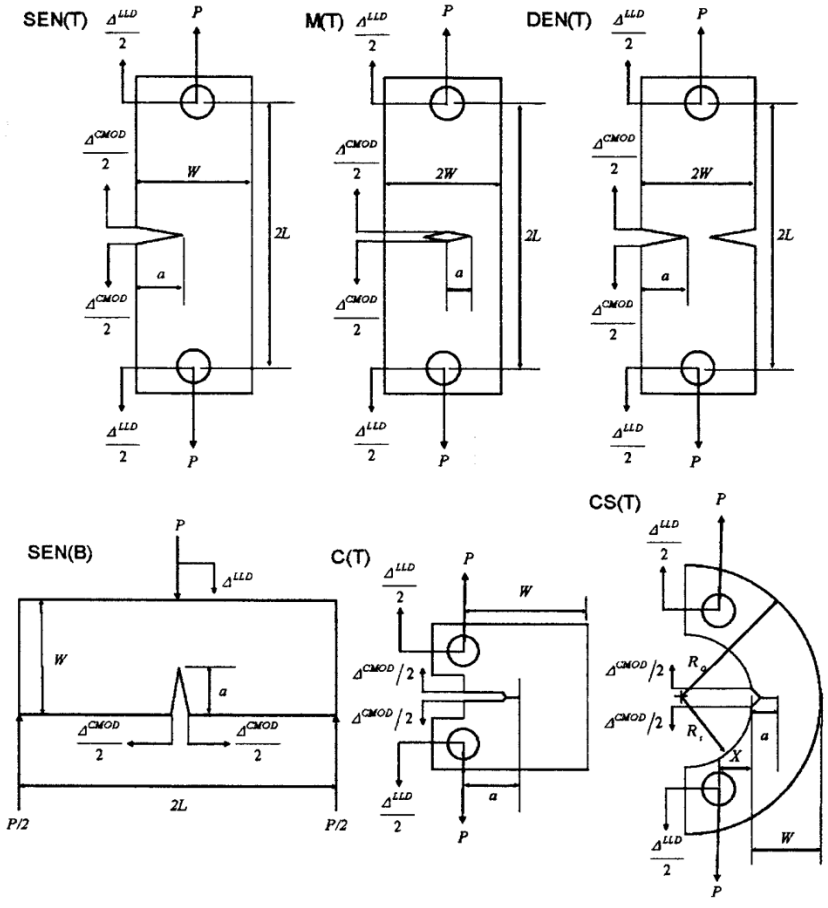

Figure 1.3. Specimen geometries used in fracture mechanics testing [13].

Thus, testing under displacement control can potentially address these shortcomings of the load-controlled tests; developing such a test is the main focus of the proposed dissertation. However, one of the challenges in such a test using C(T) specimens or any pin- loaded specimen is to do with clevis design. Although the two deflection limits are positive in these tests, the resulting minimum load is compressive. Therefore, the standard pin assemblies with universal joints permitting free rotation of the loading points are not adequate [12]. Therefore, the C(T) specimen with standard pin assembly is not a suitable choice to perform C-FCG testing under displacement controlled conditions. An alternative choice would be to choose a different specimen geometry that would facilitate a rigid clevis design to perform such testing thereby also achieving the objective of extending the ASTM standard E2760-10 to include geometries other than C(T).The proposed double-edge-notch tension-compression specimen, DEN(T-C), overcomes this limitation. The design of a DEN(T-C) specimen suitable for use in crack growth testing under tension-compression loading is systematically explored in this dissertation. All previous versions [11,14] of this specimen geometry are based on pin loading that is unsuitable for tension-compression loading; thus, suitable modifications to specimen design are made for applying tension-compression loading. Therefore, this work will also involve the development and optimization of several parameters relating to specimen geometry and dimensions of DEN(T-C) specimen. The expressions for estimating the stress intensity factor, and elastic deflections at the load-line and crack mouth, compliance will be derived using finite element and boundary element analyses. Fatigue crack growth tests will be conducted on the general purpose low strength steel, C15 steel (AISI 1015) using the DEN(T-C) specimen to validate the specimen design. Crack growth data will be generated under creep-fatigue conditions using P91 steel. These results will be compared to the crack growth data generated using the standard C(T)

specimens. Data from these tests will provide a phenomenological approach to analyze crack growth data, such that the data can be used as material properties to predict crack growth in power plant components.

1.2 Research Objectives

From the above discussion, it is clear that there are two distinct areas that need to be addressed in order to enhance the capability to obtain creep-fatigue crack growth data in creep-ductile materials and enhance the applicability of ASTM E2760-10. Accordingly, the objectives of the proposed research are:

- Design and conduct stress analyses to optimize DEN(T-C) specimen suitable for use for crack growth testing under tension-compression loading. Develop expressions for estimating the stress intensity factor, elastic deflections at the load line and crack mouth, compliance for the DEN(T-C) specimen using finite element and boundary element analyses.
- Verify the compliance and stress-intensity factor equations by conducting fatigue crack growth test using DEN(T-C) specimen and comparing the data to the standard C(T) specimen. This will be accomplished by using a general purpose low carbon steel, C15 steel (AISI 1015).
- Characterize tensile and creep rupture behavior of P91 steel for creep-fatigue crack growth analysis.
- Characterize crack growth behavior of P91 steel under creep-fatigue conditions using C(T) specimens subjected to uniaxial tensile cyclic forces in load control mode.

- Characterize crack growth behavior of P91 steel under creep-fatigue conditions using the DEN(T-C) specimen by reversing the accumulated creep displacement and compare the results to standard C(T) specimens.
- Evaluate the test results for assessing the newly developed American Society for Testing and Materials (ASTM) test standard, E2760-10 for creep-fatigue testing and suggest changes to standard if any.
- Provide a phenomenological approach to analyze crack growth data, such that the data can be used as material properties to predict crack growth in power plant components.

1.3 Overview of the Dissertation Structure

The thesis is organized such that past research on fracture mechanics approaches serves as a knowledge base and new findings of the research conducted herein are compared to the same. Chapter 2 gives a comprehensive review of the existing literature regarding various fracture mechanics approaches, creep-fatigue crack growth testing using C(T) and DEN(T) specimens, experimental methods and numerical tools for fracture analysis of cracked bodies. This chapter also covers few available literatures with regards to DEN specimen design in crack growth testing, thus setting the stage for the necessary modification and optimization work needed to the specimen for use in tension-compression testing. Chapter 3 discusses the DEN(T-C) specimen design philosophies and steps in numerical modeling using finite element and boundary element analyses. The expressions needed for crack growth testing and analyses are also derived in this chapter. A summary of the all the equations and expressions needed for the analysis of crack growth data are provided in Chapter 4. Chapter 5 covers the background of the P91 test material, machining plan for test specimen geometries and specimen configuration for C(T) and DEN(T-C) specimens. Tensile and creep rupture behavior of the P91 material are

discussed in chapter 6. Fatigue and creep-fatigue crack growth testing using C(T) and DEN(T-C) specimens are detailed in chapters 7 and 8, respectively. The unique scientific and technological contributions from this work are stated in Chapter 9. A summary of conclusions and recommendations for future work are described in Chapter 10.

CHAPTER 2

Scientific Background

Under long term service conditions, high temperature components with notches and crack-like defects may encounter crack initiation and propagation. To analyze these problems and to predict design or remaining lifetime, fracture mechanics analysis and test procedures are needed [15]. Fracture mechanics problems have been grouped into linear-elastic fracture mechanics, elastic-plastic fracture mechanics, and time dependent fracture mechanics regimes based on the dominant deformation modes in the cracked bodies.

Linear elastic fracture mechanics, LEFM, is used when the stress-strain and the load-displacement behavior is linear; in this case, the relevant crack tip parameter is the stress-intensity factor K because the plastic-zone size is small in comparison to the crack size and other pertinent dimensions of the cracked body. Elastic-plastic fracture mechanics, EPFM, is used when dominantly linear conditions can no longer be met due to large scale plasticity; the relevant crack tip parameter is the J- integral. Time-dependent fracture mechanics, TDFM, must be used when the stress-strain and load-displacement behavior is time-dependent due to dynamic loading or time-dependent creep [16]. In this dissertation, we will exclusively be concerned with TDFM in the context of creep deformation.

2.1 LEFM Approaches and Limitation

In LEFM, creep-fatigue crack growth behavior relies on ΔK to characterize the crack growth rate per cycle, da/dN, keeping the loading frequency and loading waveform constant. Figure 2(a) shows the loading waveforms typically employed in creep-fatigue experiments where t_r = rise time, t_h = hold time, t_d = decay time are the important time parameters. James [17] demonstrated the influence of loading waveform and frequency on da/dN versus. ΔK. He

showed that da/dN increases with decreasing loading frequency at a constant ΔK for 304 SS at 538°C as shown in the figure 2(b). Another similar work by Plumtree and Yu [18] on 304 SS at 570°C indicates that the time dependent damage accumulates more rapidly during the loading portion of the cycle as compared to the hold time. It is evident from the above studies that the time dependent damage plays a critical role on the fatigue crack growth behavior at elevated temperature. Creep damage at the crack tip or the influence of environment (oxidation), or microstructural changes due to loading at elevated temperatures or a combination of the above factors can be attributed to such trends. Also results from the work of several researchers [19,20,21] show that the time dependent effects at least in some materials are significantly enhanced by oxidation. Therefore it is necessary to consider environmental effects in order to predict fatigue crack growth behavior at elevated temperatures. The linear elastic parameter ΔK becomes questionable when there is significant creep deformation at the crack tip [22]. If creep deformation occurs, stresses redistribute with time near the crack tip and K no longer uniquely determines the crack tip stresses.

Instantaneous plasticity becomes significant for a large number of high temperature ductile materials where the 0.2 % yield strength decreases significantly with temperature. Under these conditions, the use of ΔK again becomes questionable. Hence, LEFM approach for creep-fatigue crack growth may be limited to highly creep resistant materials, such as nickel base super alloys and other creep-brittle materials [23,24]. Thus non-linear fracture mechanics concepts are needed for describing creep-fatigue crack growth behavior in a majority of high temperature materials which are creep-ductile in nature such as Cr-Mo steels, Cr-Mo-V steels and stainless steels.

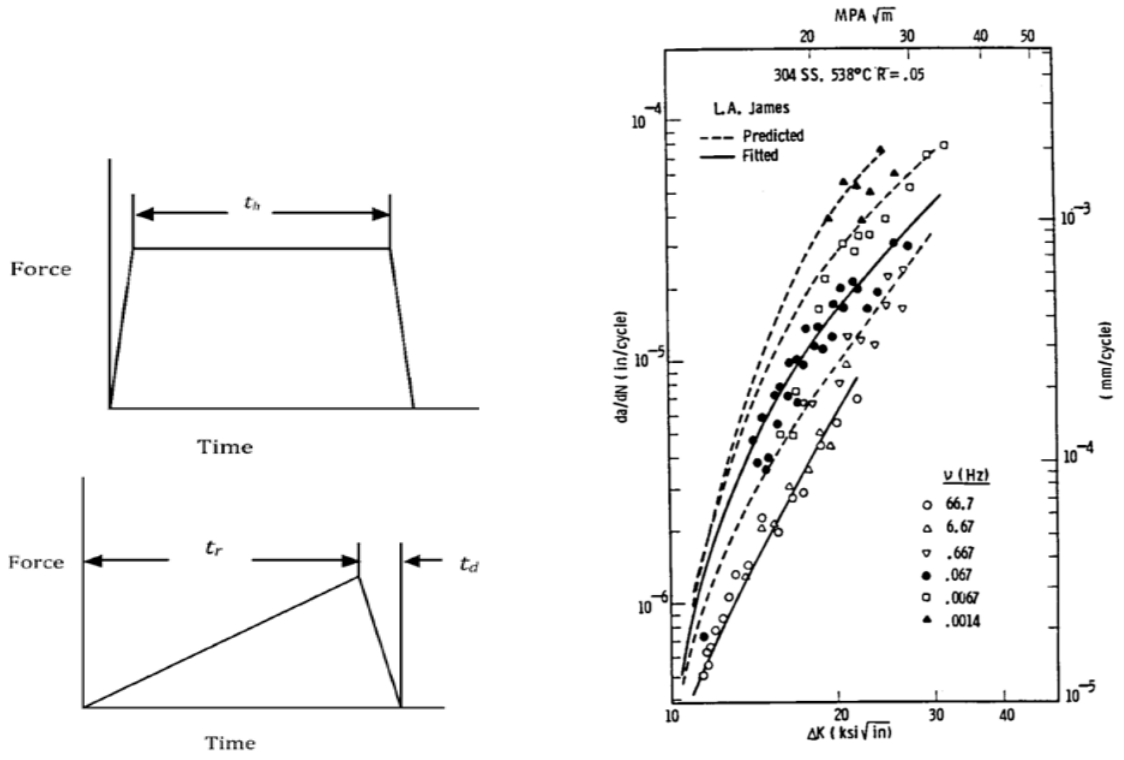

Figure 2.1. (a) Examples of loading waveform in creep-fatigue experiments; (b) Effect of loading frequency on the elevated temperature creep-fatigue crack growth behavior of creep-ductile 304 Stainless Steel [17].

2.2 Non-Linear Fracture Mechanics Approaches

"Creep-ductile materials can be defined as ones in which time-dependent crack growth at elevated temperatures is accompanied by substantial creep deformation" [2]. Therefore, it is necessary to include time-dependent creep deformation in the description of crack tip stresses and deformation fields under cyclic loading. The ΔJ integral is used to describe the fatigue crack growth behavior under gross plasticity conditions typically experienced at elevated temperatures. Dowling and Begley [25] first proposed the ΔJ parameter and later Lamba [26] gave a formal path-independent integral definition, which is analogous to Rice's J-integral [27]. For cyclically saturated material, ΔJ is given by:

$$\Delta J = \int_{\Gamma} \Delta W dy - \Delta T_i \frac{\partial \Delta u_i}{\partial x} ds \tag{2.1}$$

where ΔW is

$$\Delta W = \int_0^{\Delta \epsilon_{ij}} \Delta \sigma_{ij} d(\Delta \varepsilon_{ij}) \tag{2.2}$$

$\Delta \sigma_{ij}(x, y)$ is the range of cyclic stress at each point in the body associated with an applied external cyclic load, ΔP and $\Delta \varepsilon_{ij}(x, y)$ is the corresponding strain range, Γ is a contour beginning on the lower crack surface and ending on the upper crack surface travelling counterclockwise. T is a traction vector and u is a displacement vector. Under linear elastic conditions:

$$\Delta J = {\Delta K^2}/{E'} \tag{2.3}$$

Thus in elastic-plastic bodies the total value of ΔJ is obtained by combining the elastic and fully-plastic parts using the above equations in conjunction with non-linear finite element analyses of cracked bodies in which the stress and displacements are obtained numerically. It can also be measured experimentally at the load-point by the use of semi-empirical methods. Several studies [28,29,30] have shown the validity of ΔJ for characterizing elevated temperature growth under plasticity conditions. However, ΔJ is limited to cyclic plastic deformation and cannot be used for time dependent creep deformation which occurs if the loading frequencies are low or if there are hold times in the loading cycle. Hence, time-dependent fracture mechanics parameters are needed address those conditions.

2.3 Time Dependent Fracture Mechanics

From the above discussion it is clear that neither K nor J-integral and their cyclic versions ΔK and ΔJ do not uniquely characterize the crack tip stress fields due to accumulated creep strains at crack tip which leads to redistribution of the initial elastic-plastic stress field [26- 29, 31,32]. For short times when the crack tip creep zone is small in comparison to the relevant specimen dimension, the creep zone growth is restrained by the surrounding elastic-plastic fields characterized by K or J and time. This condition is known as small-scale-creep (SSC) condition. Under the extensive creep (EC) condition the creep zone extends through the entire uncracked ligament and the transition creep (TC) condition signifies an intermediate regime. The SSC and TC are transient conditions in which the crack tip stresses vary with time as the stresses redistribute within the uncracked ligament. The EC condition is a steady-state condition because the crack tip stresses remains constant with time. These three levels of creep deformation under which crack growth can occur are schematically shown in the figure 2.2. The commonly used uniaxial version of creep constitutive equation is [2]

$$\dot{\varepsilon} = \frac{\dot{\sigma}}{E} + A_1 \varepsilon^{-p} \sigma^{n_1(1+p)} + A\sigma^n \tag{2.4}$$

where the dots denote time derivatives, A_1, p and n_1 are material's primary creep rate parameters, and A and n are material's secondary creep rate parameters. The first term on the right hand side of the equation represents elastic strain rate that takes place as stresses redistribute in the small-scale-creep regime and can be neglected under extensive creep conditions because stresses become stationary with time. The steady-state extensive creep region is primarily used in design purposes for which the above equation reduces to

$$\dot{\varepsilon} = A\sigma^n \tag{2.5}$$

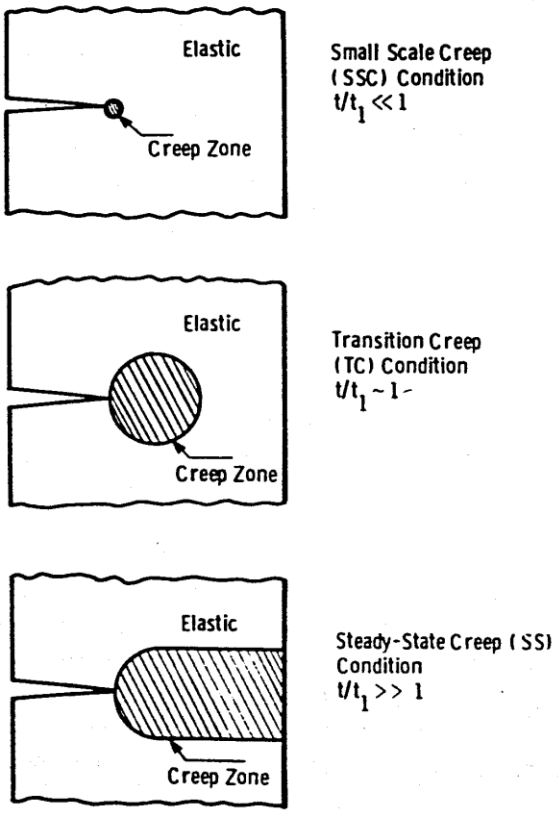

Figure 2.2. Levels of creep deformation under which creep crack growth can occur [16].

Landes and Begley [33], Nikbin et al. [34] and Taira et al. [35] defined a crack tip parameter analogous to Rice's J-integral commonly called as C^* defined as

$$C^* = \int_{\Gamma} W^* dy - T_i \left(\frac{\partial \dot{u}_i}{\partial x} \right) ds \tag{2.6}$$

where

$$W^* = \int_0^{\dot{\epsilon_{ij}}} \sigma_{ij} d(\dot{\varepsilon_{ij}}) \tag{2.7}$$

Γ is a line contour taken counterclockwise from the lower crack surface to the upper crack surface, W^* is the strain energy rate density associated with the point stress, $\dot{\sigma_{ij}}$ and strain rate, $\dot{\varepsilon_{ij}}$. T_i is the traction vector defined by the outward normal, n_j, along the path. C^* characterizes the crack tip stress and strain fields under extensive secondary creep conditions. Comparing equations 2.1 and 2.6, the analogy between C^* and J is very clear. The strain and displacement quantities are replaced with their respective time rates and stress remain as stress. Also, C^* is path independent like J when secondary creep conditions dominate as under EC condition. For these conditions, C^* can be determined for any geometry and loading conditions via the use of numerical or experimental or semi-empirical methods that are analogous to methods for determining J.

The validity of C^* integral is limited to extensive steady-state creep conditions. But in general, structural components are designed to resist wide-spread creep deformation and may not experience extensive creep. Ohji et al. [36], Riedel and Rice [37], Bassani and McClintock [38] addressed this issue by defining crack tip stress field under small-scale creep and called it as $C(t)$ integral which is same as C^*-integral except determined close to the crack tip region where the creep strains dominate over the elastic strains. $C(t)$ for elastic, power-law creep material where small-scale creep conditions prevail, is given by the following equation for plane strain conditions:

$$C(t) \cong \frac{K^2(1-\nu^2)}{(n+1)Et} \tag{2.8}$$

where, E is elastic modulus, K is applied stress intensity factor, and ν is Poisson's ratio. The transition time t_T from small-scale-creep to extensive secondary creep condition is given by [36, 37]

$$t_T = \frac{K^2(1-\nu^2)}{E(n+1)C^*} \tag{2.9}$$

Although $C(t)$ is an attractive parameter, a major drawback is that it cannot be measured at the loading pins under small-scale-creep conditions. It has to be always calculated from the equation 2.8. Saxena [39] addressed this issue by defining the C_t parameter, another extension of C^*-integral concept to characterize creep crack growth under a wide range of conditions from small-scale to extensive steady state creep. It is given by

$$C_t = -\frac{1}{B}\frac{\partial U_t^*\left(a, t, \dot{V}_c\right)}{\partial a} \tag{2.10}$$

where B is thickness, a is crack size, t is time, $\dot{V}_c$ is load-line deflection rate, and U_t^* is energy dissipated. Under extensive creep conditions, C_t reduces to $C^*(t)$ which is also equal to $C(t)$, but in the small scale creep condition $C_t \neq C(t)$, Instead, it is given by [40] and related to creep zone expansion rate.

$$(C_t)_{ssc} = 2(1-\nu^2)\frac{K^2}{EW}(F'/F)\beta\dot{\gamma}_c \tag{2.11}$$

Where F is K calibration factor $(K/P)BW^{1/2}$, $F' = dF/d(\frac{a}{W})$, β = 1/3, a factor determined from FEA, and $\gamma_c$is creep zone size with $\dot{\gamma}_c$ being its time derivative. $(C_t)_{ssc}$ can be estimated

analytically by substituting expressions of $\dot{\gamma}_c$ in the equation [41,42]. In terms of the measured load-deflection rate, $(C_t)_{ssc}$ is expressed as follows:

$$(C_t)_{ssc} = \frac{P\dot{V}_c}{BW} F'/F \tag{2.12}$$

For wide range of creep conditions, C_t can be estimated from the following formula [41]

$$C_t \cong (C_t)_{ssc} + C^* \tag{2.13}$$

The equation 2.13 is useful in test specimens to determine C_t for $t < t_T$. The above equations have been verified numerically by several researchers [41,43,44]. In summary, three crack tip parameters are relevant for characterizing elevated temperature crack growth behavior under static loading in ductile materials. These are the $C^*(t)$ - integral, $C(t)$ - integral and the C_t parameter. Thus, the above discussion provides the necessary analytical tool to analyze the more complex creep-fatigue problem which is one of the focuses of the current work.

2.4 Crack Tip Parameter for Creep-Fatigue Crack Growth

Several components operated at high temperature are subjected to cyclic loading making crack growth behavior under creep-fatigue conditions significant. Service condition is simulated in the laboratories by using different loading waveforms shown earlier. Elastic, plastic and creep deformation at the crack tip is achieved by the use of such wave shapes at elevated temperature [2]. Creep deformation can take place at the crack tip during the hold time as well as during the loading portion of the cycle in a trapezoidal loading waveform. The extent of creep deformation at the crack tip during loading will depend on the rate of loading and is generally accompanied by elastic and plastic deformation. Stress relaxation take place during the hold period resulting in accumulation of creep strains and if the hold period is sufficiently long extensive creep conditions will eventually occur. Thus, crack tip stress solutions are needed for a wide range of

loading and material deformation conditions in order to analyze creep-fatigue problems. Studies [5-7,45] performed on creep-ductile power plant materials using C(T) specimens have shown $(C_t)_{avg}$ to be the most effective crack tip parameter in correlating C-FCG rates in such materials. The time dependent crack growth, $(da/dt)_{avg}$, are expressed as a function of the average magnitude of the C_t parameter, $(C_t)_{avg}$. $(C_t)_{avg}$ for creep-fatigue crack growth during the hold time is given by [46]

$$(C_t)_{avg} = \frac{1}{t_h}\int_0^{t_h} C_t dt \tag{2.14}$$

where, $(da/dt)_{avg}$ is related to $(da/dN)_{time}$ by:

$$\left(\frac{da}{dt}\right)_{avg} = \frac{1}{t_h}\left(\frac{da}{dN}\right)_{time} \tag{2.15}$$

$(C_t)_{avg}$ can be determined for test specimens in which both load and load-line deflection behavior with time are measured from the following equation:

$$(C_t)_{avg} = \frac{\Delta P \Delta V_c}{BW t_h}\frac{F'}{F} \tag{2.16}$$

Where, ΔP is the applied load range, ΔV_c is the load-line deflection rate due to creep during hold time, t_h. $(C_t)_{avg}$ can be determined via the use of analytical methods outlined in the literature [5,46].

2.5 Creep-Fatigue Crack Growth Correlation

Combined creep and fatigue crack growth may take place at elevated temperatures. In most cases fatigue dominates at higher frequencies (f > 1 *Hz*) and creep dominates at lower

frequencies (f < 0.1 *Hz*) and hold times [47] (see figure 2.3). The models for creep-fatigue interaction can be separated by ones that account for hold-time effects and those that apply for continuous cyclic situations. Linear summation damage model and the damage summation model are the widely used approaches in evaluating the creep fatigue crack growth data for lifetime predictions. The purpose of these models is to provide the ability to interpolate/extrapolate time-dependent crack growth effects. The linear summation damage model proposed to evaluate crack growth under creep-fatigue condition is given by:

$$\frac{da}{dN} = \left(\frac{da}{dN}\right)_{cycle} + \left(\frac{da}{dN}\right)_{time} \tag{2.17}$$

where $(da/dN)_{time}$ is related to $(da/dt)_{avg}$ by:

$$\left(\frac{da}{dt}\right)_{avg} = \frac{1}{t_h}\left(\frac{da}{dN}\right)_{time} \tag{2.18}$$

The first term on the right hand side of the equation 2.17 accounts for cycle dependent crack growth rate and the second term represent the time-dependent part.

The cycle-dependent crack growth rate, $(da/dN)_{cycle}$ is determined from fatigue tests without hold time. By re-arranging the equation, $(da/dt)_{avg}$, can be calculated by:

$$\left(\frac{da}{dt}\right)_{avg} = \frac{1}{t_h}\left[\left(\frac{da}{dN}\right) - \left(\frac{da}{dN}\right)_{cycle}\right] \tag{2.19}$$

The alternate approach for predicting creep-fatigue crack growth is the dominant damage approach [48]. The governing equations for estimating the crack growth rate from this model is as follows:

$$\frac{da}{dN} = max\left[\left(\frac{da}{dN}\right)_{cycle}, \left(\frac{da}{dN}\right)_{time}\right] \tag{2.20}$$

where $(da/dt)_{avg}$, is expressed as:

$$\left(\frac{da}{dt}\right)_{avg} = \frac{1}{t_h}\left(\frac{da}{dN}\right)_{time} \tag{2.21}$$

In this approach, the cycle-dependent and the time-dependent crack growth rates during creep-fatigue conditions are assumed to be competing mechanisms and the crack growth rate is determined by the greater of the two. In general equation 2.20 is more conservative and is preferred for analyzing creep-fatigue data [48] while equation 2.19 is more conservative in application when creep-fatigue crack growth rates are being predicted.

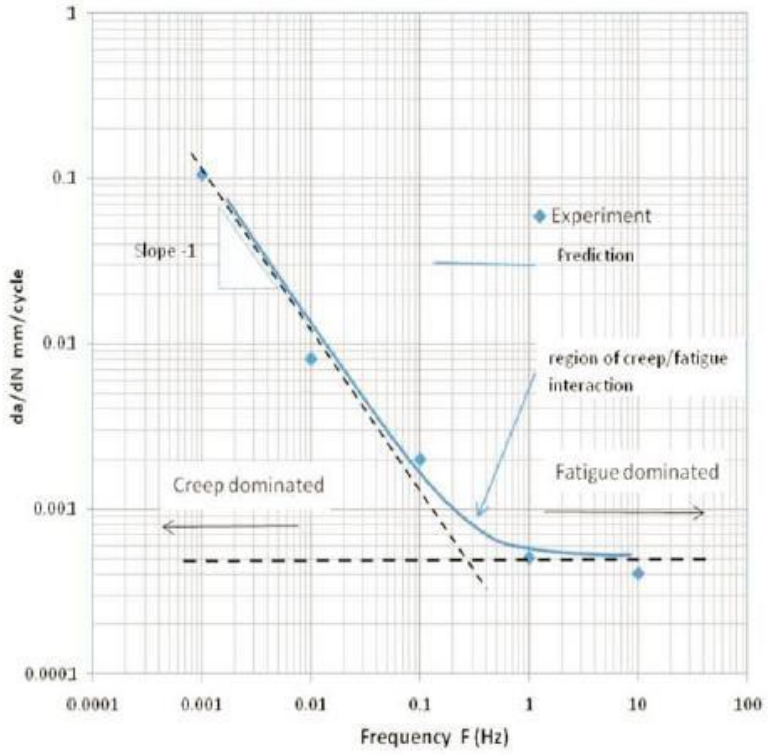

Figure 2.3. Fatigue, creep, creep-fatigue interaction regimes [47].

The figure 2.4 shows the plot of crack growth rate versus ΔK for Cr-Mo-V steels at 1000° F (538° C) at various hold times [49]. It can be observed from the figure that the crack growth rate increases with increase in hold time and stress-intensity factor range, ΔK. However, there are other concerns about the use of ΔK at elevated temperature as discussed in section 2.1. It is apparent that time dependent creep deformation is more wide-spread and there is lack of correlation between crack growth rate and ΔK.

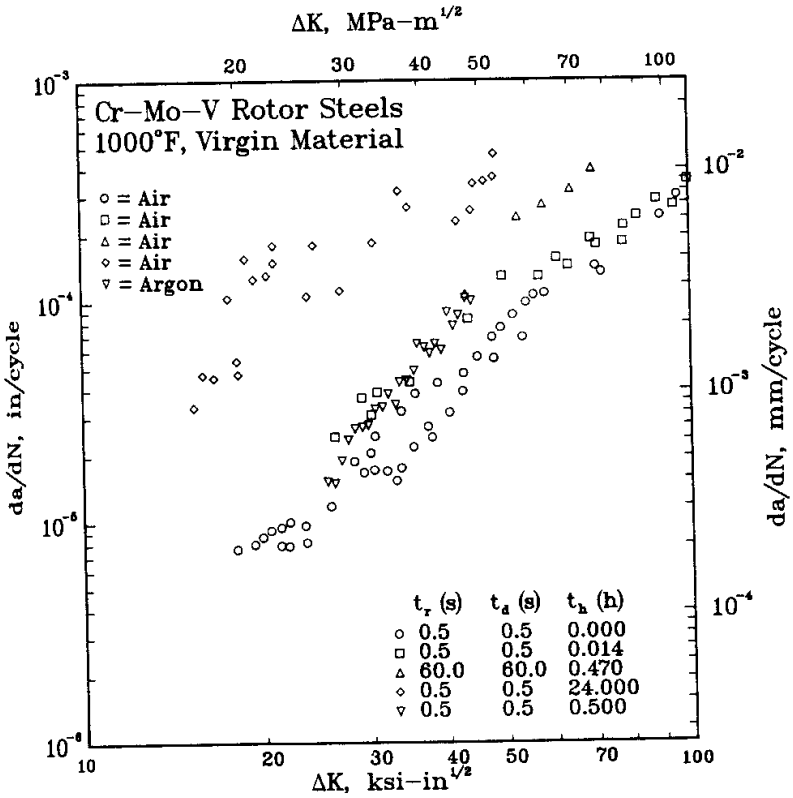

Figure 2.4. Effect of hold time on crack growth behavior of Cr-Mo-V at 538°C [49].

Under cyclic and static loadings of metals at elevated temperature, crack growth behavior are affected by transients [39]. A characteristic hook is a typical response in this transient regime. It can be observed in figures 2.4 and 2. 5 that several of the Cr-Mo steel exhibited this characteristic hook during the early portion of the test. Several studies [46,50,51] have reported

this transient trend in the crack growth behavior during the early part of the creep-fatigue crack growth tests. This transient behavior implies that even for constant loading frequency and waveform, da/dN does not uniquely correlate with ΔK during the early portion of the tests for creep-ductile materials even though the specimen is in dominantly in the LEFM regime. This trend can be important in service life predictions as it can occupy a major portion of the fracture life.

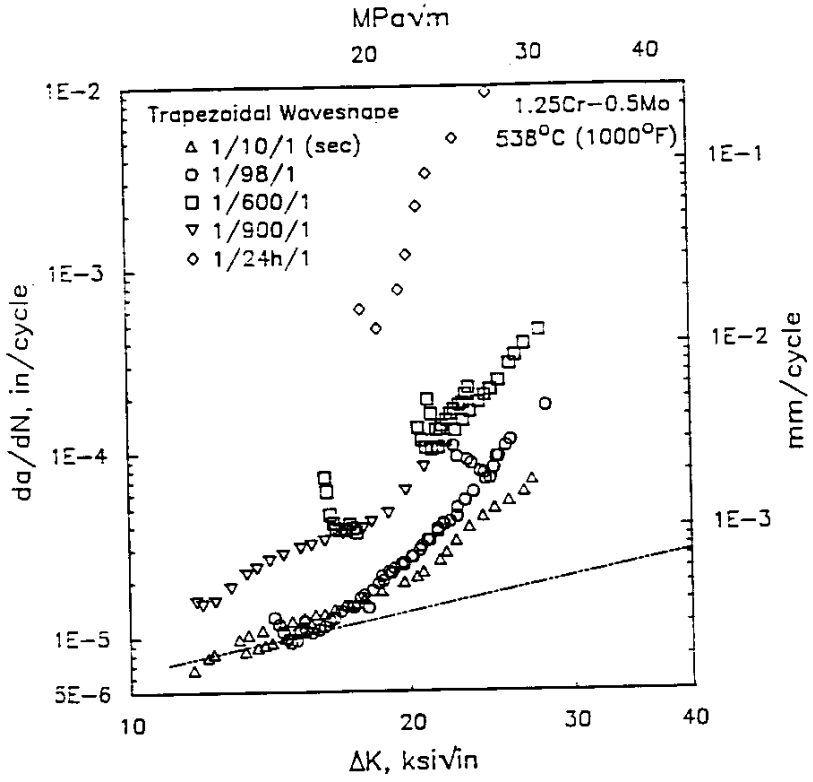

Figure 2.5. Transient crack growth behavior at the beginning of the test for 1.25Cr-0.5Mo steel [7].

By measuring the displacement at the loading pins as a function of time during the hold time, the effects of instantaneous plasticity and creep are included in the estimation of $(C_t)_{avg}$ and, thus, the transients from the expanding creep-zone are normalized when the crack growth rates are correlated with the $(C_t)_{avg}$ parameter. Figure 2.6 shows the correlation between

$(da/dt)_{avg}$ and $(C_t)_{avg}$ for 1.25Cr-0.5 Mo at 538° C for various hold time tests ranging from 10 seconds to 24 hours. The plot also includes creep crack growth data for the same material. It can be observed from the plot that all the data lie in the same scatter band implying that the time-dependent crack growth data during creep-fatigue is identical to creep-crack growth data provided the correct parameter is used to correlate the trends. Several such studies have been conducted by Saxena and co-workers [2] on various Cr-Mo-V, steels which are predominantly creep-ductile in nature (see also figure 2.7). These studies indicated a unique correlation exists between average rate of crack growth during the hold time and the average value of the C_t parameter for wide range of hold time conditions.

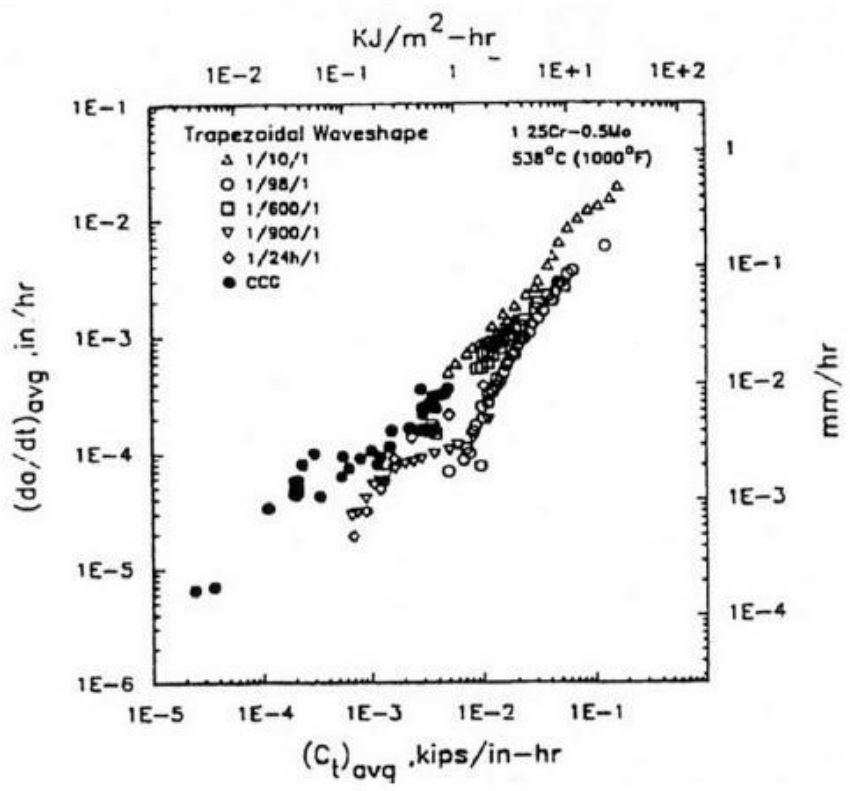

Figure 2.6. Average time rate of crack growth as a function the average value of $(C_t)_{avg}$ for several hold-times ranging 10 seconds to 24 hours and including creep crack growth rates for 1.25 Cr -0.5Mo Steel at 538°C [7].

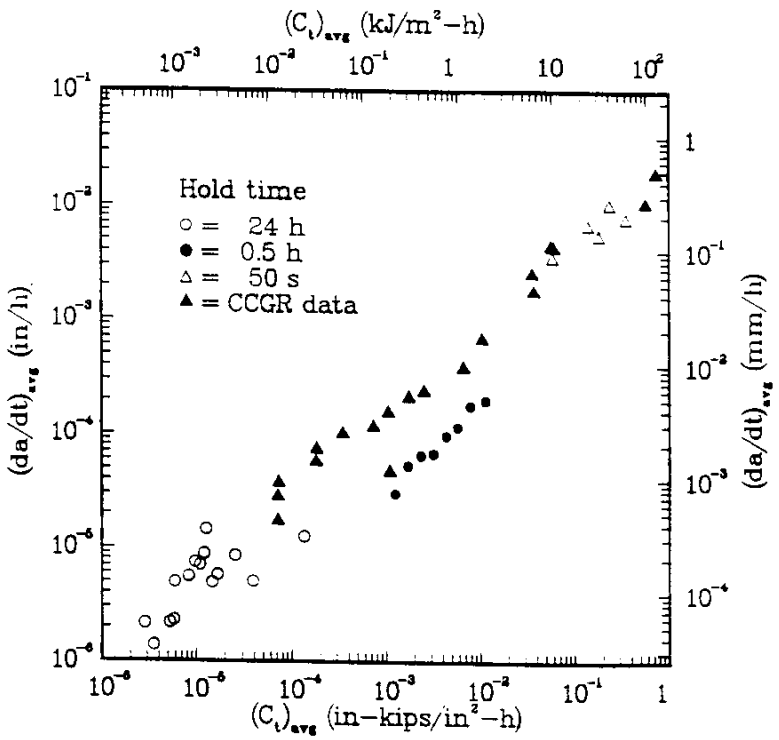

Figure 2.7. Correlation between $(da/dt)_{avg}$ and $(C_t)_{avg}$ in Cr-Mo-V steels [49].

2.6 Experimental Methods for Characterizing Creep-fatigue Crack Growth

Two methods have been primarily used to obtain creep-fatigue crack growth data. The first is a conventional fracture mechanics method based on testing compact specimens subjected to uniaxial cyclic forces in load control mode [2]. In this method, C(T) specimens are subjected to constant-amplitude loading using a prescribed waveform and frequency under a positive load ratio. The load-line displacements at maximum, minimum and during the hold time are measured for the entire loading cycle. The extensometers now available are capable of making such measurements. Crack size can be measured by either electric potential drop, (EPD) or unloading compliance method. Figure 2.8 shows the comparison between the crack length measured by the EPD technique and unloading compliance technique [52]. The unloading compliance can produce considerable scatter in the data. But, this generally depends on the response dynamics of

the extensometer used for testing. Extensometers used during C-F testing must have a higher dynamic response.

In C-FCG tests, the crack length is averaged across the specimen thickness, as the crack front will be usually curved. The figure 2.9 shows the crack front on a side-grooved C(T) specimen [52]. Side grooves are essential in elevated temperature testing. Without side grooves, tunneling can be very severe and it can contribute to more scatter in the data. The angle for the side grooves needs to be optimized for a given material but guidelines for that are available in the ASTM standards [11,8].

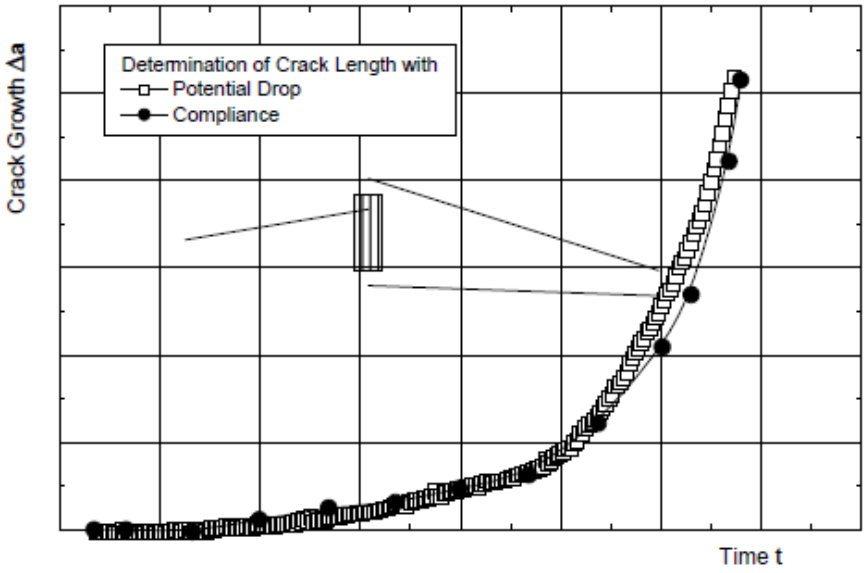

Figure 2.8. Comparison between crack length measured by unloading compliance and potential drop [52].

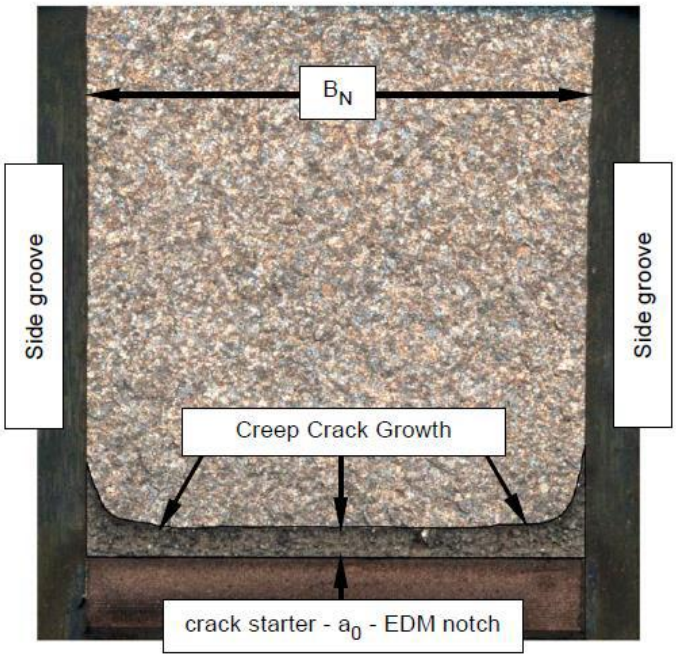

Figure 2.9. Crack front on a side grooved C(T) specimen [52].

This method generally yields satisfactory results provided linear-elastic conditions can be maintained in the specimens. But during C-F testing, the accumulated creep and plastic deformation increase with each cycle leading to ratcheting of specimen, thereby not being able to maintain linear elastic conditions in the test specimen. This is prone to become even more severe during longer hold time tests where there is significant accumulation of creep deformation with each cycle. Researchers [7] have observed that if the initial a/W values in 50 mm wide C(T) specimens are about 0.3, sufficient crack growth data can be obtained in creep-ductile power plant materials such as Cr-M0 and Cr-Mo-V steels in the temperature of interest before LEFM conditions are violated.

The majority of the C-FCG tests performed to date have been under load-controlled conditions, mostly out of convenience. Displacement controlled tests require specially designed grips to ensure that the specimen does not buckle when reversing the displacement to a

minimum, which results in compressive stress. However, this type of testing is more representative of the conditions experienced by some of the power plant components (e.g. cyclic thermal stresses). Some other advantages of displacement controlled tests over load controlled tests are as follows:

In load-controlled tests, the net section stress ahead of the crack-tip rises continuously as the crack advances. This generally leads to decrease in constraint because there is a tendency for the stress state to change from plane strain to plane stress. This is more prevalent in thinner specimens although there is an increase in triaxiality of the stress state in thick specimens as well. These thickness effects can cause the crack growth rates to vary. In displacement controlled test the constraint is not lost as the load decreases with time. Thus, the state of the stress essentially remains unchanged during the duration of the tests [53].

The issue of the ratcheting can be avoided with displacement controlled test as discussed earlier in section 1.1 and significant crack extension can be obtained than the load controlled tests. During the load controlled tests, the crack growth rate accelerates rapidly as the tests progresses causing specimens to open up beyond the operational range of high temperature extensometer. Thus, the tests must be conducted at low loads for long durations of time to obtain valid crack growth data. This is not the case with the displacement controlled tests because the crack growth rates decrease as the tests progresses and crack growth data can be obtained in shorter times than the load-controlled tests.

Gladwin et al. [54] observed other complications such as static mode of fracture (e.g. tearing) can influence the creep-fatigue damage process in positive R load-controlled C-FCG tests. Thus, the crack growths associated with the hold time may be a result of stable tearing

rather than the true creep-fatigue interactions. This problem is also avoided in displacement controlled tests. The Japanese researchers have largely contributed to the second method for generating creep-fatigue crack growth data [28,30,55]. In this method, hollow cylindrical specimens containing small crack along the circumference are subjected to prescribed displacement or stress. Crack size is generally monitored by EPD. Because the test specimens are in general, smaller in size (10-13 mm), it is unlikely that significant crack growth data can be obtained under any conditions.

2.7 Creep-Fatigue Crack Growth Testing using DEN(T) Specimens

Figure 2.10 shows a schematic of the DEN specimen where a is the crack size, h is the height and W is the width of the specimen. Figure 2.11 shows DEN specimen designs used by researchers [14,56] to conduct creep testing. Pin loading is commonly used to facilitate such testing. But as discussed earlier, pin loading is not suitable for performing displacement controlled creep-fatigue crack growth testing because the pin configuration is not suitable under compressive loading.

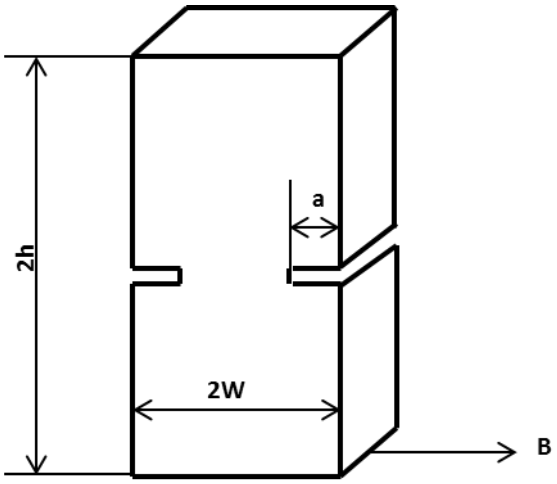

Figure 2.10. DEN specimen configuration.

Although DEN is a common specimen used in research and practice of fracture mechanics, very limited experimental work has been performed on creep-fatigue crack growth using DEN specimens. Such work has been by Mueller et al. [57], Scholz et al. [15], Kussmaul et al. [58], Gengenbach et al. [59] and Yokobori et al. [60] using side grooved DEN specimen for characterizing creep-fatigue crack initiation and growth under constant amplitude load controlled conditions. It is also suggested from the literature [56 - 60] that bulk of work has been performed on C(T) specimens which is dominantly under bend type loading and the experimental data under dominantly tension type loading using DEN specimens are scarce in the literature. Furthermore, there is no standardized DEN specimen available in the ASTM standards to perform creep-fatigue crack growth testing. Hence, it is imperative to review the published literature and its findings.

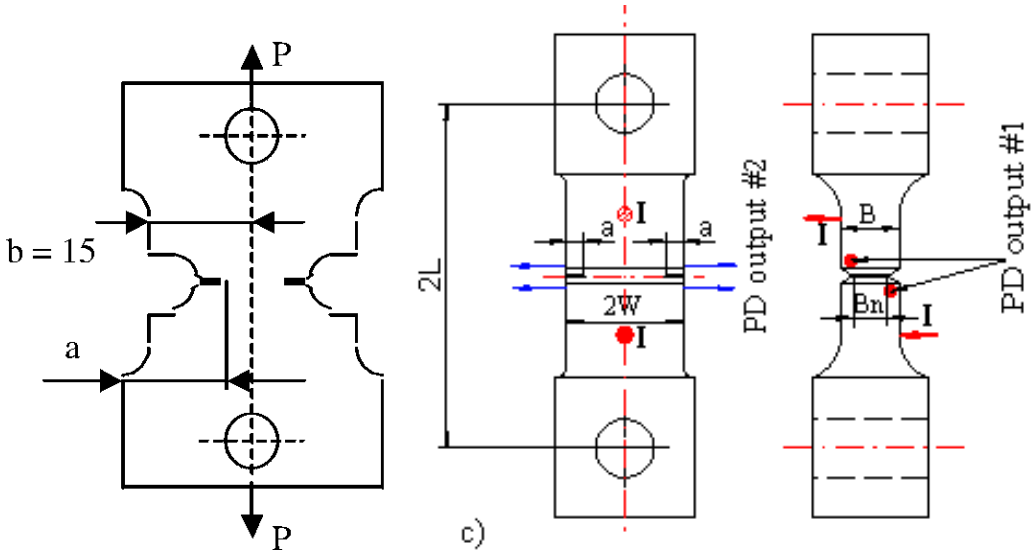

Figure 2.11. DEN specimens used in creep testing [14, 56].

Gengenbach et al. [59] investigated the creep crack initiation of 9-12 % Cr steels at 600°C using C(T) and DEN(T) specimens. The DEN(T) specimens tested had thickness of 60 mm while the C(T) specimens had 25 mm and 50 mm respectively. Figures 2.12 and 2.13 show the results of creep crack initiation times of C(T) and DEN(T) specimens for the tested materials. Their studies indicate that there can be strong influence of specimen geometry on the crack initiation behavior. This is largely due to the constraint in the larger specimen and was under investigation at the time of this publication.

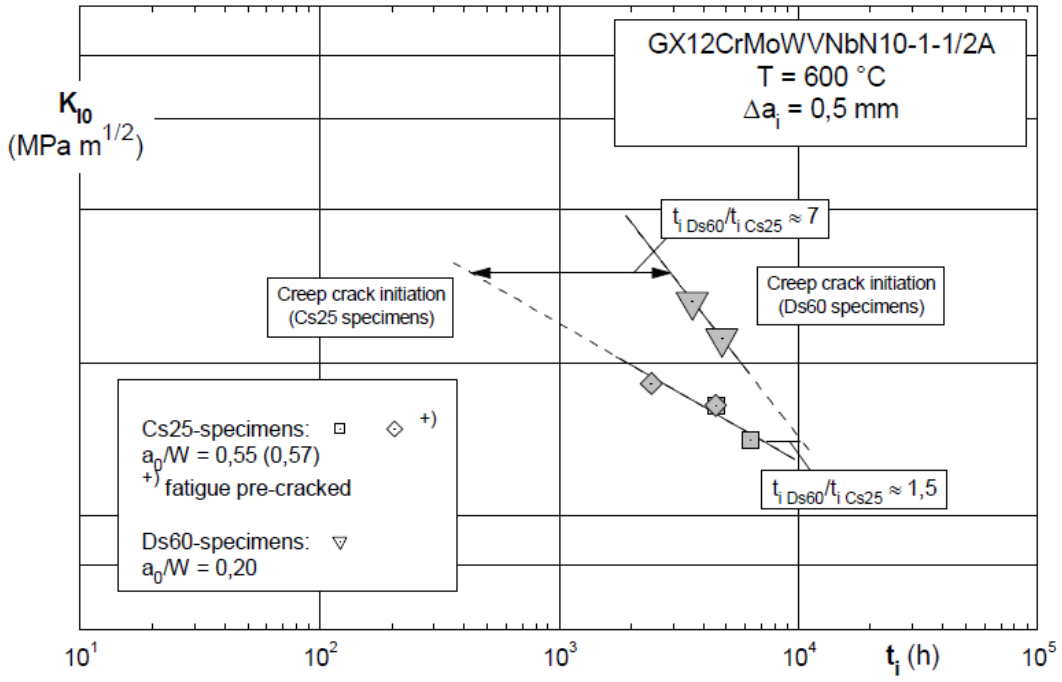

Figure 2.12. Creep crack initiation time of C(T) and DEN(T) specimens for GX12 cast steels at 600°C [59].

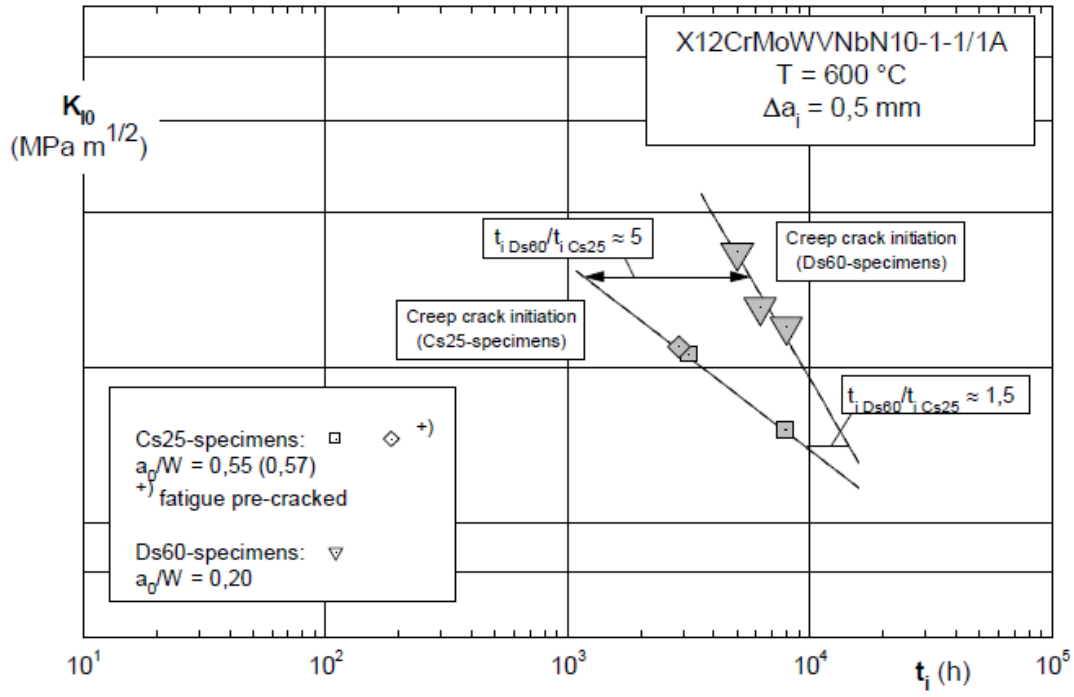

Figure 2.13. Creep crack initiation time of C(T) and DEN(T) specimens for GX12 forged steels at 600°C [59].

Mueller et al. [57] studied the crack behavior of 10 Cr-steels at 550°C and 600°C under creep and creep-fatigue conditions using C(T) and DEN(T) specimens. C(T) specimens had thicknesses of 25 mm and 50 mm and the DEN(T) specimens tested had thickness of 60 mm. Figure 2.14 shows the creep crack growth rate. They observed that although the DEN(T) and C(T) specimen data lie within tight scatter band, the DEN(T) specimens had a higher crack growth rate as shown in the figure. They noted that higher crack tip constraint conditions and the size of the DEN(T) geometry can cause such increase in crack growth rates. But, similar such effects were not present under creep-fatigue crack growth conditions as shown in figures 2.15 and 2.16.

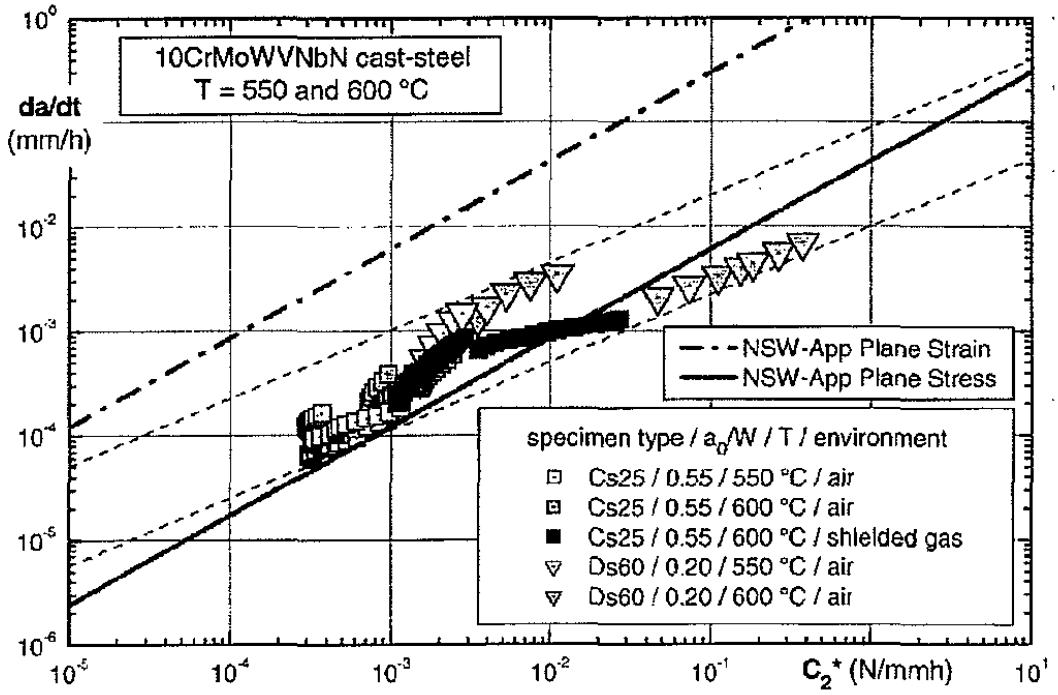

Figure 2.14. Creep crack growth rate versus parameter C^* for 10Cr-cast steel at 550 and 600°C [57].

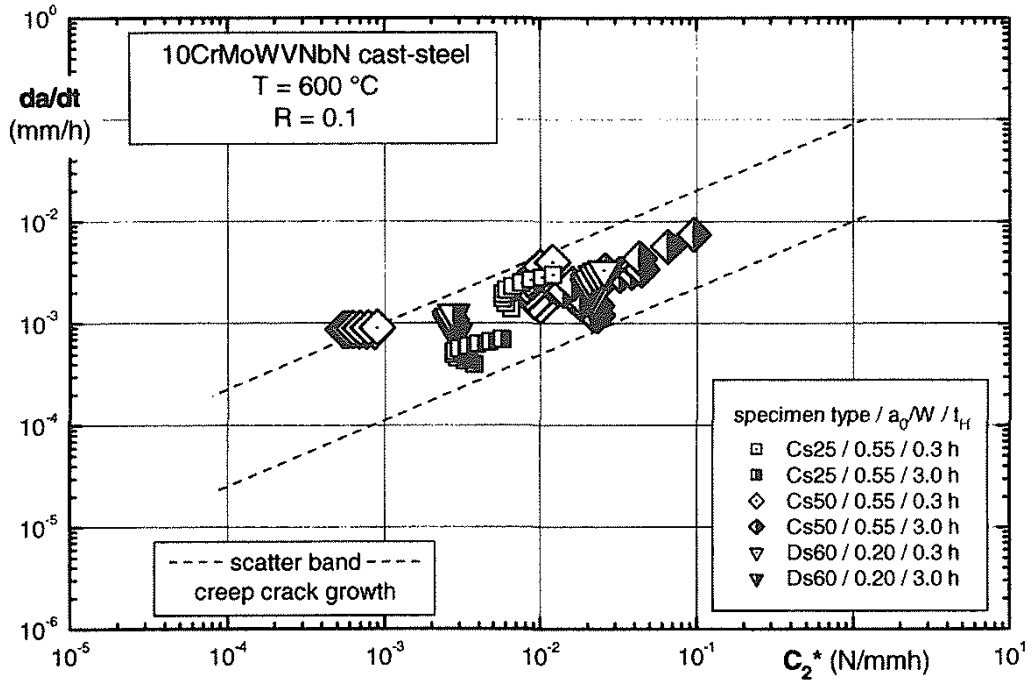

Figure 2.15. Creep-fatigue crack growth rate versus C^* parameter for 10Cr-cast steel at 600°C [57].

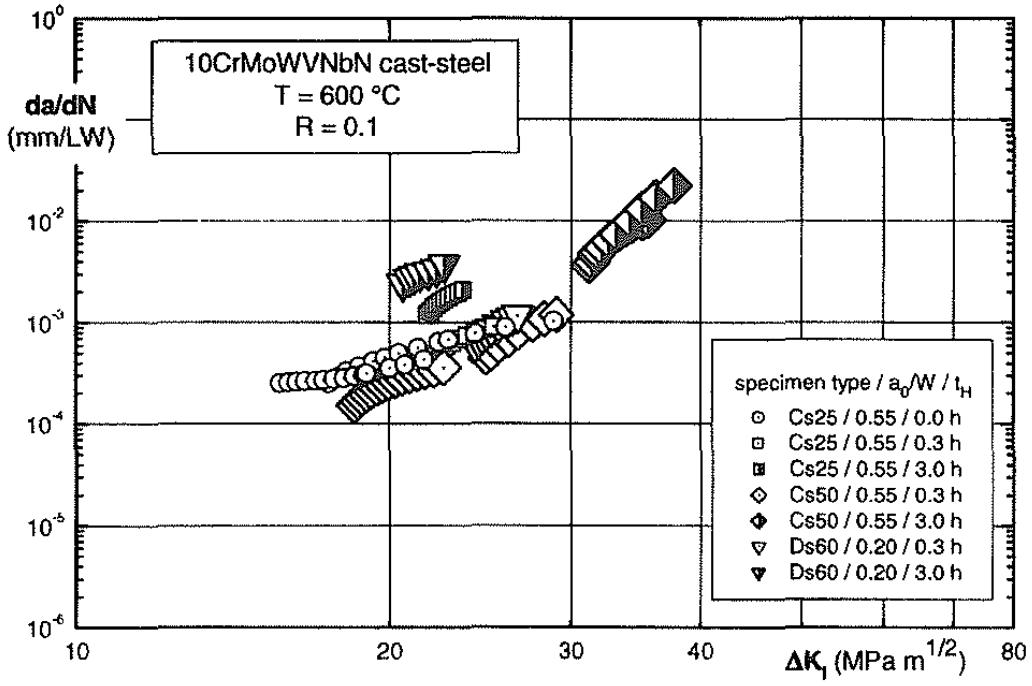

Figure 2.16. Creep-fatigue crack growth rate versus ΔK for 10Cr-cast steel at 600°C [57].

2.8 DEN Specimen Designs

Since this work will involve modification and optimization of DEN specimen geometry parameters, the few published literature, which are relevant to our proposed specimen design methodologies will be discussed here.

Allen et al. [61] at NASA Marshall Space Flight Center explored the various approaches to develop a fatigue crack growth coupon to investigate highly plastic stress field to simulate large separation bolt in a flight hardware. The various fatigue coupons are illustrated in figure 2.17. They started with a notched plate specimen and noted that this specimen was very sensitive to load alignment and resulted in varying stress fields in the notch region. Thus, to reduce the alignment sensitivity, they developed a modified DEN(T) specimen. This specimen, being symmetric has an advantage over the notched plate specimen in reducing the bending sensitivity. Although this specimen had an improvement over the NP specimen, the transition sections below

the pin holes were found to be stiffer resulting in stress concentrations. Thus fillets were cut into the transition section below the pin holes. Two different fillet radii resulted in MDEN(T)-2 and MDEN(T)-3 specimens respectively. These fillets sections essentially act as flexure and helps preserve the stress state in the notch regions.

It is noted that all the coupons are primarily pin loaded with deep notch to produce plastic stress field and cannot be used in tension-compression testing. But it is prudent to take advantage of their scientific approaches towards reducing load misalignment and stress concentrations.

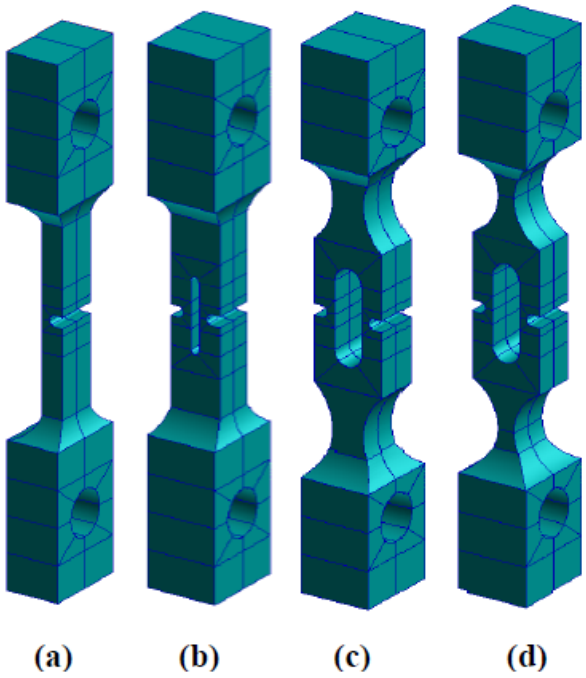

Figure 2.17. Illustration of: (a) Notched plate, (b) MDEN(T), (c) MDEN(T)-2, (d) MDEN(T)-3 [61].

The closest modification that exists to the DEN specimen to accommodate tension-compression loading are from the early works of Dowling et al. [62] and more recently from Wire et al [63]. The figure 2.18 shows the various specimen geometries used by Dowling to

study the fatigue crack growth and closure at high cyclic strains. One among those test specimens, is the DEN specimen modified to conduct fatigue tests under fully reversed loading (R = -1). The figure 2.19 shows the fatigue crack growth rate, da/dN versus ΔK for short and long cracks using double edge notch, center hole and compact specimens at R = -1. These results show that the crack growth data for the tested specimen geometries fall into a tight scatter band. But, a clear description of the various geometric parameters of the DEN specimen is not available in his work.

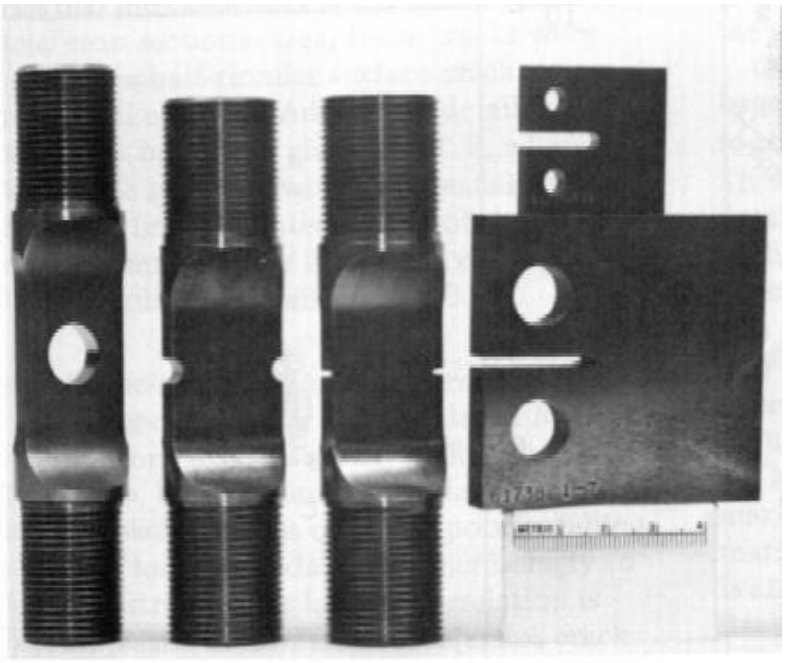

Figure 2.18. Test specimen geometries (Center-hole, blunt double-edge-notch, sharp double edge notch, blunt notched compact (top), pre-cracked compact (bottom) [62].

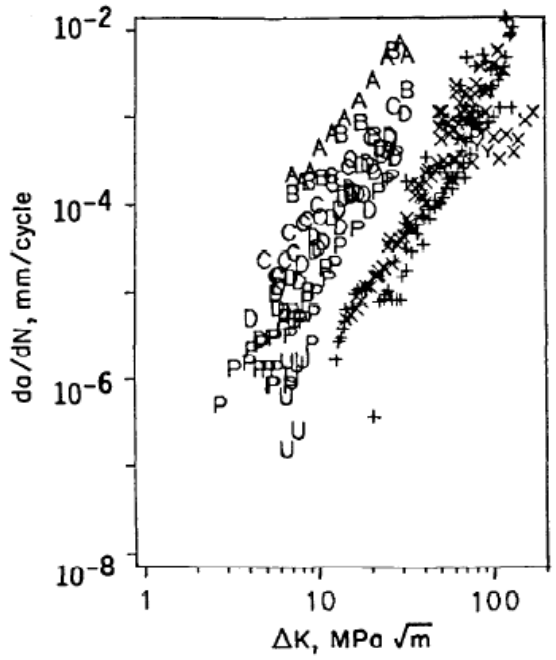

Figure 2.19. Fatigue crack growth rate versus ΔK for short cracks (A, $\Delta\varepsilon$ =0.029; B, $\Delta\varepsilon$ = 0.018; C, $\Delta\varepsilon$ =0.010; D, $\Delta\varepsilon$ =0.0066; P, $\Delta\varepsilon$ =0.0047; U, $\Delta\varepsilon$ =0.0037 and long cracks (X, double-edge notch; T, center hole; +,compact) at R = -1 with no plasticity correction. [62].

Wire and Mills [63] modified a pin-loaded DEN specimen to accommodate tension-compression testing as shown in figure 2.20. They conducted fatigue crack growth rate testing using 304 SS in air and elevated temperature water using C(T) and DEN specimens. Strain gauges attached to the specimen monitored the bending stress and alignment was achieved by manually adjusting the pull rods. The strain gauges were then removed and EPD leads were attached to the specimen to monitor the crack growth. As noted by Wire and Mills and several other investigators, crack asymmetry is a potential problem with DEN specimens. Hence, a systematic procedure is required to validate and qualify the crack growth data. The crack growth rate trends from the DEN test data and the conventional C(T) test data are shown in the figure 2.21. It can be observed from the plot that the DEN and C(T) data are in good agreement in the

intermediate growth rate regimes. Thus, one of the objectives in this work will be to show that the C(T) and DEN fatigue crack growth data can be collapsed into a reasonable scatter band.

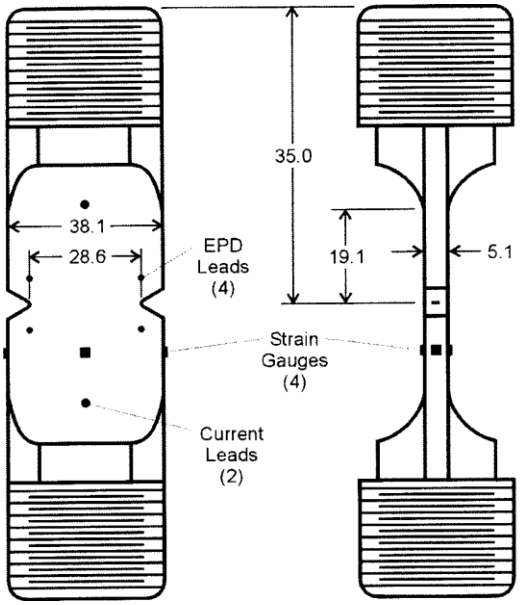

Figure 2.20. Modified DEN specimen used by Wire and Mills [63].

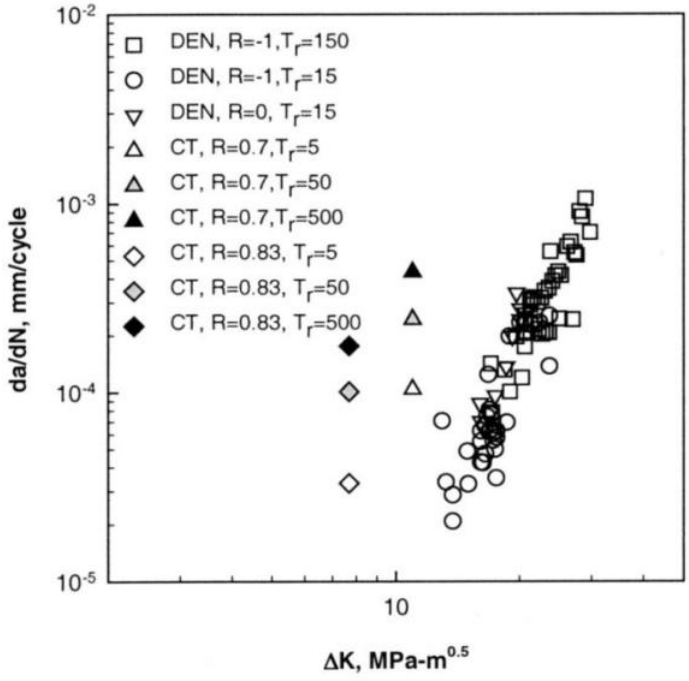

Figure 2.21. DEN and C(T) crack growth data from the work of Wire and Mills [63].

2.9 Numerical Analyses

2.9.1 Finite Element Analysis

FEA is a versatile numerical tool used in the fracture analysis of cracked bodies. A fracture analysis involves a combination of stress analysis and fracture mechanics parameters calculation. Figure 2.22 shows the three modes of fracture possible under the relative movement of the two surfaces of the crack. They are

- Mode I – Opening or tensile mode
- Mode II – Shearing or sliding mode
- Mode III – Tearing or out-of-plane mode

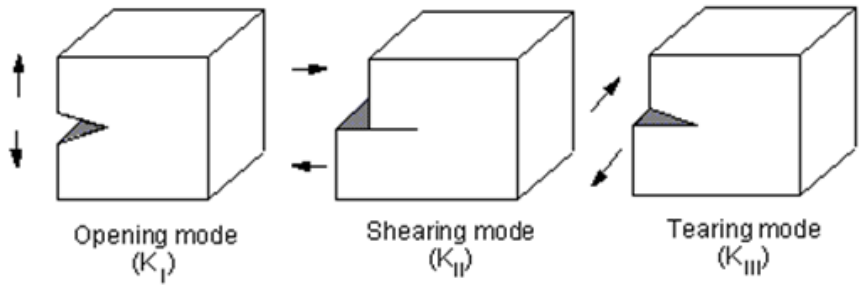

Figure 2.22. Schematic of the fracture modes [64].

Fracture mechanics parameters describe either the energy-release rate or the amplitude of the stress and deformation fields ahead of the crack tip. Stress-intensity factor, energy-release rate and J -integral are the widely used parameters in fracture analysis. While the former two are limited to linear elastic fracture mechanics, the J -Integral is applicable to both linear elastic and nonlinear elastic-plastic materials. In LEFM, the stress and strain fields ahead of the crack tip are expressed as:

$$\sigma_{ij} = \frac{K}{\sqrt{r}} f_{ij}(\theta) \tag{2.22}$$

$$\varepsilon_{ij} = \frac{K}{\sqrt{r}} g_{ij}(\theta) \tag{2.23}$$

Here K is the stress-intensity factor, r and θ are coordinates of a polar coordinate system as shown in the figure 2.23.

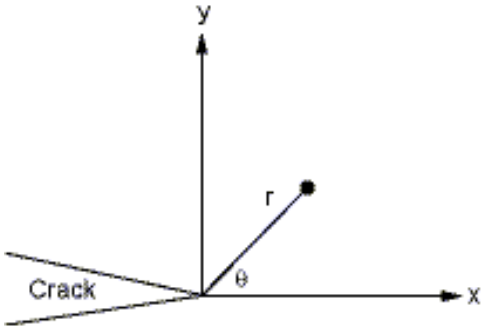

Figure 2.23. Schematic of a crack tip [64].

The stress fields for a mode I crack are given by:

$$\sigma_x = \frac{K_I}{\sqrt{2\pi r}} cos\left(\frac{\theta}{2}\right)\left(1 - sin\left(\frac{\theta}{2}\right) sin\left(\frac{3\theta}{2}\right)\right) \tag{2.24}$$

$$\sigma_y = \frac{K_I}{\sqrt{2\pi r}} cos\left(\frac{\theta}{2}\right)\left(1 + sin\left(\frac{\theta}{2}\right) sin\left(\frac{3\theta}{2}\right)\right) \tag{2.25}$$

$$\sigma_{xy} = \frac{K_I}{\sqrt{2\pi r}} cos\left(\frac{\theta}{2}\right) sin\left(\frac{\theta}{2}\right) cos\left(\frac{3\theta}{2}\right) \tag{2.26}$$

Some of the earlier approaches for determining fracture mechanics parameters from numerical analysis can be broadly classified into two categories: point matching and the energy method. The point matching method involves inferring the stress intensity factor from the stress or the displacement fields in the body, while energy methods compute the energy release rate in the body and relate it to stress intensity factor. In LEFM, the stress-intensity factor can be estimated from stresses in front of the crack tip or displacements behind the crack tip. The edge or tip of the crack is known as a crack tip in a 2-D model and crack front in a 3-D model, as illustrated in figure 2.24.

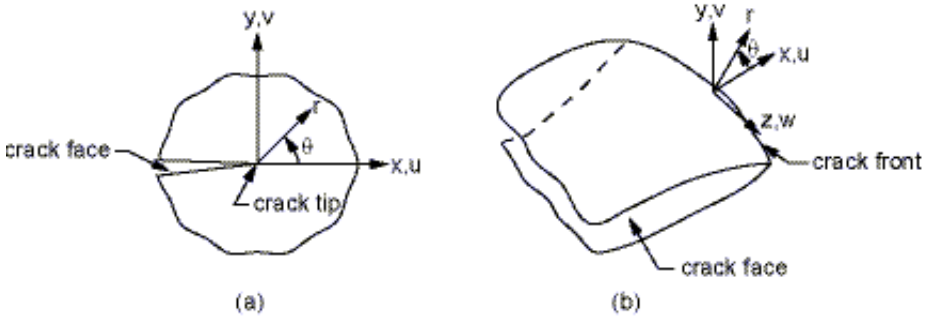

Figure 2.24. Crack tip in (2d model) and Crack front in (3D model) [64].

For linear elastic problems, the displacements are proportional to $\sqrt{r}$ near the crack tip where r is the distance from the crack tip, making stresses and strains singular at the crack tip and varying as $1/\sqrt{r}$. Hence, singular elements are needed to model the crack tip region to produce this singularity [65]. Some of the singular elements commonly used in 2-D and 3-D analysis are shown in the figure 2.25.

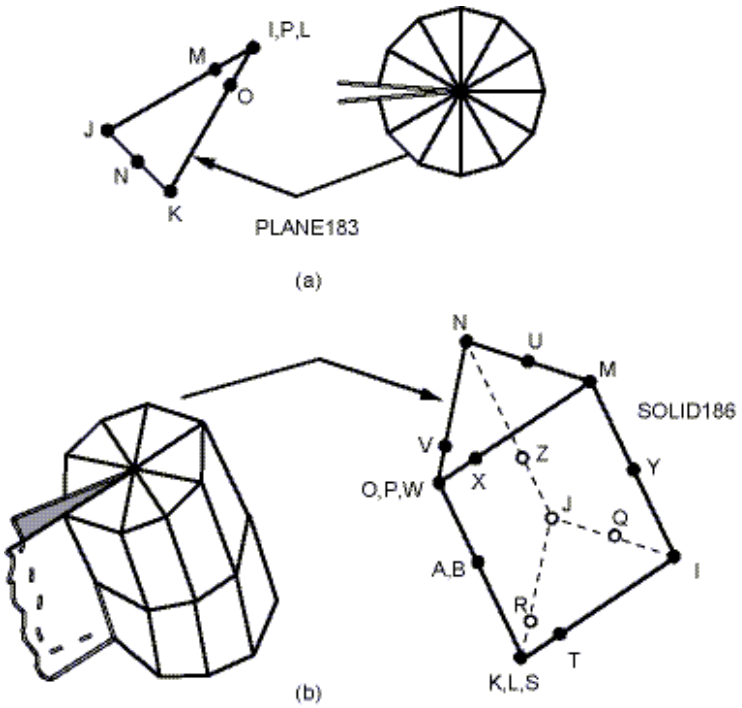

Figure 2.25. Examples of singular elements [64]

The finite element modeling of a component containing a crack requires special attention because of high stress gradients that exist in the crack tip region. Two-dimensional (2-D) linear elastic fracture problems can be modeled using PLANE183, the 8-node quadratic solid. Nore that the quadratic solid element have 3 collapsed nodes at the crack tip. The first row of elements around the crack tip should be singular, as illustrated in figure 2.25. Figure 2.26 shows the 2-D FE model of C(T) specimen. It is advantageous to use symmetry wherever possible to reduce time and computation effort [64].

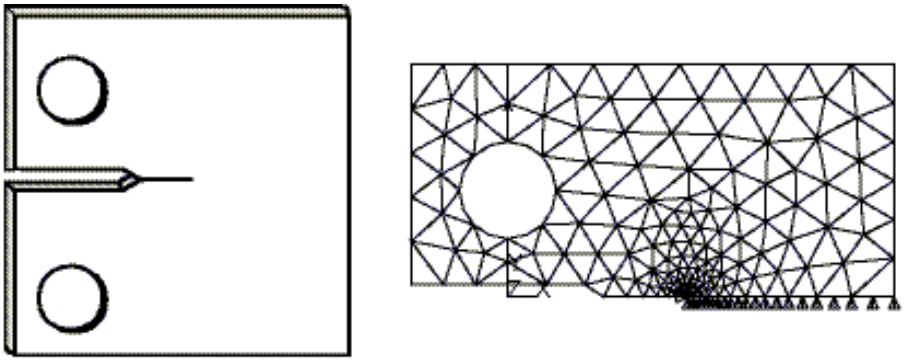

Figure 2.26. C(T) specimen and its 2-D FE model [64].

The other approach to estimate the stress-intensity factor in the LEFM regime is based on J - integral. The J - integral can be calculated numerically along a contour around a crack tip. In a linear elastic material, the J - integral represents the energy release rate. The stress-intensity factor and the energy-release rate are related by $G = K^2 / E'$ (where G denotes the energy-release rate and E' is the effective modulus). The advantages of this method are that it can be applied to both linear and nonlinear problems, and path independence (in elastic materials) enables one to calculate J at a far field where numerical accuracy is greater. The J - integral calculation built in ANSYS is based on the domain integral method formulated by Shih [66]. The domain integral applies area integration for 2-D problem and volume integration for 3-D problems and yields more accurate results, easier to implement than the contour integrals [64]. Hence, this methodology will be used in this work to estimate the values of *J*. Hutchinson [67] and Rice and Rosengren [68] independently demonstrated that the J - integral characterizes the crack tip field in a nonlinear elastic material. J - integral is also one the most widely accepted parameters for elastic-plastic fracture mechanics. In this work, the commercial software ANSYS® is used for FEA.

2.9.2 Boundary Element Analysis

The boundary element analysis is another powerful method used for the analysis for elastic structures [69]. In this method, only the boundary of the body needs discretization (in the absence of body forces). This is key advantage over the other methods as it simplifies the modeling procedure. In this work, the 2D-BEA code, FADD2D-Fracture Analysis by Distributed Dislocations will be utilized for fracture mechanics and stress analysis of two-dimensional (2D) cracked (or uncracked) bodies. FADD2D integrates a fracture mechanics and stress analysis code to perform fracture mechanics analysis. In this approach, cracks are modeled by series of point dislocations. Quadratic boundary elements are used to model internal and external boundaries. Cracks are modeled by linear boundary elements and stress-intensity factors are computed from dislocation densities. The code can be used to analyze multiple body, multiple and non-straight crack(s) as shown in the figure 2.27.

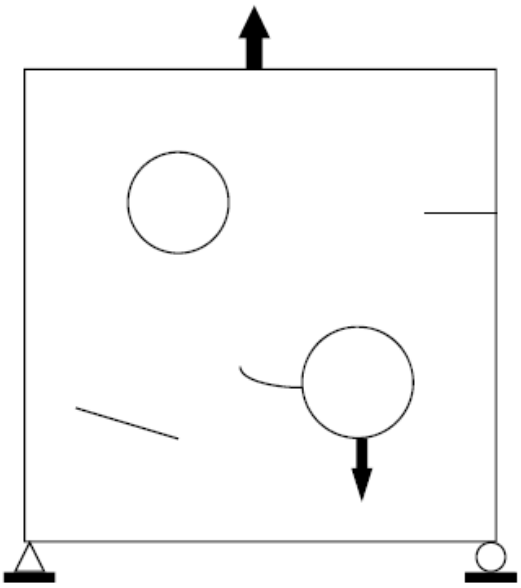

Figure 2.27. Example of multiple and non-straight crack(s) [70].

The model is created by accessing the various toolbars shown in the figure 2.28. The five steps involved in defining the model are:

1. Control Parameter [**CP**] (Title of problem, problem type)
2. Materials[**M]** (Material properties, number of boundaries, number of cracks, number point loads in the selected material)
3. Cracks and Crack segment[**Ck, Cs**] (crack parameters)
4. Boundaries and Boundary segments[**B**] (Boundary definition)
5. Points Load [**PL**] (location of the load, load in normal and tangential directions and material code)

It is then followed by Mesh generation and Analysis. Depending on the type of analysis, View Mesh, Stresses, Displacements, Stress Int. Factors, Propagate Crack and Crack (x,y) are selectively activated. Stresses and Displacement buttons are not activated if there are no boundaries and if if there are no cracks in the configuration, Stress Int. Factors, Propagate Crack and Crack (x,y) are not activated. Similarly, if the crack propagation steps are zero, Propagated Crack is not activated. More information regarding this technique can be found from the work of Chang and Mear [69,70].

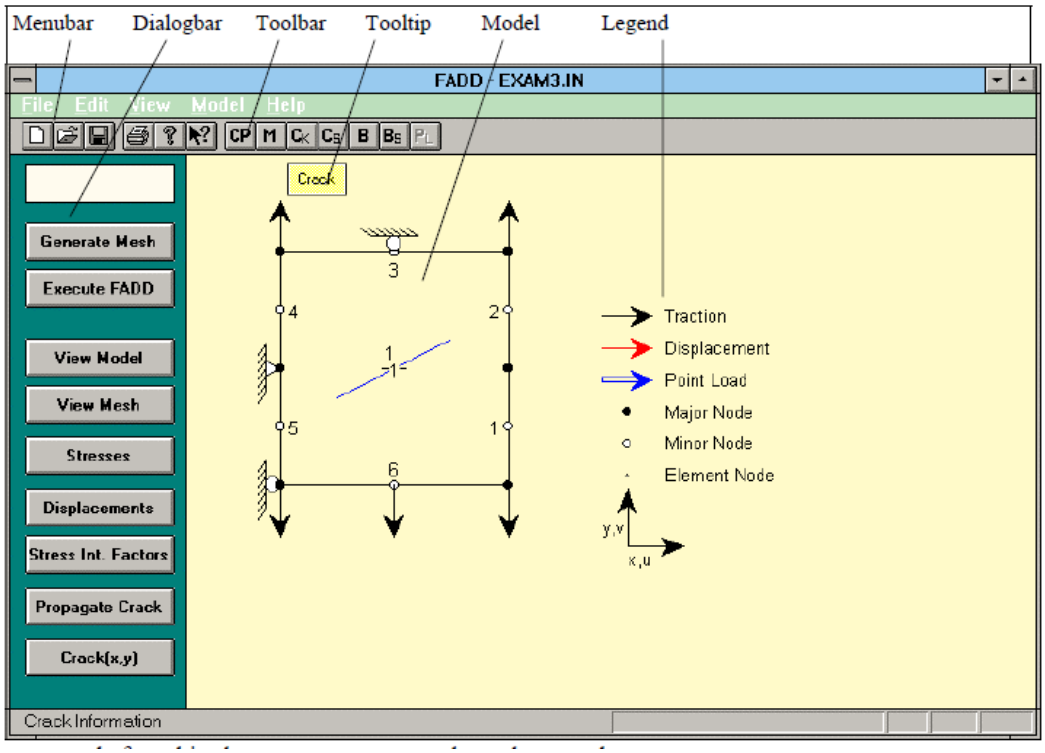

Figure 2.28. FADD2D main window screen showing the functionality of key user interface components [70].

2.10 Summary

In summary, the previous discussion indicated substantial amount of research has been conducted on C-FCG using C(T) specimens under load controlled conditions. This has translated into the current standard - ASTM E-2760-10: Standard test method for creep-fatigue crack growth testing. Research results are needed to extend the standard to other specimen geometries and loading conditions in order to understand and correlate their effects on creep-fatigue crack growth properties. Thus, there is a need to develop or modify a fracture mechanics test specimen that can be capable of reversing the specimen displacement at the load-line by maintaining LEFM conditions and, thereby, extracting more crack extension data from each tests. The

proposed double-edge-notch tension-compression specimen, DEN(T-C), overcomes this limitation. The design of a DEN(T-C) specimen suitable for use for crack growth testing under tension-compression loading is systematically explored in the Chapter 3 and also published in Narasimhachary et al., A Double Edge Notch Specimen Design for Tension-Compression Fatigue Crack Growth Testing, Engineering Fracture Mechanics, v92, 126-136 (2012).

CHAPTER 3

Development of Double-Edge-Notch-Tension-Compression Specimen

3.1 Design of DEN(T-C) Specimen

The proposed DEN(T-C) specimen is shown in figure 3.1. The specimen is similar to standard DEN specimens used previously, except the specimen is adapted for tension-compression loading**.** In addition to the rectangular member with notches on either side, the specimen contains cylindrical regions at the top and bottom that are an integral part of the specimen. The cylindrical ends are threaded and allow the user to rigidly mount the specimen to the hydraulic ram on one end and to the load cell fixtures on the other. The DEN(T-C) specimen is capable of being loaded both in tension and compression without the need for complex clevis design, thereby, allowing the user to perform tests in which the forces are both tensile and compressive during each loading cycle. The cylindrical region ensures rigidity; thereby the loads and displacements are uniformly distributed to the rectangular member of the specimen. Gentle fillet radius was chosen in all the transition regions of the specimen to reduce stress concentrations. The specimen size should be chosen with consideration to material availability, capacity of the loading system, and the size of the heating furnace in the case of high temperature testing. The thickness, B, and width, W, of the specimens are chosen based on above considerations and the remainder of the specimen dimensions are proportioned to the selected value of W. An additional consideration in choosing thickness should be avoidance of crack tunneling during crack growth testing and room for side-grooving, if necessary. The range, $4 \leq W/B \leq 2$, was chosen based on these considerations [11]. These specimen dimensions including the height were optimized as described below.

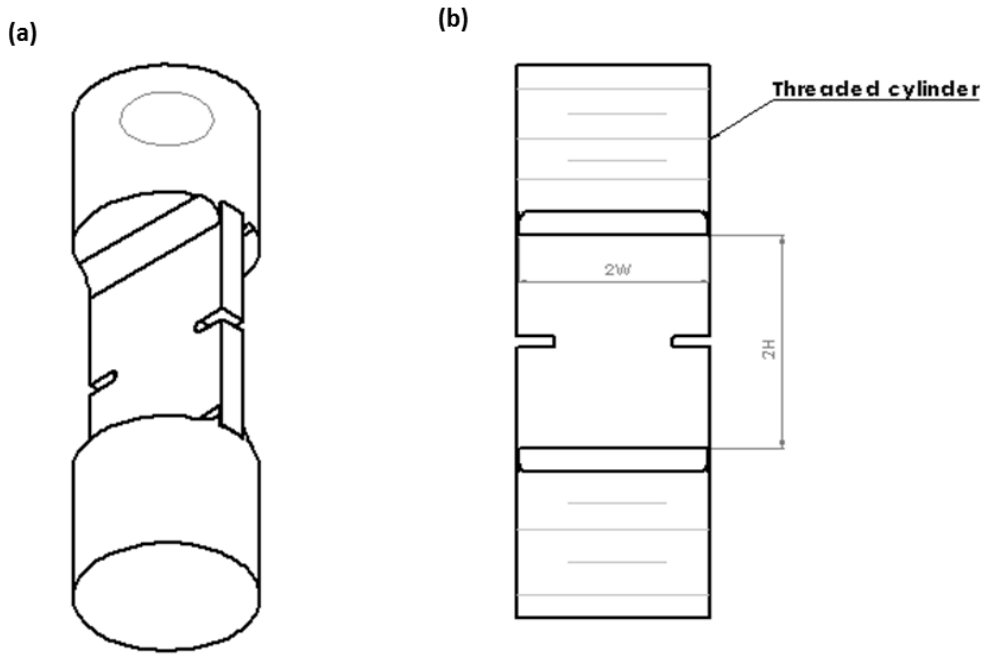

Figure 3.1. Schematic of the proposed double-edge-notch specimen (a) Isometric view (b) Front view.

3.1.1 Estimating the Height of the Specimen

Displacement controlled testing involves both tensile and compressive loads during a loading cycle; thus, specimen buckling during the compressive loading is a major concern in designing the specimen. Reducing the height of the loading train can reduce the risk of buckling. Hence, the height of the DEN(T-C) specimen is kept as short as possible in order to avoid buckling. On the other hand, the height should be large enough so that the stress-intensity factor values become very insensitive to the height. In order to optimize the height of the DEN(T-C) specimen for creep-fatigue crack growth testing, a linear elastic FEA approach was performed. Since the K-values for DEN specimens in the literature [71] are only valid only for $H/W \geq 3$, it is vital to fully understand the dependence of the stress intensity factor on the specimen height.

The aim is to choose the shortest H/W value that yields stress-intensity factor values that are not very sensitive to the height. The optimization requires reducing the specimen height to minimize the chances of buckling but also keep it such that the stress intensity factor is not highly sensitive to the H/W value.

3.1.2 Overall Geometry Optimization

Stress analysis was performed for the overall specimen geometry after fixing the H/W ratio. Stress-intensity factors and displacements values were determined for DEN(T-C) specimen by modeling the stiffer cylindrical ends using an effective height to account for the fillet regions for the chosen H/W for a wide range of crack sizes.

3.2 Numerical Analyses

FEA software package, ANSYS was used to perform two-dimensional linear elastic finite element analyses on the rectangular member of the DEN(T-C) specimen (see figure 3.2). Note that the total height, $2H$, in figure 3.1 is also referred to as the gauge length of the specimen. The stress-intensity factor [66] values were estimated using the J -integral calculation, based on the domain integral method. 2-D PLANE 183 element with plane strain element behavior was chosen for the analysis. PLANE 183 is a higher order 2-D, 8-node or 6-node element and has quadratic displacement behavior [64]. A typical mesh consists about 4000 elements was used. Finer mesh sizes were utilized around the crack tip region. The boundary element code FADD2D [70] was also used to validate and conduct stress analyses for the DEN(T-C) specimen. In order to simulate the actual loading configuration of the DEN(T-C) specimen, two set of remote boundary conditions, (1) uniform stress and (2) uniform displacement were analyzed.

Several closed-form equations for Mode I stress intensity factor for DEN specimens are available in the literature. These are derived for semi-infinite plates and are applicable only to high H/W values ($H/W > 3$) [71]. The following geometric properties for DEN(T-C) specimen was analyzed: H/W of 3, 1.5, 1.2, 1 and a/W of 0.1 to 0.7, where, a is the crack length. The width, W, was chosen as 19.05 mm (0.75 in.). The material properties selected were, elastic modulus, E = 207 GPa (30E6 psi) and Poisson's ratio, ν = 0.3. The specimen was subjected to a uniform remote tensile stress, σ. Figure 3.2 shows the schematic of the DEN finite element model. Only one quarter of the specimen was modeled, due to symmetry, as shown in the figure 3.2.

The elastic component of J, J_e, is related to the linear elastic stress intensity factor, K and the effective elastic modulus, E', (E under plane stress and $E/(1-\nu^2)$ under plane strain) and is given by

$$J_e = \frac{K^2}{E'} \tag{3.1}$$

The stress intensity factor was calculated from the equation 3.1 by averaging the J -integral values for various contours . The stress intensity factor is given by

$$K_I = \sigma\sqrt{\pi a}\, F\left({}^{a}/_{W}\right) \tag{3.2}$$

where σ represents the remote uniform applied stress, $F(a/W)$ are dimensionless K -calibration function. For $H/W \geq 3$, F is given by [71]

$$F\left(a/W\right) = \frac{1.122 - 0.561\left(a/W\right) - 0.205\left(a/W\right)^2 + 0.471\left(a/W\right)^3 - 0.190\left(a/W\right)^4}{\sqrt{1 - a/W}} \quad (3.3)$$

Since the integration domain included much more than the first ring of elements, no singular elements were used [65]. It is generally accepted that the first contour closest to the crack tip does not yield accurate results because of numerical singularities, although J -integral is ideally path independent [72]. For H/W cases analyzed, there was good convergence in the stress-intensity factor values beyond contour 1. For a/W between 0.1 and 0.7, the K_I estimates for H/W = 3 were found to be within 1.5 % of the Tada's solution ($H/W \geq 3$). The stress intensity factor values are converted to the dimensionless K - calibration function - $F(a/W)$ using equation 3.2 and plotted against crack-length to width ratios (a/W).

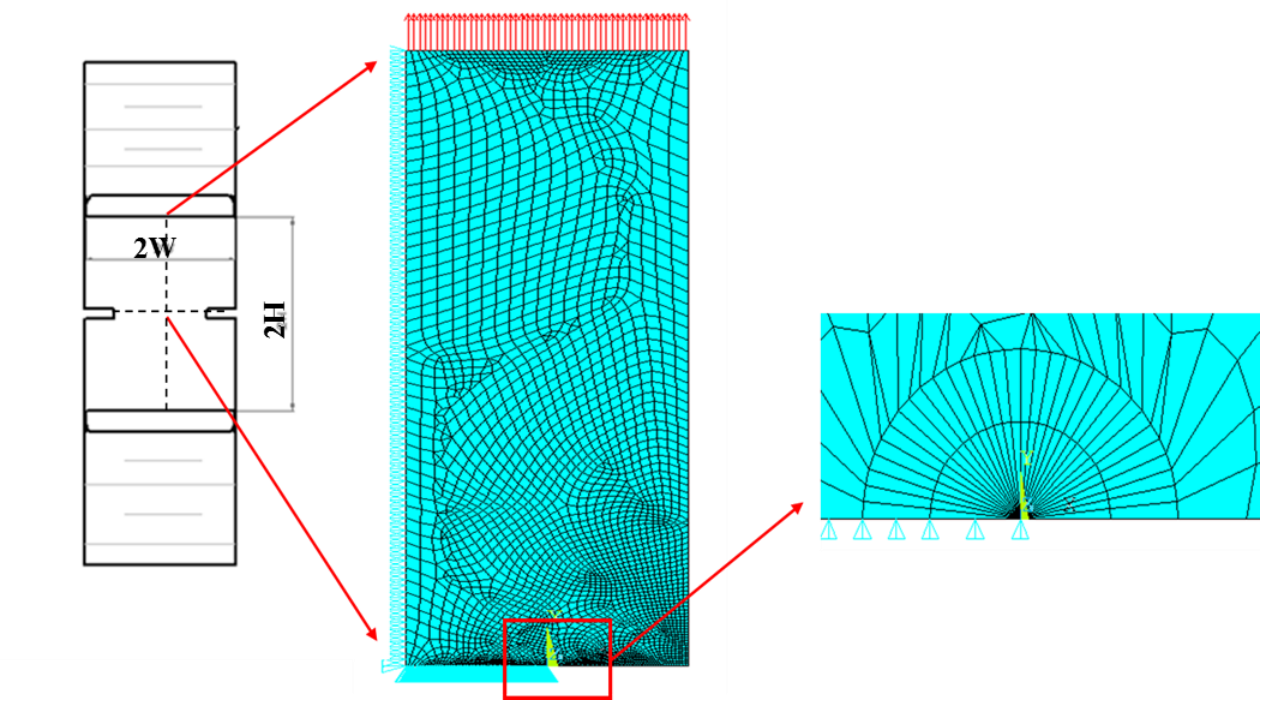

Figure 3.2. Schematic of DEN finite element model.

3.2.1 Selecting the H/W Ratio

For the various H/W ratios analyzed, it is evident from the plot of $F(a/W)$ as a function of a/W (figure 3.3) that the K values for the DEN specimen are sensitive to gage length. However, the $F(a/W)$ values between H/W = 3 and 1.2 lie within a tight range, i.e. for H/W less than 1.2, the deviation in $F(a/W)$ from equation 3.3 increased more rapidly with decreasing H/W. In comparison with Tada's solution [71] in the range $0.1 \leq a/W \leq 0.7$, the K estimates were found to be within 4.5 % for H/W = 1.2 and 12.5 % for H/W = 1. Similar trends were observed with displacement values at the crack mouth opening and the load-line location. Hence, H/W = 1.2 was chosen as being most suitable for tension-compression loading. The specimen height is also chosen keeping in mind the furnace heating limitations of maintaining uniform temperature along the specimen gage length and deflection range of extensometer. The ANSYS and FADD2D results are shown by the open symbols and closed symbols, respectively, that showed excellent agreement with one another. The results agreed within 0.09 % between ANSYS, and FADD2D.

3.2.2 Selecting the Loading Boundary Conditions

To mimic the actual loading configuration for the DEN(T-C) specimen, three different boundary conditions were analyzed:

1. Uniform tensile stress
2. Uniform displacement (v, u-free on loading boundary)
3. Uniform displacement (v, u = 0 or u-fixed on loading boundary)

Here, u and v represent the horizontal and vertical displacements, respectively.

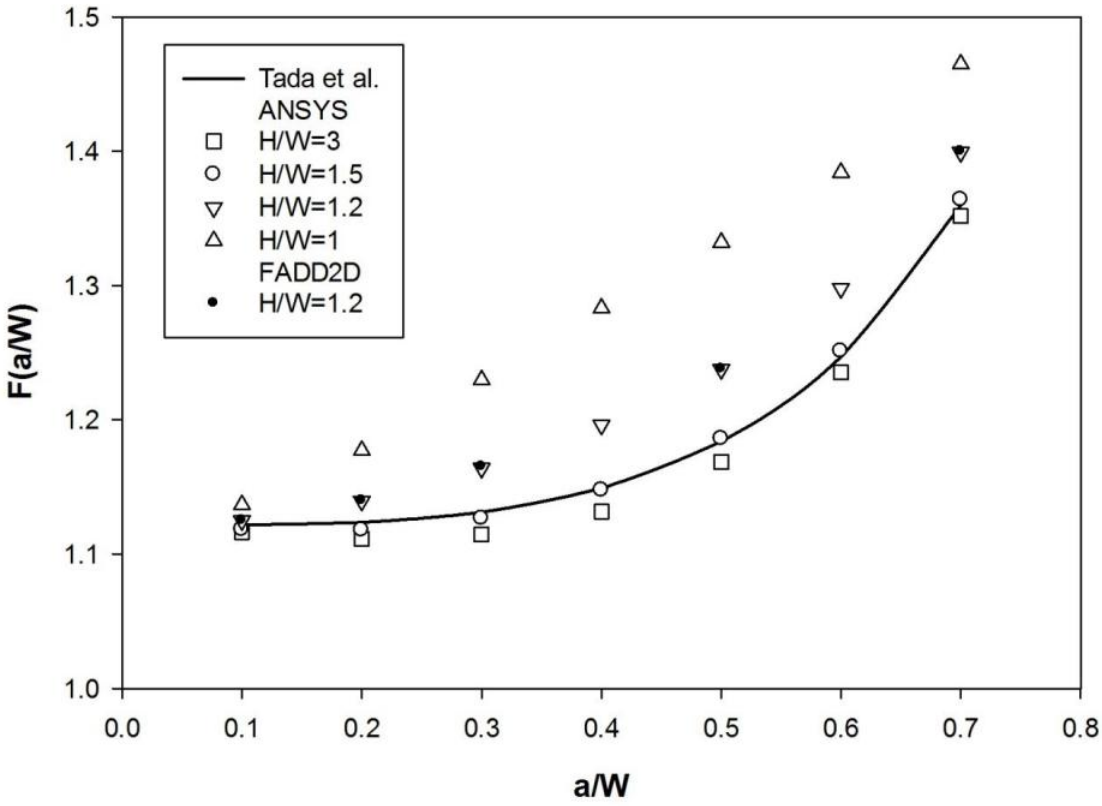

Figure 3.3. Variation in $F(a/W)$ with specimen height over a range of crack length using plane strain analyses results under remote uniform stress.

The boundary correction factor, $F(a/W)$, results from ANSYS and FADD2D, for uniform tensile stress and uniform displacement (v, u-free on loading boundary) boundary conditions for H/W = 1.2 are shown in Table 3.1. It can be noted that the results from both the finite element and boundary element codes agreed well with each other. As expected, the normal stresses, σ_{yy}, at the loading boundary showed a slight reduction above the crack location, (see figure 3.5). Note that also as expected, the boundary correction factor, $F(a/W)$, approaches 1.12 in the limit as the crack length approaches zero.

Table 3.1. Comparison of normalized stress-intensity factor, $F(a/W)$, for H/W = 1.2 using tensile stress and uniform displacement (v, u-free) boundary conditions.

BC →	Remote Uniform Tensile Stress			Remote Uniform Displacement (v,u-free)	
a/W ↓	ANSYS	FADD2D	Tada et al.	ANSYS	FADD2D
0.05	1.122	---	1.122	1.120	---
0.1	1.125	1.125	1.122	1.117	1.118
0.2	1.140	1.14	1.124	1.113	1.114
0.3	1.164	1.165	1.131	1.116	1.116
0.5	1.238	1.238	1.184	1.168	1.168
0.7	1.399	1.4	1.360	1.351	1.35

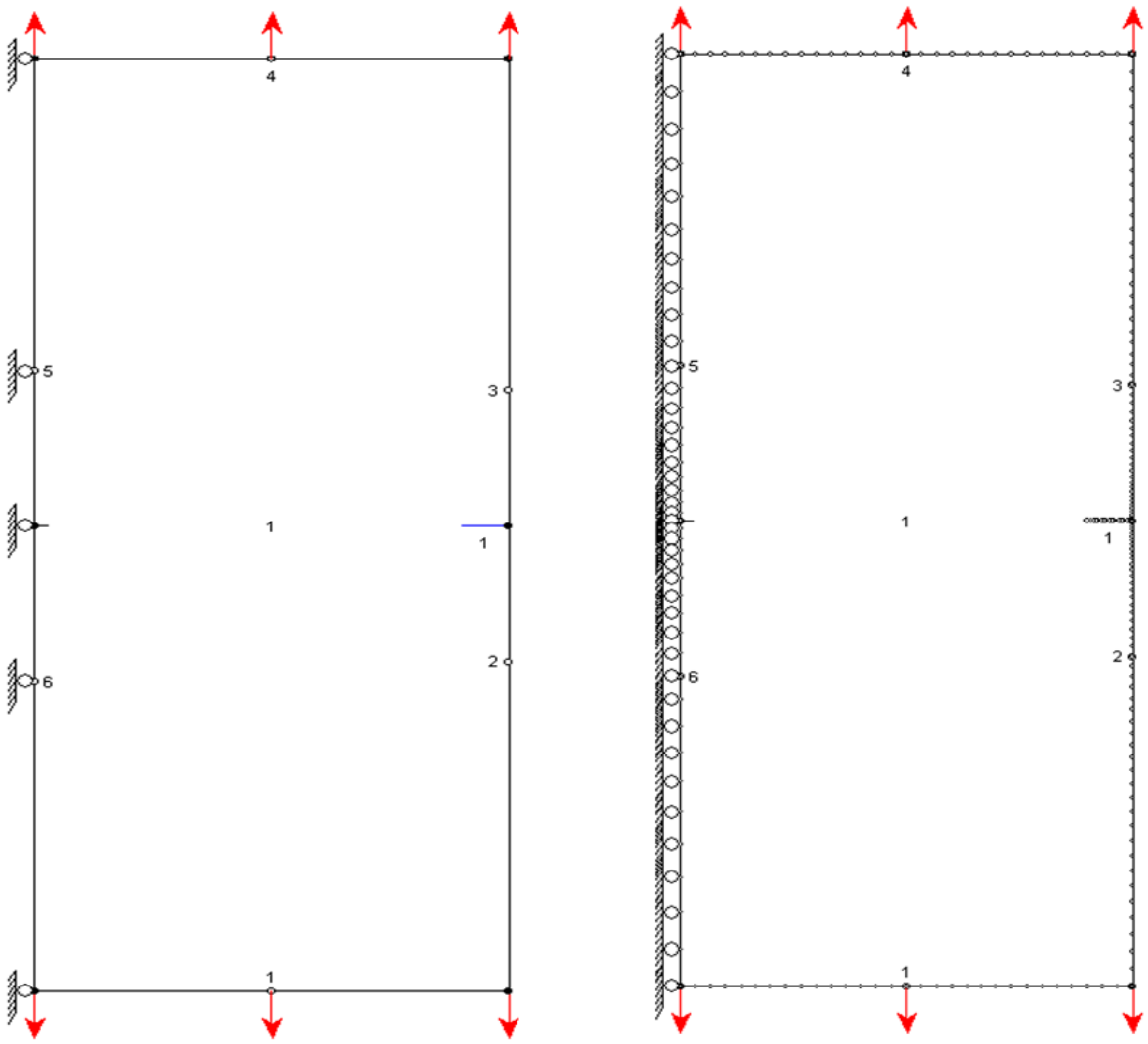

Figure 3.4. FADD2D model with crack and all boundary elements (v=1; u = free).

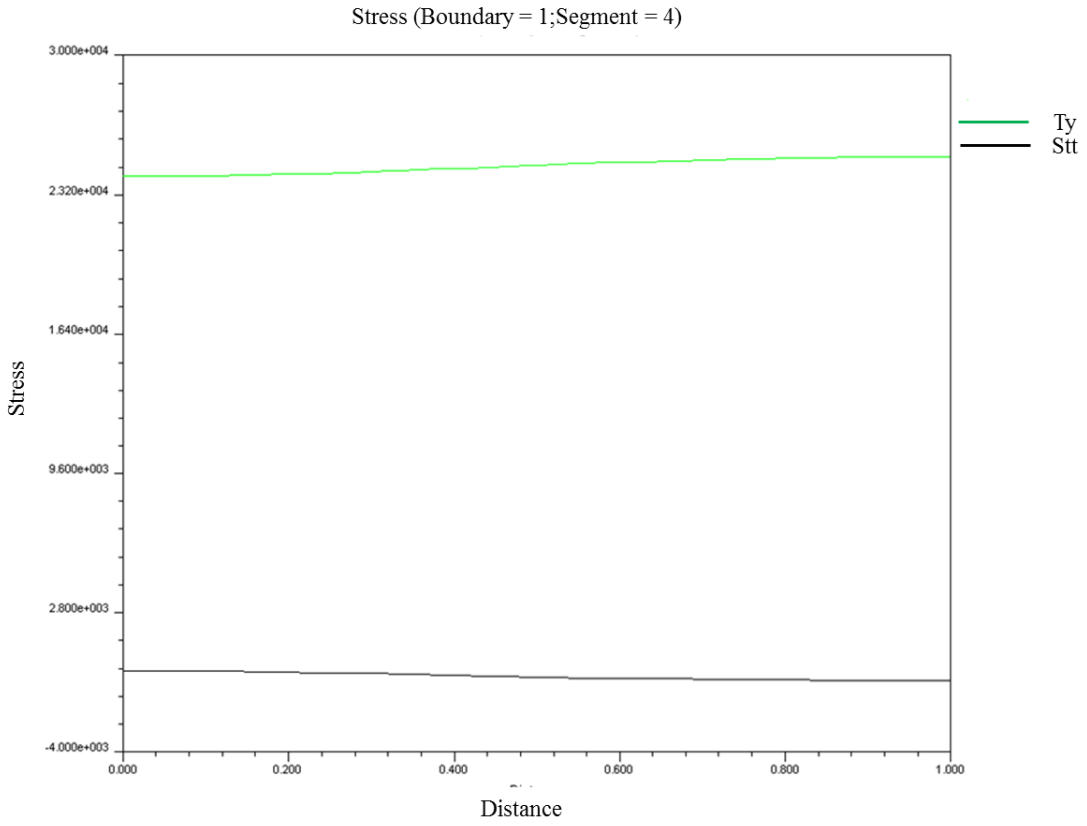

Figure 3.5. Normal and tangential stresses along Boundary 1 Segment 4 under uniform displacement (v=1; u=free).

Table 3.2 shows the boundary correction factor, $F(a/W)$, results from ANSYS and from FADD2D, respectively, for prescribed uniform displacements in the v-direction and u-fixed on loading boundary. Small differences in $F(a/W)$ values between the codes are noticed. Interestingly, both the finite-element and boundary-element codes showed that $F(a/W)$ does not go to 1.12 in the limit as the crack length approaches zero. Both the analyses showed that the normal stresses (σ_{yy}) displayed a rapid rise on the loading boundary above the crack-mouth location. The edge or corner node on the loading boundary, which is directly above the crack-mouth location showed a higher stress compared to the interior of the specimen. This variation in

stress distribution on the loading boundary influences the stress-intensity factor values. The differences in F values were as much as 10 % in comparison to the previous two boundary conditions Thus, a "singularity" exists at the outer edge of the double-edge notch-plate under v-uniform, u-fixed displacement boundary condition.

Table 3.2. Comparison of the normalized stress-intensity factor, $F(a/W)$, for H/W = 1.2 using uniform displacement (v,u-fixed) boundary conditions.

BC →	Uniform displacement (v,u-fixed)	
a/W ↓	ANSYS	FADD2D
0.05	1.010	
0.1	1.014	1.044
0.2	1.020	1.045
0.3	1.033	1.054
0.5	1.110	1.123
0.7	1.321	1.328

In order to further understand the effect of singularity, the standard DEN specimen with a crack was subjected to prescribed uniform displacement in v-direction, with u-fixed except at the edge node (see figure 3.6). Analyses were also performed without a crack subjected to prescribed uniform displacement in v-direction and u-fixed boundary condition (see figures 3.8 and 3.10). The normal stresses again showed a rapid rise on the loading boundary above the crack-mouth location for the cracked body (see figure 3.7). The normal stresses also showed a similar increase at the edge for the plate with no crack (see figure 3.9 and 3.11). Thus, the appropriate boundary condition for the DEN(T-C) specimen with larger cylindrical ends would be that of a prescribed uniform displacement in the v-direction and u-fixed on the loading boundary. The K-calibration

expressions for the new specimen design will be influenced by this assumption. The precise boundary conditions chosen for the analysis of the DEN(T-C) specimen are described in detail in section 3.3.

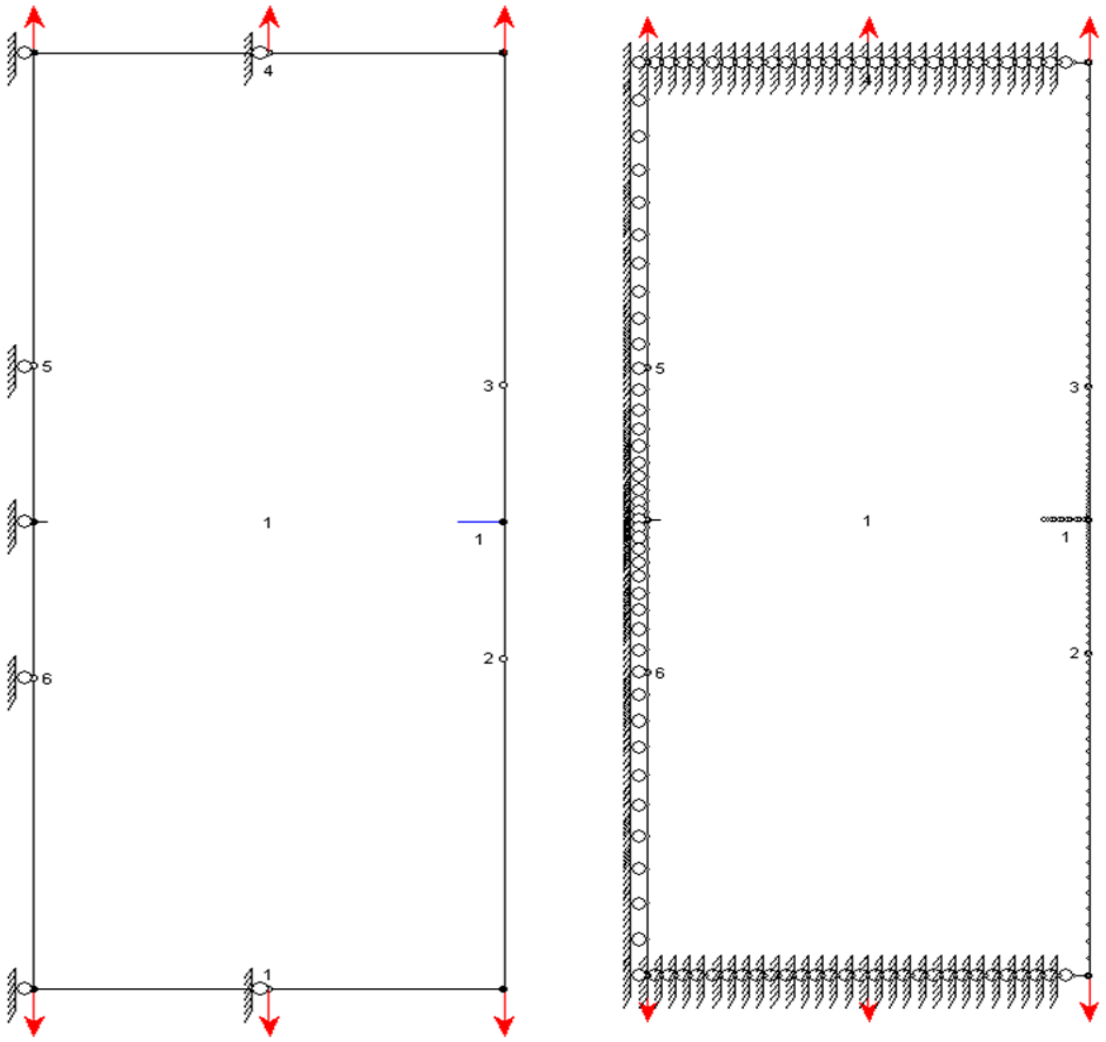

Figure 3.6. FADD2D model with crack and all boundary elements (v=1; u = 0 except edge node).

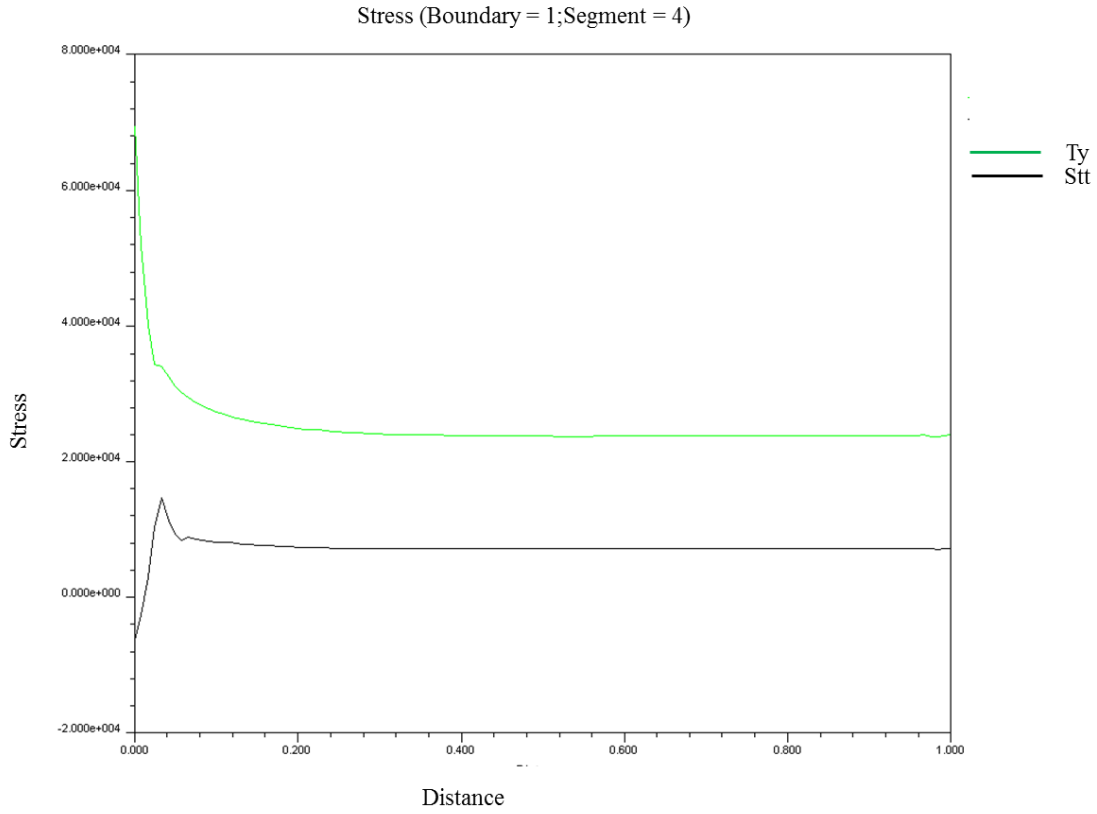

Figure 3.7. Normal and tangential stresses along Boundary 1 Segment 4 under uniform displacement (v=1; u=0 except edge node).

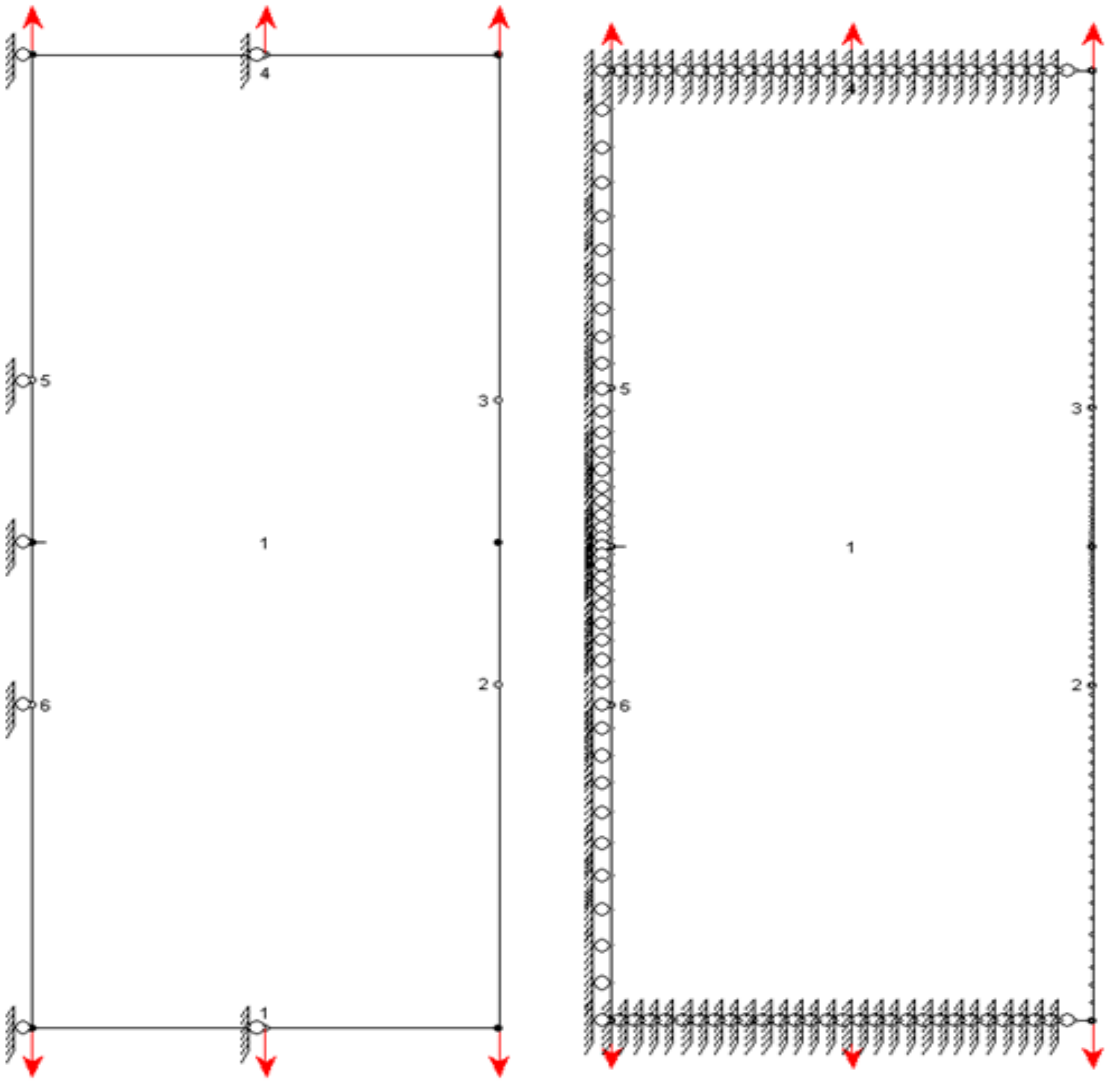

Figure 3.8. FADD2D model with no crack and all boundary elements (v=1; u = 0 fixed except edge node).

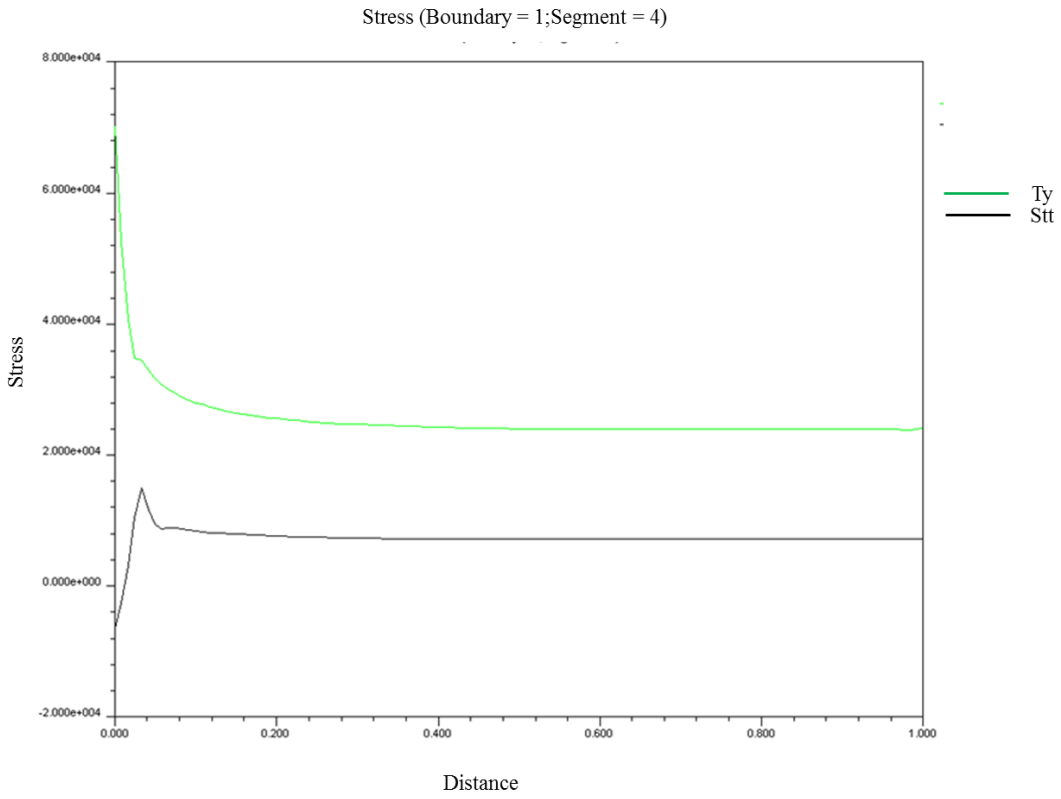

Figure 3.9. Normal and tangential stresses along Boundary 1 Segment 4 under uniform displacement (no crack,v=1; u= 0 except edge node).

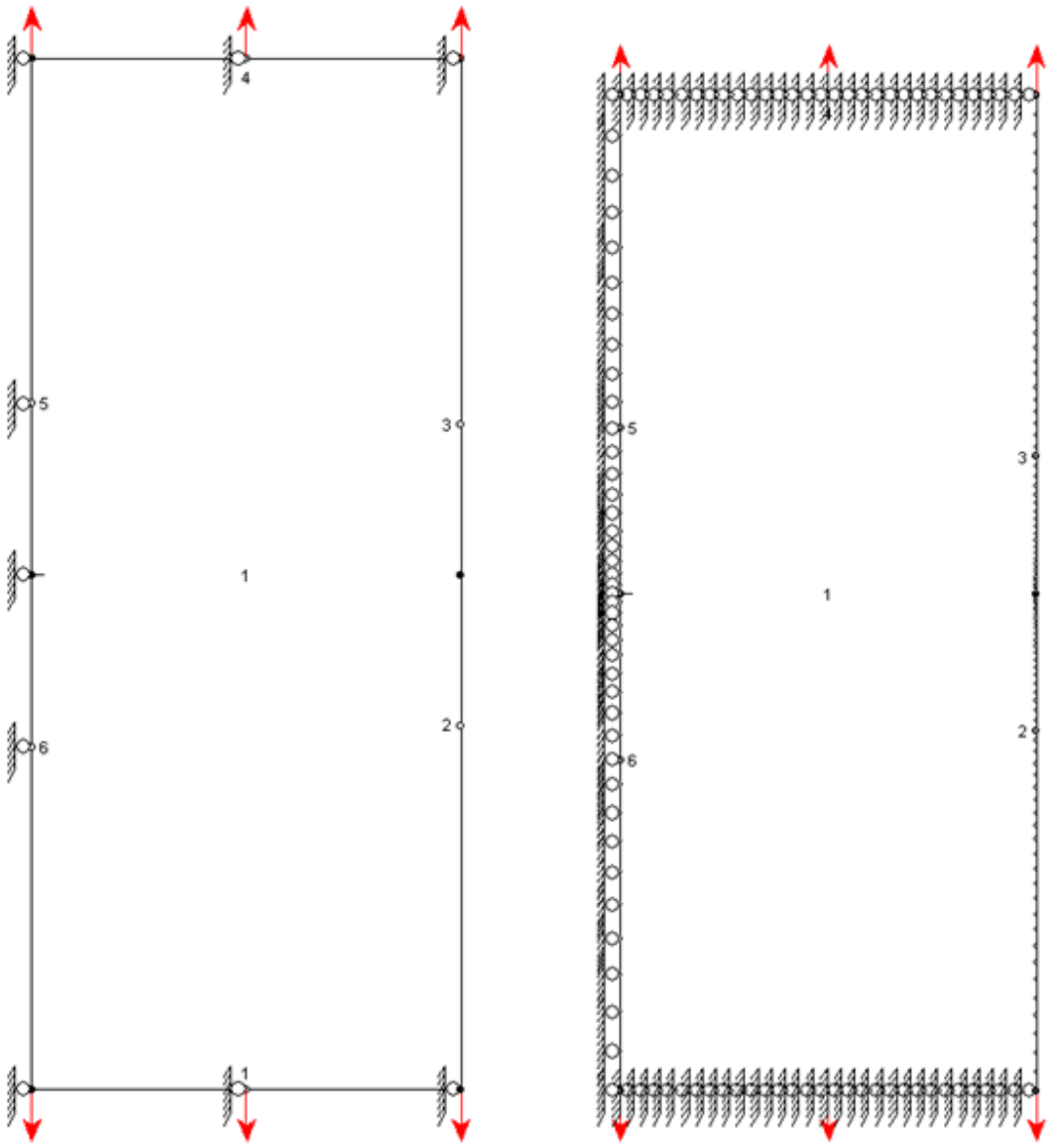

Figure 3.10. FADD2D model with no crack and all boundary elements (v=1; u = 0 all nodes).

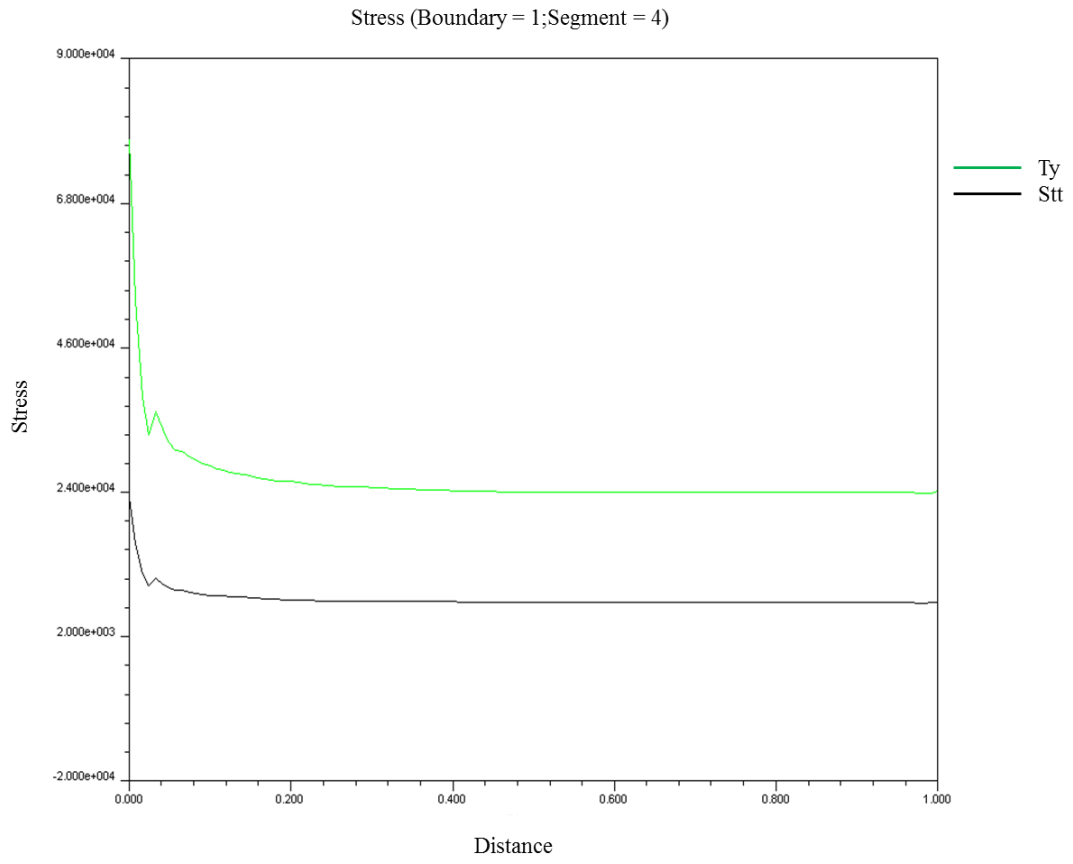

Figure 3.11. Normal and tangential stresses along Boundary 1 Segment 4 under uniform displacement (no crack, v=1; u=0 all nodes).

3.2.3 Overall Geometry Optimization

Figure 3.12 shows the dimensions of the DEN(T-C) specimen. H/W = 1.2 and a fillet radius of 5.08 mm (0.2 in.) are selected. An effective height to width ratio (h_{eff}/W) of 1.46 is chosen to account for the fillet region which extends to the bottom of the cylindrical region. The cylindrical ends measures 31.75 mm (1.25 in.) in length, of which about 24 mm (0.95 in.) is threaded. Specimen load is transmitted via shear loads that are applied through the threaded section. Hence, uniform displacement at a height of about 35.6 mm (1.4 in) from the center of the specimen (H/W = 1.87) was chosen as the location for applying the loading boundary

condition. The finite element and the boundary element models were created using multiple bodies as shown in figures 3.13 and 3.14 to accurately obtain the stress-intensity factors and the displacements for the DEN(T-C) specimen. The cylindrical ends are modeled as rectangular plates with higher young's modulus (E) to account for the heavier section/higher stiffness.

Two different Young's modulus values have been used to model the stiffness change. The mesh size in FEM was composed of about 7000 elements (PLANE 183 in ANSYS) with finer mesh around the crack tip region. Uniform displacement in Y-direction (v = constant) and fixed displacements in X-direction (u = 0) along L10 which is at the end of the threaded section was chosen to apply loading BC. The FADD2D model had boundary elements along external boundaries and the crack surfaces as shown in the figure 3.15. Boundary 1 and 3 (upper and lower regions) had 48 elements each, while boundary 2 (containing the two equal length cracks) had 112. The two cracks had from 4 to 36 elements each for a/W values ranging from 0.1 to 0.9.

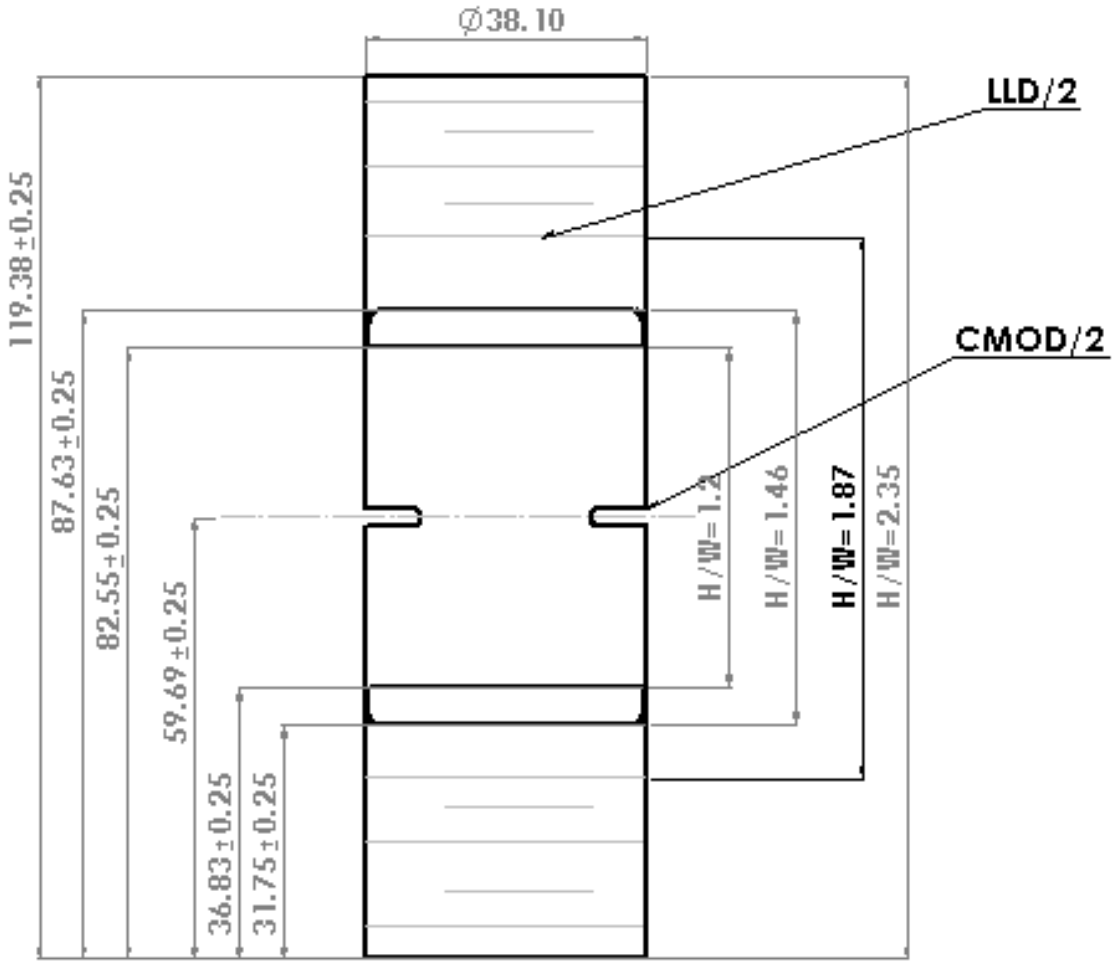

Figure 3.12. Schematic showing the various dimensions of DEN(T-C) specimen configuration.

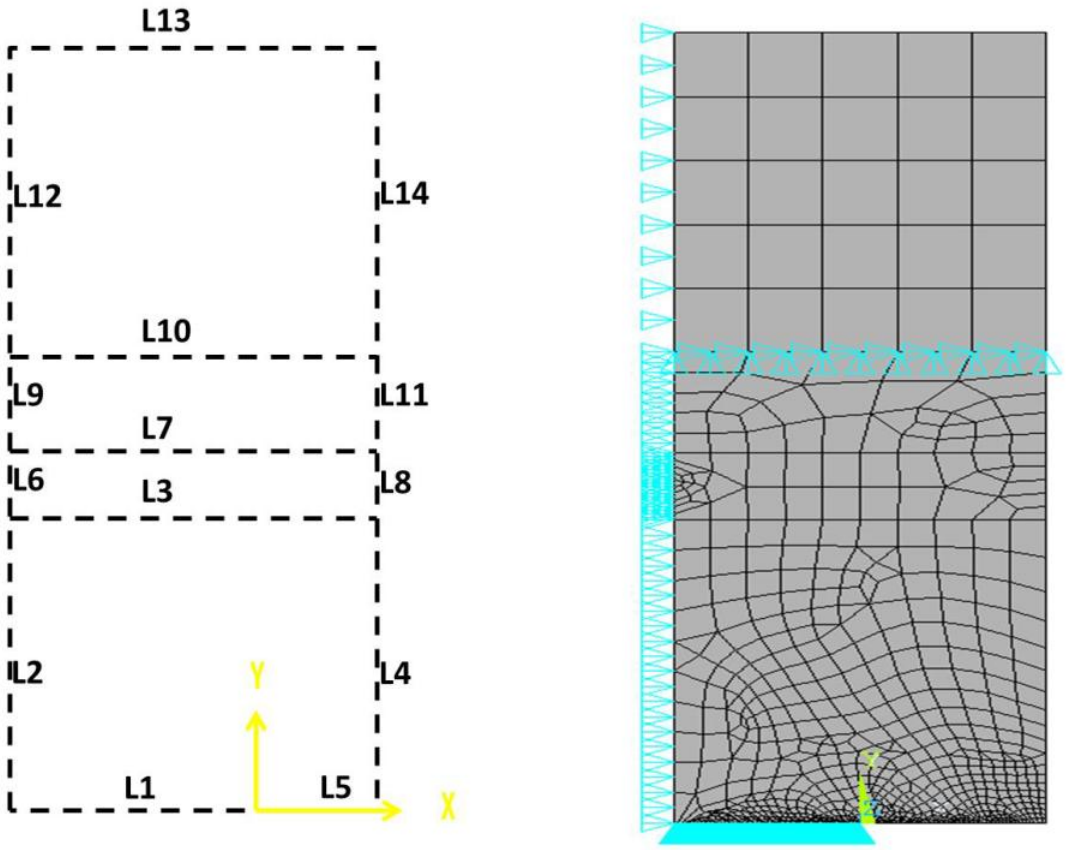

Figure 3.13. The ANSYS model of DEN(T-C) specimen. Shown here is a one-quarter rectangular plate with crack. The cracktip is located at the origin with Line 5(L5) representing the length of the crack. L3 represents H/W = 1.2, L7 represents H/W = 1.46, L10 represents H/W = 1.87 and L13 represents the end of the cylindrical section, H/W = 2.35. The section of the top plate between L10 and L13 has no impact on the stress-intensity factors.

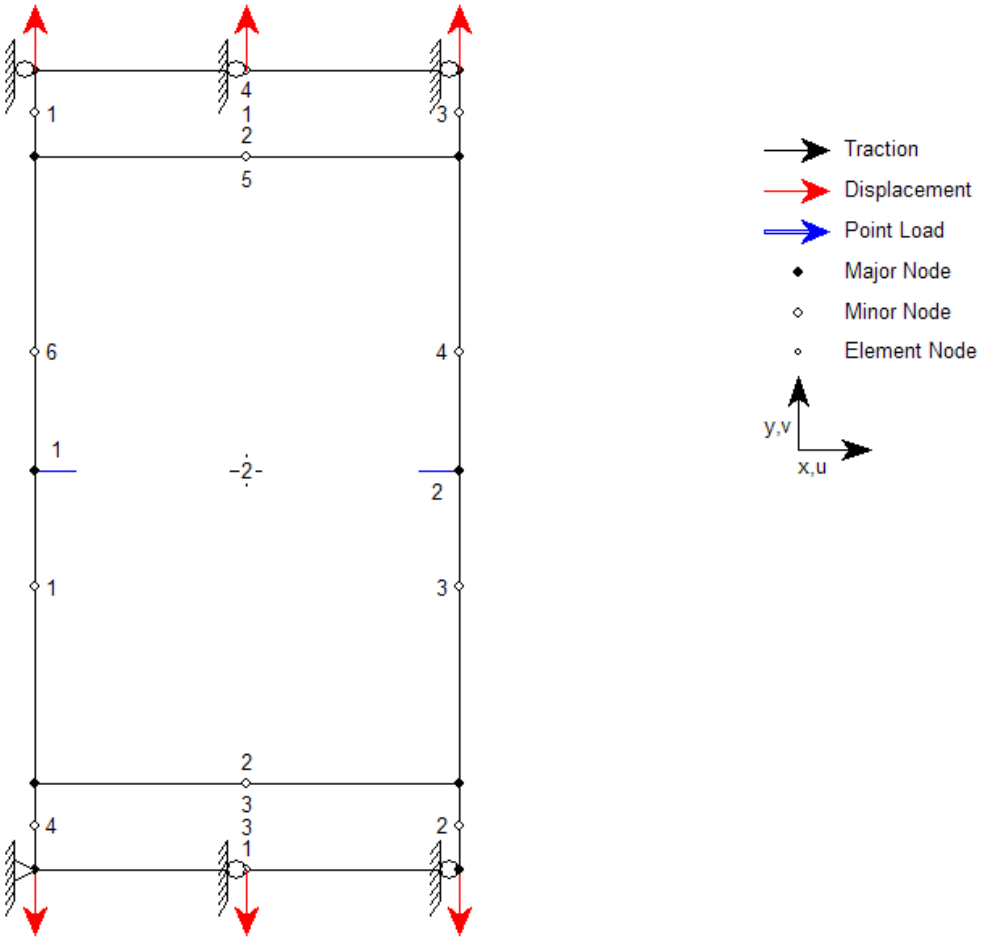

Figure 3.14. FADD2D model of double-edge-notch tension-tompression tpecimen with region 2 at H/W = 1.46 and the threaded region (1, 3) at H/W = 1.87. The applied loading was uniform displacement in y-direction (v = constant) and fixed displacements in x-direction (u = 0) at the edge of the threaded section.

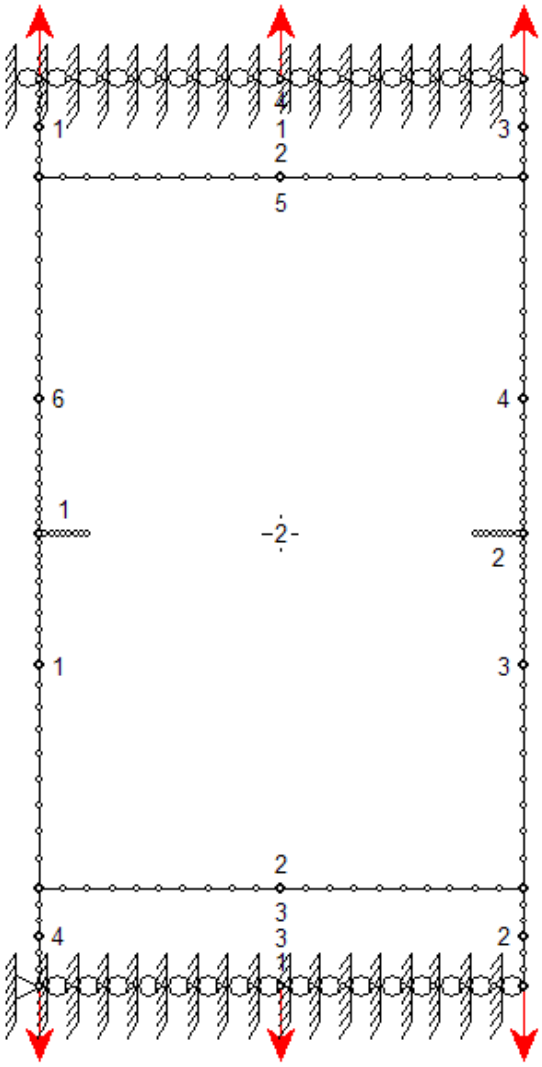

Figure 3.15. FADD2D model showing boundary elements along external boundaries and the crack surfaces. Boundary 1 and 3 (upper and lower regions) had 48 elements each, while boundary 2 (containing the two equal length cracks) had 112. The two cracks had from 4 to 36 elements each for a/W ranging from 0.1 to 0.9.

3.3 Results and Discussions

3.3.1 K - Calibration Expressions

The normalized stress-intensity factor results, $F(a/W)$, for the DEN(T-C) specimen from the finite element, boundary element analysis and the Tada et al. equation [71] are compared in table 3.3. The difference between FEA and BEA results was within 1%, while the difference between FEA result and Tada et al. equation was within 5 %. One can again note that the $F(a/W)$ does not go approach 1.12 in the limit as the crack length goes to zero. The addition, of the top plate with a higher elastic modulus does soften the singularity at the edge node directly above the crack location, but the normal stresses still show a rise on the loading boundary above the crack location. The key difference between Tada et al.'s solution and the FEA solution of DEN(T-C) specimen are primarily due to the stiffer plate of DEN(T-C) specimen and the loading boundary conditions employed and some also due to a shorter specimen gage length here that are more representative of the specimen geometry and how the loads will be applied during testing.

Stress analyses of the DEN(T-C) specimen subjected to uniform displacement for various crack sizes were performed to obtain the *K*-calibration expression, $F(a/W)$. The parameter $(1-a/W)^2$ was used in normalization as it enables a fit to be carried out over a wide range of a/W values. The Tada et al. solution [71] for DEN specimen for Mode I loading has the same normalizing parameter . The normalized boundary correction factor, $F\left(\frac{a}{W}\right).(1-a/W)^2$, is plotted against a/W in figure 3.16. The diamond symbols are the results from FEA and dashed curves are the fitted values from regression as described below.

Table 3.3. Comparison of normalized stress-intensity factor, $F(a/W)$, for DEN(T-C) specimen.

a/W	F_{BEA}	F_{FEA}	Tada et al.[71]
0.1	1.080	1.068	1.122
0.2	1.080	1.068	1.124
0.3	1.087	1.076	1.131
0.4	1.108	1.099	1.149
0.5	1.149	1.142	1.184
0.6	1.221	1.216	1.247
0.7	1.343	1.339	1.360
0.8	1.568	1.564	1.577
0.9	2.113	2.109	2.118

The SOLVER© software routine available as an additional plug-in in Microsoft Excel, was utilized to perform regression analysis of the available FEA data. The data are fitted by minimizing the squares of errors. Figure 3.16 demonstrates the fitting efficiency of the polynomial equation for DEN(T-C) specimen by comparing predicted and the FEA data. The prediction correlates well with the analytical data.

The following equation represents normalized stress-intensity factor, $F(a/W)$, for $0.05 \leq a/W \leq 0.9$ and has an accuracy of fit that is better than 0.07 % for our DEN(T-C) specimen:

$$F\left(a/W\right) = \frac{1.072 - 0.6033\left(a/W\right) + 0.0019\left(a/W\right)^2 + 0.4294\left(a/W\right)^3 - 0.27\left(a/W\right)^4}{\sqrt{1 - a/W}} \quad (3.4)$$

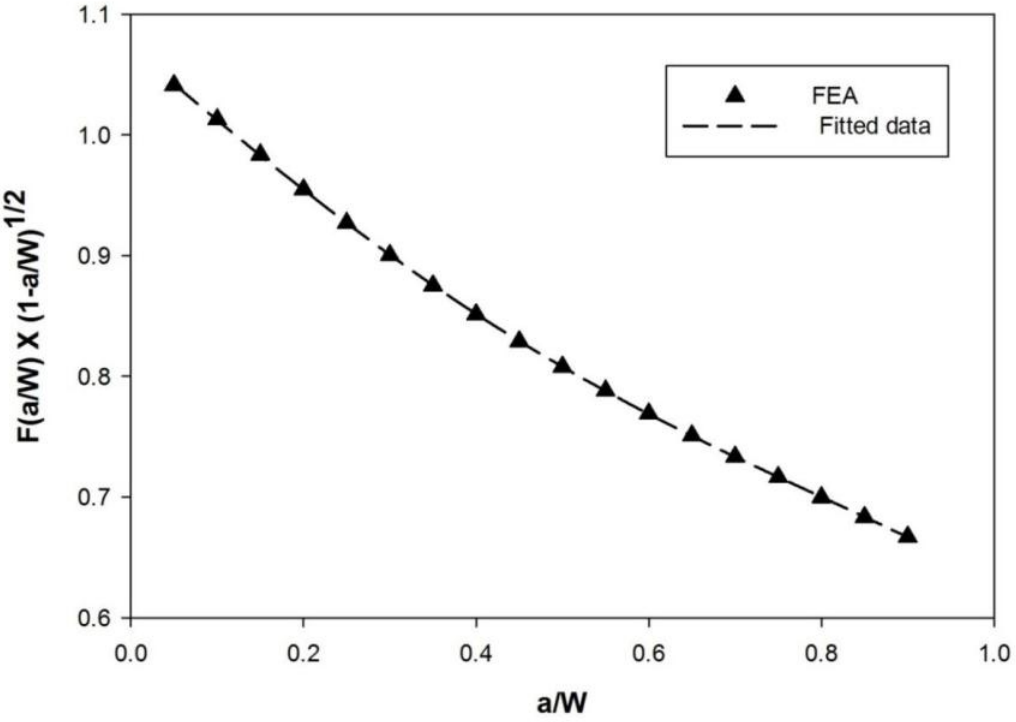

Figure 3.16. Comparison of fitted normalized boundary correction factor with the FEA data used to generate the fitted constants.

3.3.2 CMOD and LLD Expressions

The crack mouth and load line displacements are extracted from the relevant location on the DEN(T-C) specimen as shown the figure 3.12. The CMOD is given by the following equation [71]:

$$\delta_e = \frac{4\sigma a}{E'} V_1(a/W) \tag{3.5}$$

where $V_1(a/W)$ has the following form:

$$V_1(a/W) = \frac{1}{\left(\frac{\pi a}{2W}\right)}\left(C_0\left(\sin\frac{\pi a}{2W}\right) + C_1\left(\sin\frac{\pi a}{2W}\right)^3 + C_2\left(\sin\frac{\pi a}{2W}\right)^5 + cosh^{-1}\left(\sec\frac{\pi a}{2W}\right)\right) \tag{3.6}$$

The normalized CMOD function, $V_1(a/W)$ for the DEN(T-C) specimen is obtained by rearranging terms in equation 3.6 by fitting the FEA data to obtain the three regression coefficients. Figure 3.17 demonstrates the fitting efficiency of the equation for DEN(T-C) specimen by comparing predicted and obtained FEA data. Once again, the prediction matches well with the analytical data. Equation 3.7 is valid for $0.1 \leq a/W \leq 0.9$ and has an accuracy of fit better than 1 %.

$$V_1(a/W) = \frac{1}{\left(\frac{\pi a}{2W}\right)}\left(0.3783\left(\sin\frac{\pi a}{2W}\right) - 0.2108\left(\sin\frac{\pi a}{2W}\right)^3 + 0.078\left(\sin\frac{\pi a}{2W}\right)^5 + cosh^{-1}\left(\sec\frac{\pi a}{2W}\right)\right) \tag{3.7}$$

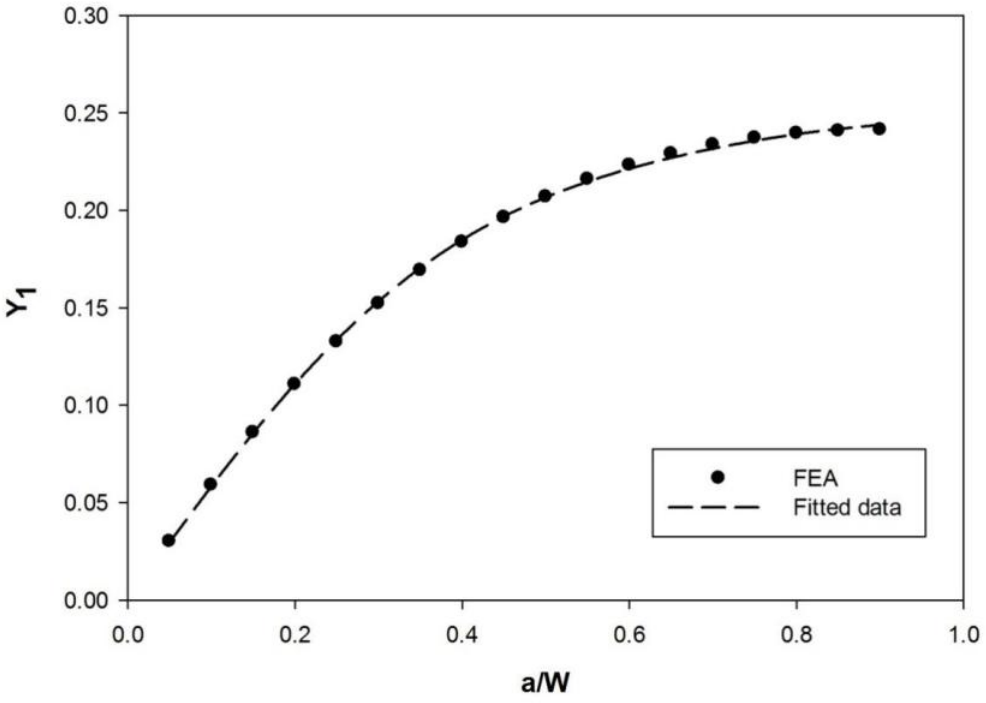

Figure 3.17. Comparison of fitted normalized CMOD function with the FEA data, Where $\mathbf{Y_1} = C_0\left(\sin\frac{\pi a}{2W}\right) + C_1\left(\sin\frac{\pi a}{2W}\right)^3 + C_2\left(\sin\frac{\pi a}{2W}\right)^5$.

The total load-line displacement is given by the following equation [71]

$$\Delta_{total} = \Delta_{crack} + \Delta_{no\ crack} \tag{3.8}$$

Where Δ_{total} = LLD , $\Delta_{crack} = \frac{4\sigma a}{E'} V_2(a/W)$ and $\Delta_{no\ crack} = \frac{\sigma}{E'} 2H$ (3.9)

where $V_2(a/W)$ has the following form

$$V_2(a/W) = \frac{1}{\left(\frac{\pi a}{2W}\right)}\left(C_0 + C_1\left(\cos\frac{\pi a}{2W}\right)^4 + C_2\left(\cos\frac{\pi a}{2W}\right)^8 + ln\left(\sec\frac{\pi a}{2W}\right)\right) \tag{3.10}$$

Since the loading boundary is under uniform displacement, $V_2(a/W)$ is obtained from FEA using the following procedure. Under uniform displacement, the total load-line displacement is constant (C) . The reference stress (σ_0) was taken from the finite element model of DEN(T-C) specimen with no crack. σ is the stress corresponding to each crack size. Thus equation 3.8 is normalized as

$$C = \Delta_{crack} + \frac{\sigma}{\sigma_0} C \tag{3.11}$$

Thus, $V_2(a/W)$

$$V_2(a/W) = \frac{C\left(1 - \frac{\sigma}{\sigma_0}\right)E'}{4\sigma a} \tag{3.12}$$

$V_2(a/W)$ for the DEN(T-C) specimen is obtained by rearranging terms in equation 3.10, by fitting the FEA data to obtain the three regression coefficients. Figure 3.18 demonstrates the fitting efficiency of the equation for DEN(T-C) specimen. Alternate forms of the fit were attempted since some differences occurred for very deep crack size (a/W > 0.8) between the

predicted data and the FEA data, thus. The following formula for $V_2(a/W)$ is derived from regression analysis and shown to represent the numerical data very well. The equation is valid for $0.1 \le a/W \le 0.8$ and has an accuracy of fit better than 2 %.

$$V_2(a/W) = \frac{1}{\left(\frac{\pi a}{2W}\right)}\left(0.027 - 0.0201\left(\cos\frac{\pi a}{2W}\right)^4 - 0.00687\left(\cos\frac{\pi a}{2W}\right)^8 + ln\left(\sec\frac{\pi a}{2W}\right)\right) \qquad (3.13)$$

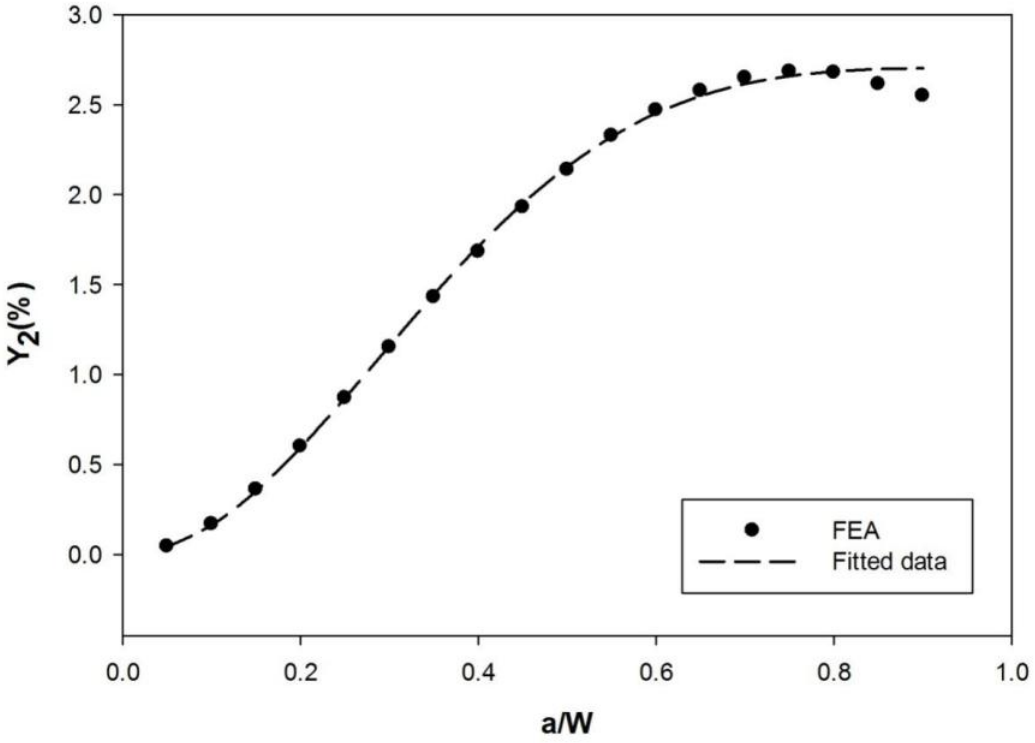

Figure 3.18. Comparison of fitted normalized LLD function with the FEA data, where $\mathbf{Y_2} = \boldsymbol{C_0} + \boldsymbol{C_1}\left(\mathbf{cos}\frac{\boldsymbol{\pi a}}{\mathbf{2W}}\right)^{\mathbf{4}} + \boldsymbol{C_2}\left(\mathbf{cos}\frac{\boldsymbol{\pi a}}{\mathbf{2W}}\right)^{\mathbf{8}}$.

A polynomial fit for $V_1(a/W)$ and $V_2(a/W)$ is also derived from regression analysis and shown to represent the numerical data very well (figure 3.19). The following formula for $V_1(a/W)$ is valid for $0.1 \le a/W \le 0.85$ and has an accuracy of fit better than 1 %:

$$V_1(a/W) = 1.411 - 0.5624\left(a/W\right) + 2.466\left(a/W\right)^2 - 4.873\left(a/W\right)^3 + 3.965\left(a/W\right)^4 \qquad (3.14)$$

Similarly, the following formula for $V_2(a/W)$ is valid for $0.1 \leq a/W \leq 0.85$ and has an accuracy of fit better than 1.7 %

$$V_2(a/W) = 0.0044 + 0.768\left(a/W\right) + 0.967\left(a/W\right)^2 - 2.671\left(a/W\right)^3 + 2.691\left(a/W\right)^4 \quad (3.15)$$

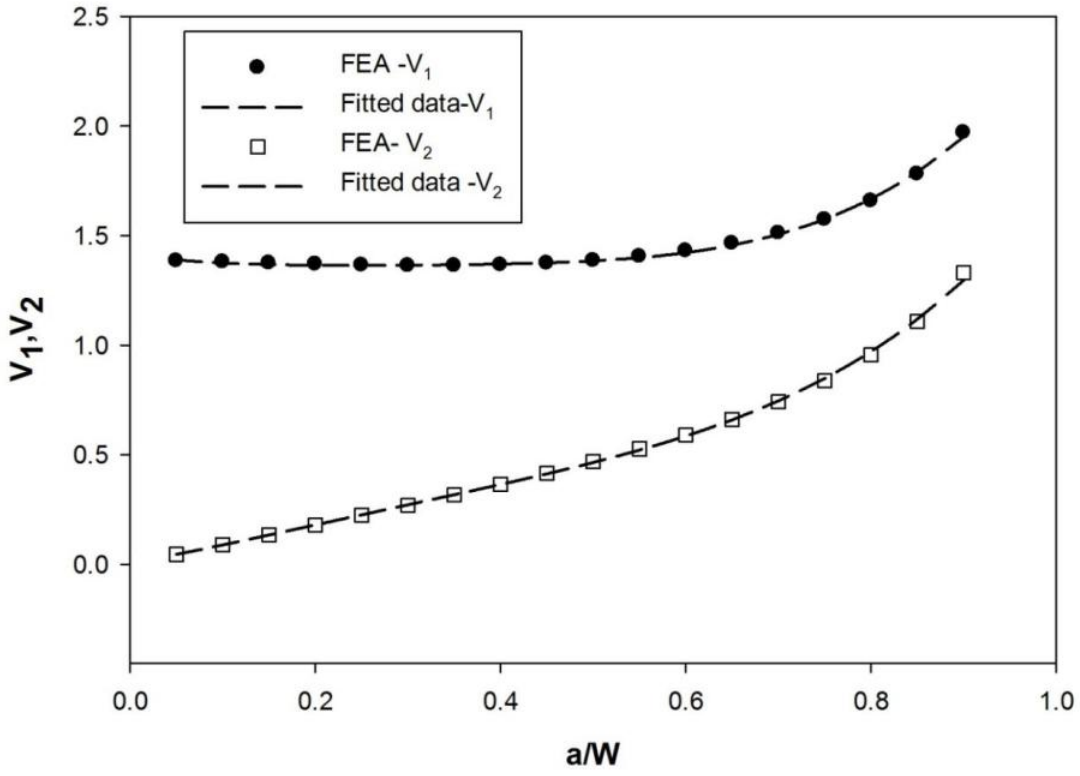

Figure 3.19. Comparison of fitted normalized LLD and CMOD function with the FEA data using polynomial functions.

3.3.3 Compliance Expressions

Since the purpose of the specimen is for use in crack growth testing, expressions are also developed for crack size as a function of specimen compliance and compliance as a function of crack size. Compliance technique has been used for many years to monitor subcritical crack

growth in fracture mechanics and fatigue crack growth testing [73,74]. This technique can be very useful for a specimen like DEN(T-C) because of the complexities involved with the other methods like potential drop. Potential drop method requires a total of 6 independent leads (4 output voltage leads and 2 current leads) to monitor the crack length. Environmental chambers and other process related issues are also to be considered. For example, current leakage into the crack solution could alter the electrochemical reaction in corrosion-fatigue tests [75]. But on the other hand, potential drop provides us with independent measurement of the crack sizes.

3.3.3.1 Compliance as a Function of Crack Length

Elastic deflections were calculated at the load line [H/W = 1.87] as shown previously in the figure 3.12 for various crack lengths. The normalized compliance (BEV/P) in terms of crack length were developed in the range for $0.1 \leq a/W \leq 0.9$. The parameter $1-(a/W)^2$ was used in normalization to enable a fit to be carried out over a wide range of a/W values. The open square symbols are the results from FEA and dashed curves are the fitted values in the Figure 3.20. The figure demonstrates the fitting efficiency of the polynomial equation for DEN(T-C) specimen by comparing predicted and the FEA data. The prediction seems to correlate well with the analytical data. The following equation represents normalized compliance in terms of crack length in the range $0.1 \leq a/W \leq 0.9$ and has an accuracy of fit that is better than 0.3 % for our DEN(T-C) specimen:

$$BEV/P = \left(1.477 + 0.55\left(\frac{a}{W}\right) - 2.24\left(\frac{a}{W}\right)^2 + 4.28\left(\frac{a}{W}\right)^3 - 3.86\left(\frac{a}{W}\right)^4\right) \Big/ 1-\left(\frac{a}{W}\right)^2 \quad (3.16)$$

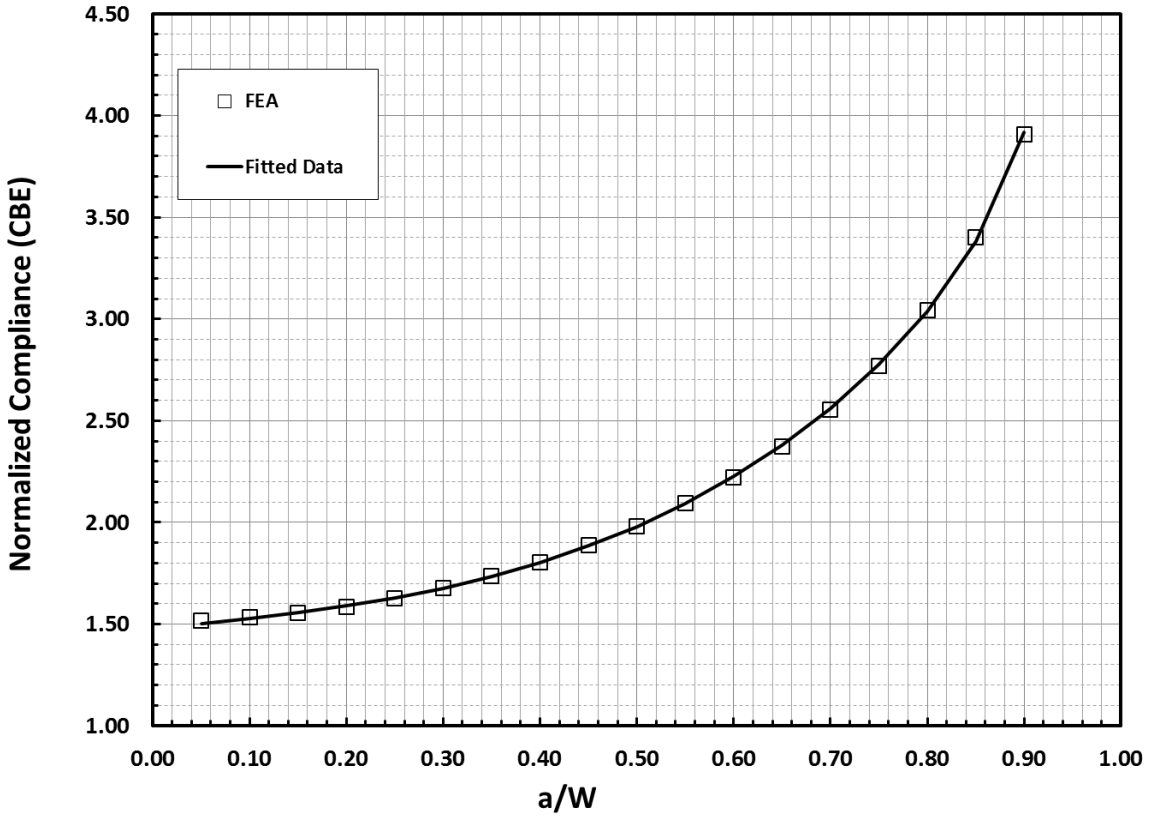

Figure 3.20. Normalized compliance results from the FEA for DEN(T-C) specimens.

3.3.3.2 Crack Length as a Function of Compliance

The analytically predicted compliance results (figure 3.20) have been refit using the same form used for C(T) specimen available in the ASTM E-647 standard [12]. This standard form allows the user to simply input the coefficient's in the crack growth measuring software. The functional form of the relationship is given by

$$\frac{a}{W} = C_0 + C_1(U_x) + C_2(U_x)^2 + C_3(U_x)^3 + C_4(U_x)^4 + C_5(U_x)^5 \tag{3.17}$$

where $$U_x = \frac{1}{\left(\frac{BEV}{P}\right)^{1/2}+1}$$

The C_0, $C_1 \ldots C_5$ are regression coefficients for the load-line location given by:

C_0 = 8.90, C_1 = -36.20, C_2 = 11.77, C_3 = 0.02, C_4= 520.89, C_5 = -881.3

Equation 3.17 is valid in the range $0.2 \leq a/W \leq 0.85$. The a/W values predicted from the polynomial equations are within ±0.005 of the actual values. Figure 3.21 shows the percent difference in predicted a/W values from the analyses. The results show that the current equation is within 2 % for a/W ratios less than 0.85.

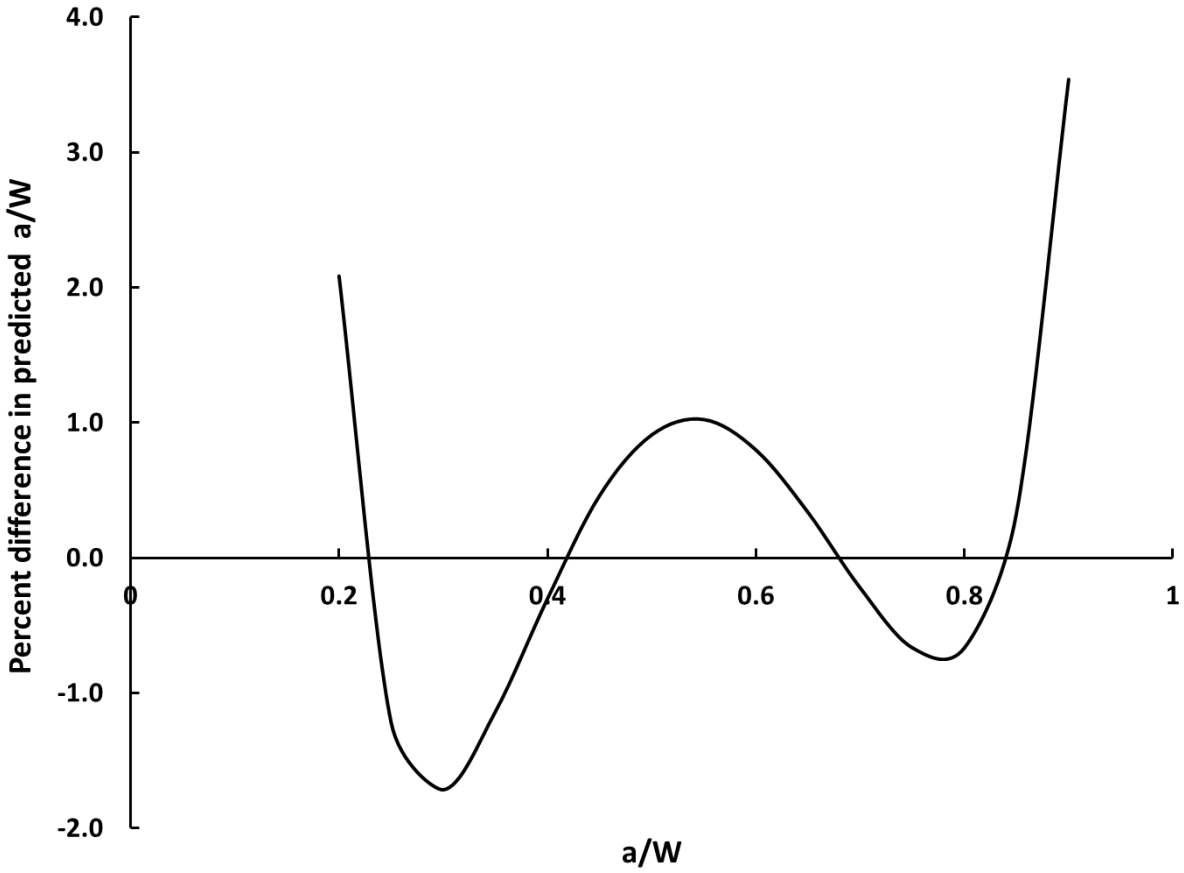

Figure 3.21. Percent difference in crack-length difference determination from the current equation 3.17.

Chapter 4

Expressions for Crack Growth Analysis

A phenomenological approach is needed to analyze crack growth data, such that the data can be used as material properties to predict crack growth in power plant components. Since a number of equations and expressions are needed to analyze crack growth data under fatigue and creep-fatigue conditions, it is prudent to summarize the expressions for C(T) and DEN(T-C) specimens respectively.

4.1 Experimental Equations for *C*(T) Specimens

4.1.1. Stress-Intensity Factor Equations

The stress-intensity factor K_I is strictly valid only for linear elastic behavior, but it can be used as an approximation if the plastic zone size and/or creep deformation zone near the crack tip is limited. For a side-grooved C(T) specimen subjected to mode I loading, the stress-intensity parameter is given by [8]

$$K = \frac{P}{(BB_N)^{1/2} W^{1/2}} F(a/W) \tag{4.1}$$

where, $F(a/W)$, is given by

$$F(a/W) = \left[\frac{2 + a/W}{\left(1 - a/W^{3/2}\right)}\right]\left(0.886 + 4.64(a/W) - 13.32(a/W)^2 + 14.72(a/W)^3 - 5.6(a/W)^4\right) \tag{4.2}$$

The variation in the stress-intensity factor in a cycle is given by the stress-intensity factor range:

$$\Delta K = K_{max} - K_{min} \tag{4.3}$$

The load ratio,R, is related to stress-intensity factor range by :

$$\Delta K = (1 - R)K_{max} \; for \; R \geq 0 \tag{4.4}$$

$$\Delta K = K_{max} \; for \; R \leq 0 \tag{4.5}$$

4.1.2 Determination of Delta-J:

The ΔJ integral is used to describe the fatigue crack growth behavior under gross plasticity conditions typically experienced at elevated temperatures [25]. The total value of ΔJ is given by:

$$\Delta J = \Delta J_e + \Delta J_p \tag{4.6}$$

where ΔJ_e is given by:

$$\Delta J_e = {\Delta K^2}/{E'} \tag{4.7}$$

and ΔJ_p is given by:

$$\Delta J_p = \frac{\Delta A_p}{B(W - a)} \eta \tag{4.8}$$

where ΔA_p is the area under the load versus the plastic part of the load-displacement diagram.

Eta (η) is the plastic correction factor given by:

(4.9)

$$\eta = \left(2 + 0.522 \left(1 - {a}/{W}\right)\right)$$

4.1.3 Determination of $(C_t)_{avg}$ Parameter:

The average value of the (C_t) parameter during the hold-time of the cycle is given by [16, 46]

$$(C_t)_{avg} = \frac{\Delta P \Delta V_c}{(BB_N)^{1/2} W t_h} (F'/F) \tag{4.10}$$

where, ΔP is the applied load range, ΔV_c is the difference in force-line displacement between the end and start of the hold time, th, during a cycle. F'/F is given by:

$$\frac{F'}{F} = \left[\left(\frac{1}{2 + a/W)}\right) + \left(\frac{3}{2(1 - a/W)}\right)\right] + \left[\frac{\left(4.64 - 26.64(a/W) + 44.16(a/W)^2 - 22.4(a/W)^3\right)}{0.886 + 4.64(a/W) - 13.32(a/W)^2 + 14.72(a/W)^3 - 5.6(a/W)^4}\right] \tag{4.11}$$

4.2 Numerical Expressions for C(T) Specimens

4.2.1 Estimating J-Plastic

The plastic component of J, J_p may be estimated using the following equation [31]

$$J_p = \alpha \varepsilon_0 \sigma_0 (W - a) h_1(a/W, m) \left(P/P_0\right)^{m+1} \tag{4.12}$$

Similarly the crack mouth displacement, δ_p, and the load-line displacement, V_p, are given by

$$\delta_p = \alpha \varepsilon_0 a \, h_2(a/W, m) \left(P/P_0\right)^{m} \tag{4.13}$$

$$V_p = \alpha \varepsilon_0 a \, h_3(a/W, m) \left(P/P_0\right)^{m} \tag{4.14}$$

where h_1, h_2, h_3 are functions of $a / W, m$ are given in EPRI Handbook solution [31] for plane stress and plane strain and can be obtained from FEA for the desired geometry. $\alpha, \varepsilon_0, \sigma_0, m,$ are

deformation properties of the material. The limit load, P_0, for unit thickness for plane strain and plane stress are given by the following equation, respectively:

$$P_0 = 1.455\,\eta_1(W-a)\sigma_0 \tag{4.15}$$

$$P_0 = 1.071\,\eta_1(W-a)\sigma_0 \tag{4.16}$$

where η_1 is given by:

$$\eta_1 = \left[\left(\frac{2a}{W-a}\right)^2 + 2\left(\frac{2a}{W-a}\right) + 2\right]^{1/2} - \left[\left(\frac{2a}{W-a}\right) + 1\right] \tag{4.17}$$

4.2.2 Estimating C^*

C^* can be estimated by substituting the value of P_0 from the equation 4.15 into equation 4.12 and replacing ${}^{\alpha\varepsilon_0}/_{\sigma_0^m}$ by A and m by n, we get the following equation for plane-strain conditions:

$$C^* = A\,(W-a)h_1\left({}^{a}/_{W}, n\right)\left(\frac{P}{1.455\,\eta_1 B\,(W-a)}\right)^{n+1} \tag{4.18}$$

The corresponding expressions for crack tip opening displacement (CTOD) due to creep, $\dot{\delta_{ss}}$ and the load-line displacement rate are given by the following equations:

$$\dot{\delta_{ss}} = A\,a\,h_2\left({}^{a}/_{W}, n\right)\left(\frac{P}{1.455\,\eta_1 B\,(W-a)}\right)^{n} \tag{4.19}$$

$$\dot{V_{ss}} = A\, a\, h_3\left(a/W, n\right)\left(\frac{P}{1.455\,\eta_1 B\,(W-a)}\right)^n \tag{4.20}$$

The functions of h_1, h_2, h_3 in the above equations are the same as ones listed in EPRI Handbook solution [31]. A and n are constants in power-law creep. Substituting equation 4.20 into equation 4.18 and comparing the terms with equation 4.9, it can be shown that

$$\eta = \frac{h_1}{h_3}\ \frac{\left(1-a/W\right)}{1.455\,\eta_1(a/W)}\ \frac{n+1}{n}\ \approx\ \left(2+0.522\left(1-a/W\right)\right) \tag{4.21}$$

4.2.3 Estimating $(C_t)_{avg}$

When hold times are too small for reliable measurement of difference in force-line displacement because of the resolution limitations of the extensometer, $(C_t)_{avg}$ can be estimated using the following equation. This equation has been derived for materials that creep in accordance with the power law [5,7]. Once the value of C^* has been calculated, $(C_t)_{avg}$ can be estimated using the following equation:

$$(C_t)_{avg} = \frac{2\alpha\beta(1-\nu^2)}{E}F_{cr}(\theta,n)\ \frac{\Delta K^4}{W}(F'/F)\ (EA)^{\frac{2}{n-1}}\ t_h{}^{-\frac{n-3}{n-1}} + C^*(t) \tag{4.22}$$

where

$$\alpha = \frac{1}{2\pi}\left(\frac{(n+1)^2}{1.38n}\right)^{\frac{2}{n-1}}$$

For θ = 90°, the value of $\beta \approx 0.33$ and $F_{cr}(\theta,n)$ is given in ASTM E-2760-10 [37]. The first term on the right hand side of the equation 4.22 represents the small scale creep contribution and

second term represents the extensive creep contribution to the value of $(C_t)_{avg}$. An estimate of transition time for materials that creep according to power law is given by [36,37]

$$t_T = \frac{K^2(1-\nu^2)}{E(n+1)C^*} \tag{4.23}$$

where t_T is the time required for extensive creep conditions to occur.

4.3 Experimental Equations for DEN(T-C)

4.3.1 Stress-Intensity Factor Equations

For a DEN(T-C) specimen subjected to Model I loading, stress-intensity factor, K is calculated by the following equation [16]:

$$K = \frac{P}{(BB_N)^{1/2}W^{1/2}}F(a/W) \tag{4.24}$$

The K -calibration function, $F(a/W)$, for a DEN(T-C) specimen has been modified from the standard function [Tada et al.] to include the influence of specimen height [$H\ /\ W$= 1.2]. The procedure to develop this function for the DEN(T-C) specimen was discussed in chapter 3.

$F(a/W)$ is given by:

(4.25)

$$F\left({}^{a}/_{W}\right) = \left[\frac{\frac{1}{2}\left(\frac{\pi a}{W}\right)^{1/2}}{\left(\sqrt{1-{}^{a}/_{W}}\right)}\right]\left(1.072 - 0.6033\left({}^{a}/_{W}\right) + 0.0019\left({}^{a}/_{W}\right)^2 + 0.4294\left({}^{a}/_{W}\right)^3 - 0.27\left({}^{a}/_{W}\right)^4\right)$$

4.3.2 Determination of Delta- J:

The total value of Delta-J is given by:

$$\Delta J = \Delta J_e + \Delta J_p \tag{4.26}$$

Where the contribution of the elastic part of Delta- J is given by:

$$\Delta J_e = {\Delta K^2}/{E'} \tag{4.27}$$

The plastic contribution can be calculated from:

$$\Delta J_p = \frac{\Delta A_p}{2Bc}\,\eta \tag{4.28}$$

where ΔA_p is the area under the load versus the plastic part of the load-displacement diagram and c is the un-cracked ligament. η is given by [76]:

$$\eta = \frac{2}{\left(0.72 + 1.82\ {c}/{W}\right)}\,\frac{c}{W}\,\frac{n+1}{n}\,\frac{h_1}{h_3} \tag{4.29}$$

4.3.3 Determination of $(C_t)_{avg}$ Parameter:

The average value of the (C_t) parameter during the hold-time of the cycle is given by [16, 46]

$$(C_t)_{avg} = \frac{\Delta P \Delta V_c}{(BB_N)^{1/2} W t_h}\,(F'/F) \tag{4.30}$$

Where, ΔP is the applied load range, ΔV_c is the difference in force-line displacement between the end and start of the hold time, t_h, during a cycle. F'/F is given by:

$$\frac{F'}{F} = \left[\frac{2}{x}\ \frac{\left(0.475 - 0.80199\left(a/W\right) + 0.5388\left(a/W\right)^2 + 1.3285\left(a/W\right)^3 - 2.218\left(a/W\right)^4 + 0.9571\left(a/W\right)^5\right)}{\left(1.072 - 0.6033\left(a/W\right) + 0.0019\left(a/W\right)^2 + 0.4294\left(a/W\right)^3 - 0.27\left(a/W\right)^4\right)}\right]$$

(4.31)

Where,

$x = (1 - a/W)(a/W)(\sqrt{\pi})$

4.4 Numerical Expressions for DEN Specimens

4.4.1 Estimating J -Plastic:

The plastic component of J, J_p may be estimated using the following equation [31]

$$J_p = \alpha\varepsilon_0\sigma_0 c h_1\left(a/W, m\right)\left(P/P_0\right)^{m+1} \tag{4.32}$$

Similarly the crack mouth displacement, δ_p, and the load-line displacement, V_p, are given by

$$\delta_p = \alpha\varepsilon_0 c\ h_2\left(a/W, m\right)\left(P/P_0\right)^{m} \tag{4.33}$$

$$V_p = \alpha\varepsilon_0 c\ h_3\left(a/W, m\right)\left(P/P_0\right)^{m} \tag{4.34}$$

where h_1, h_2, h_3 are functions of $a\ /\ W, m$ are given in EPRI Handbook solution [31] for plane stress and plane strain conditions and can be obtained from FEA for the desired geometry.

$\alpha, \varepsilon_0, \sigma_{0,} m,$ are deformation properties of the material. The limit load, P_0, for unit thickness for plane strain and plane stress are given by the following equation respectively:

$$P_0 = \left(0.72 + 1.82\ \frac{c}{W}\right)\sigma_0 W \tag{4.35}$$

$$P_0 = \frac{4}{\sqrt{3}}\ c\sigma_0 \tag{4.36}$$

4.4.2 Estimating C^*

C^* can be estimated by substituting the value of P_0 from the equation 4.35 into equation 4.32 and replacing ${}^{\alpha\varepsilon_0}/_{\sigma_0^m}$ by A and m by n, we get the following equation for plane-strain conditions:

$$C^* = Ach_1\left({}^{a}/_{W}, n\right)\left(\frac{P}{\left(0.72 + 1.82\ \frac{c}{W}\right)BW}\right)^{n+1} \tag{4.37}$$

The corresponding expressions for crack tip opening displacement (CTOD) due to creep, $\dot{\delta_{ss}}$ and the load-line displacement rate are given by the following equations

$$\dot{\delta_{ss}} = Ach_2\left({}^{a}/_{W}, n\right)\left(\frac{P}{\left(0.72 + 1.82\ \frac{c}{W}\right)BW}\right)^{n} \tag{4.38}$$

$$\dot{V_{ss}} = Ach_3\left({}^{a}/_{W}, n\right)\left(\frac{P}{\left(0.72 + 1.82\ \frac{c}{W}\right)BW}\right)^{n} \tag{4.39}$$

The functions of h_1, h_2, h_3 in the above equations are the same as ones listed in EPRI Handbook solution [31]. A and n are constants in power-law creep. In the context of this dissertation, we will exclusively focus on the measured value of $(C_t)_{avg}$ for the DEN(T-C) specimen.

CHAPTER 5

Test Material and Specimen Configuration

5.1 Test Material

The candidate test materials considered were from a wide variety of materials that are used in elevated temperature applications that include gas turbine materials for aircraft and land-based engines, fossil-power plant and nuclear reactor materials. The chosen test material is ASTM Grade P91 steel that has creep strength of 94 MPa at 600°C for a life of 100,000 hours. Modified 9Cr-1Mo steel (P91/T91 as per ASTM A335/A213 respectively) was developed by Oak Ridge National Laboratory in the early 1980's. The Grade 91 material, classified as martensitic steel is typically used in main steam pipes, superheaters headers, boilers and turbines in supercritical and ultra-supercritical fossil power generation plants (see figure 5.1) [77]. The Grade 91 has higher creep rupture strength permitting its use in thinner-wall components. As an alternative to low alloy ferritic and austenitic stainless steels owing to it superior elevated temperature strength, it also offers other advantages such as low thermal expansion, high thermal conductivity, high corrosion cracking resistance, a low oxidation rate, good inspectability and weldability [78]. These advantages allow this material to be a candidate to replace currently used ASTM Grade P22 (2¼ Cr-Mo) steel and an alternative for future applications in power plants operating at service conditions greater than 600°C and a steam pressure of 300 bar. The chemical composition of P91 steel used in this study is shown in the Table 5.1 [79].

Table 5.1. Actual chemical composition of P91 steel (wt %).

C	Si	Mn	P	S	Ni	Cr	Mo
0.11	0.31	0.45	0.011	0.009	0.19	8.22	0.94

As	V	Nb	Al	Cu	N	Sb, Sn	Fe
0.005	0.21	0.07	0.006	0.16	0.039	0.001	Bal.

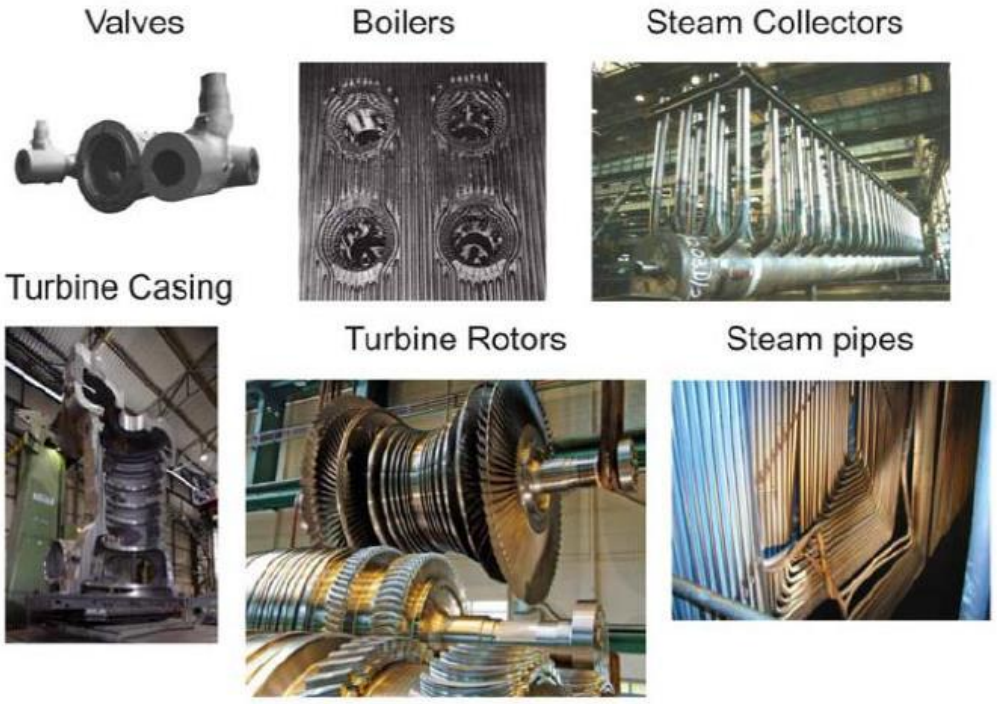

Figure 5.1. Various applications of the 9-12% chromium martensitic/ferritic steels in the fossil-fired steam power plant industry [80].

Figure 5.2 (a) shows the microstructure of the renormalized P91 material which contains fine martensitic laths arranged in packets (30-40 μm in size) within prior austenite grains that are on the average 100 μm in diameter. Optical micrographs at high magnifications revealed that the

austenite grain boundaries and lath boundaries are filled with $M_{23}C_6$ particles, where M=Cr (sizes up to 100 nm) and numerous fine MX particles M=Nb or V and X=C and/or N, inside the packets, similar to the schematic shown in figure 5.2 (b). It has been found that the martensitic transformation occurring in P91 steel produces high dislocation density that contributes to excellent creep resistance in this material with additional strengthening by precipitation of carbides, nitrides and carbonitrides of Nb and V [81]. These steels are typically heat treated to produce a martensitic microstructure followed by tempering to improve the ductility and impact strength at lower temperatures.

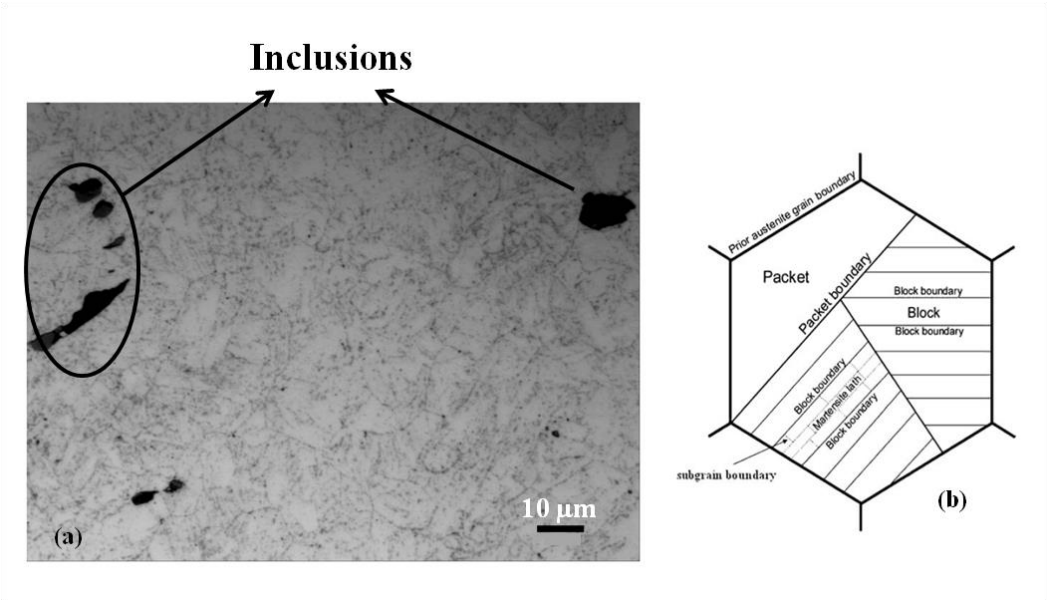

Figure 5.2. (a) Optical micrograph of P91 steel microstructure with the inset showing inclusions and (b) shows a schematic of the microstructure [82].

5.2 Machining Plan

The test material P91 steel was obtained from an ex-service pipe section with an outer diameter of 480 mm and a wall thickness of 45 mm from which specimens blanks were machined. The material was re-heat-treated to ensure consistency with original microstructure. The P91 steel was first sectioned into three segments along its length as shown in the figure 5.3.

Piece 2 was used for the round-robin on creep and creep-fatigue crack formation. The specimen blanks for tensile and creep-rupture testing were machined from this pipe section 2 as detailed in [83]. Piece 3 was heat treated for this test program and Piece 1 is being stored for future use.

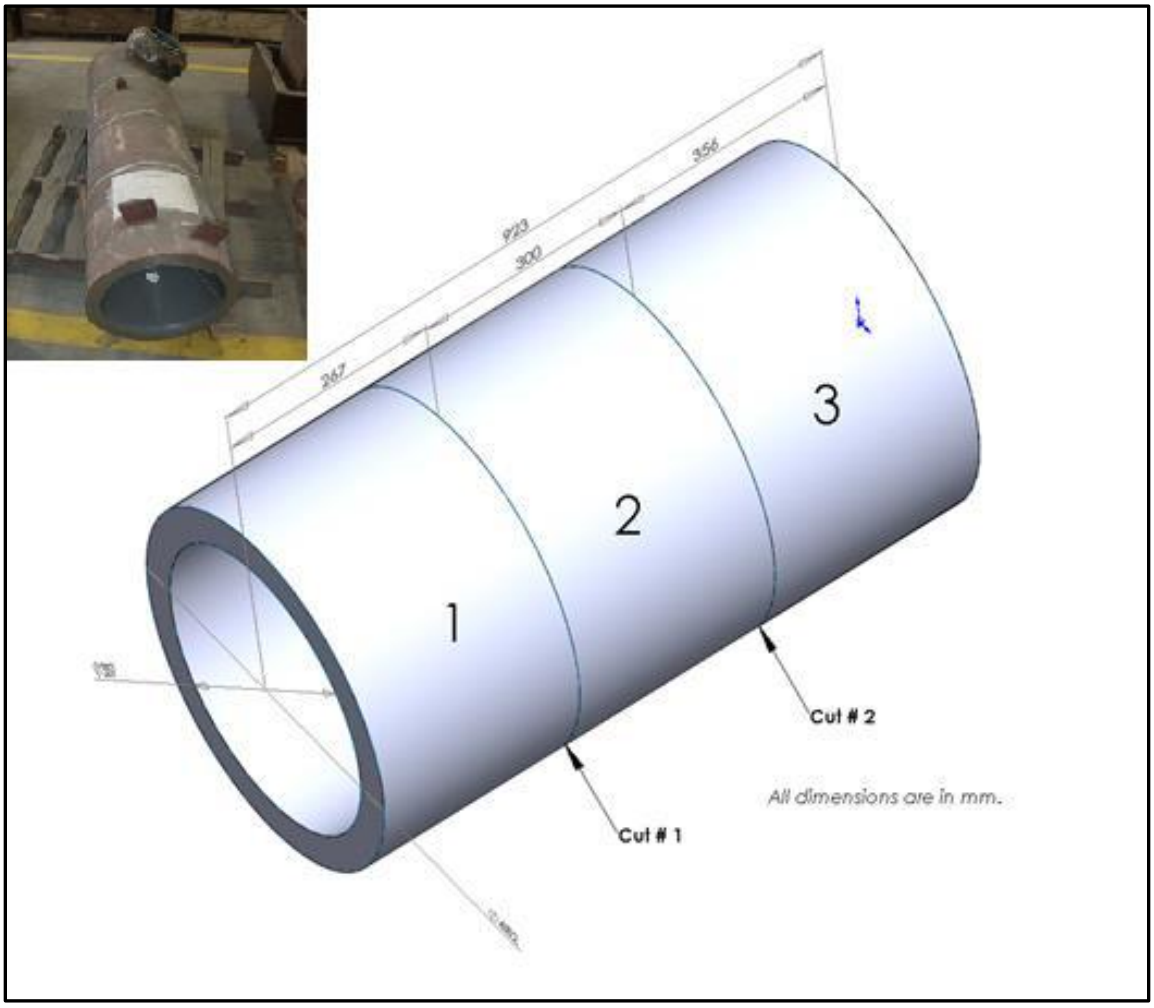

Figure 5.3. Graphical illustration of the ex-service P91 pipe section with the inset showing the actual pipe provided by EPRI, Charlotte, North Carolina, USA.

Piece number 3 was sectioned into 6 sections and marked as 3-1, 3-2, 3-3, 3-4, 3-5 and 3-6 respectively. This is graphically ilustrated in figure 5.4. A total of 30 square blanks measuring 65 mm x 63 mm x 15 mm were machined from piece 3-1 for load controlled testing using C(T) specimens. Out of the 30 blanks, 10 were used by UA and the remaining 20 blanks are reserved to be used by the future ASTM-RR participants.

Similarly, a total of 4 cylindrical blanks measuring 42 mm in diameter and 356 mm long were machined for displacement controlled testing using DEN(T-C) specimens from piece 3-2. A total of 8 specimens were machined from the 4 cylindrical blanks. The machining layouts of the subsections 3-1 and 3-2 used for machining the specimen blanks are illustrated in figure 5.5 and 5.6. Both the C(T) and DEN(T-C) test specimens were machined in such a way that the loading and crack growth are in the longitudinal and circumferential directions respectively.

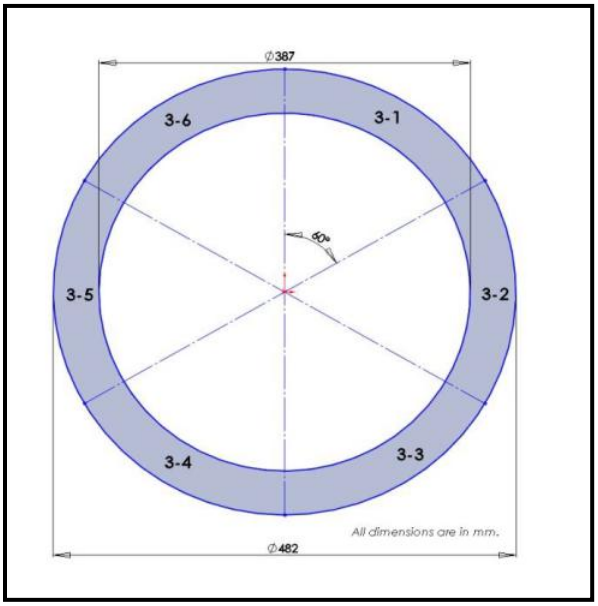

Figure 5.4. **Cross-sectional view of the piece number 3 as used for the test program.**

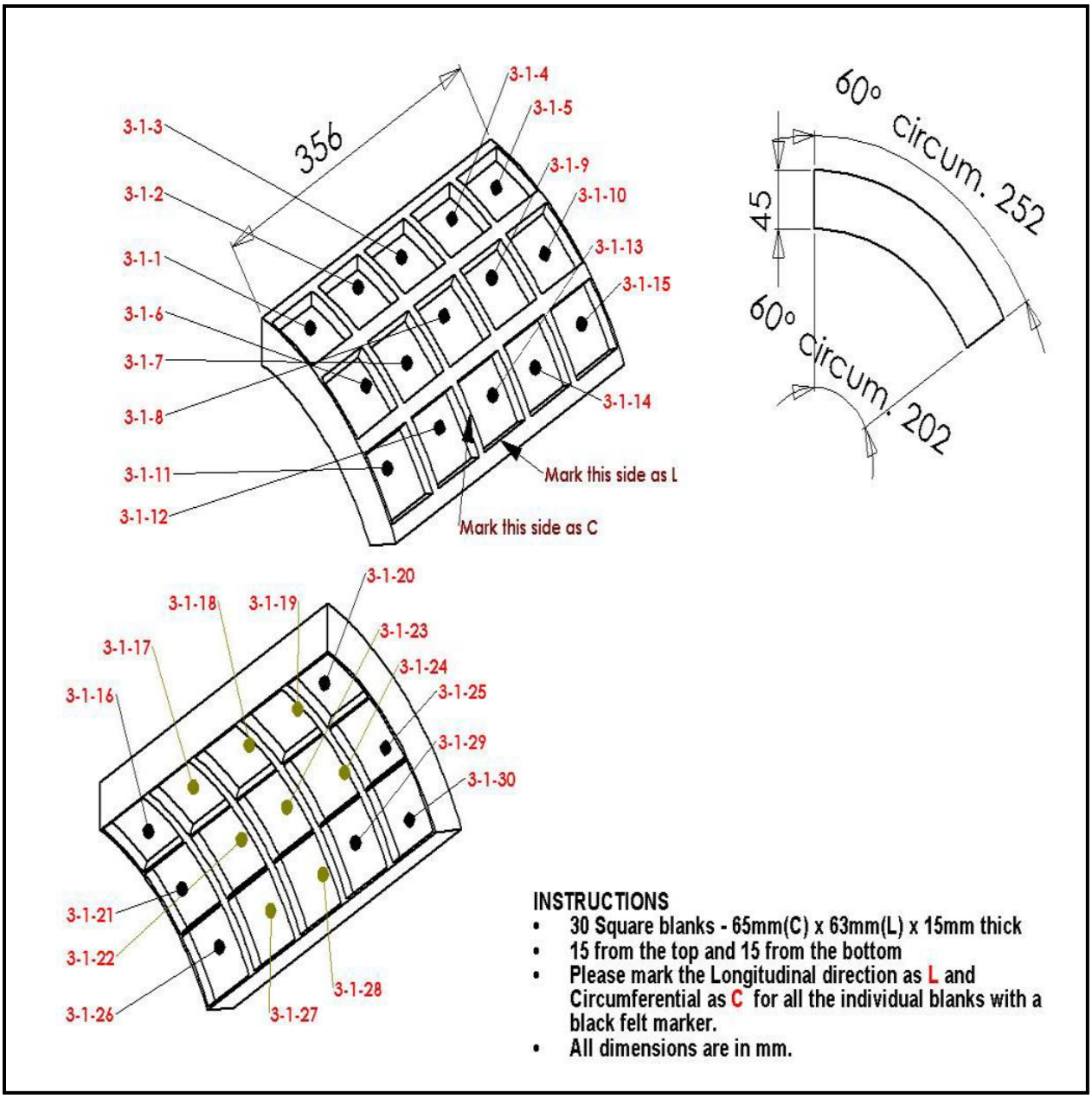

Figure 5.5. Machining layout for C(T) specimen blanks.

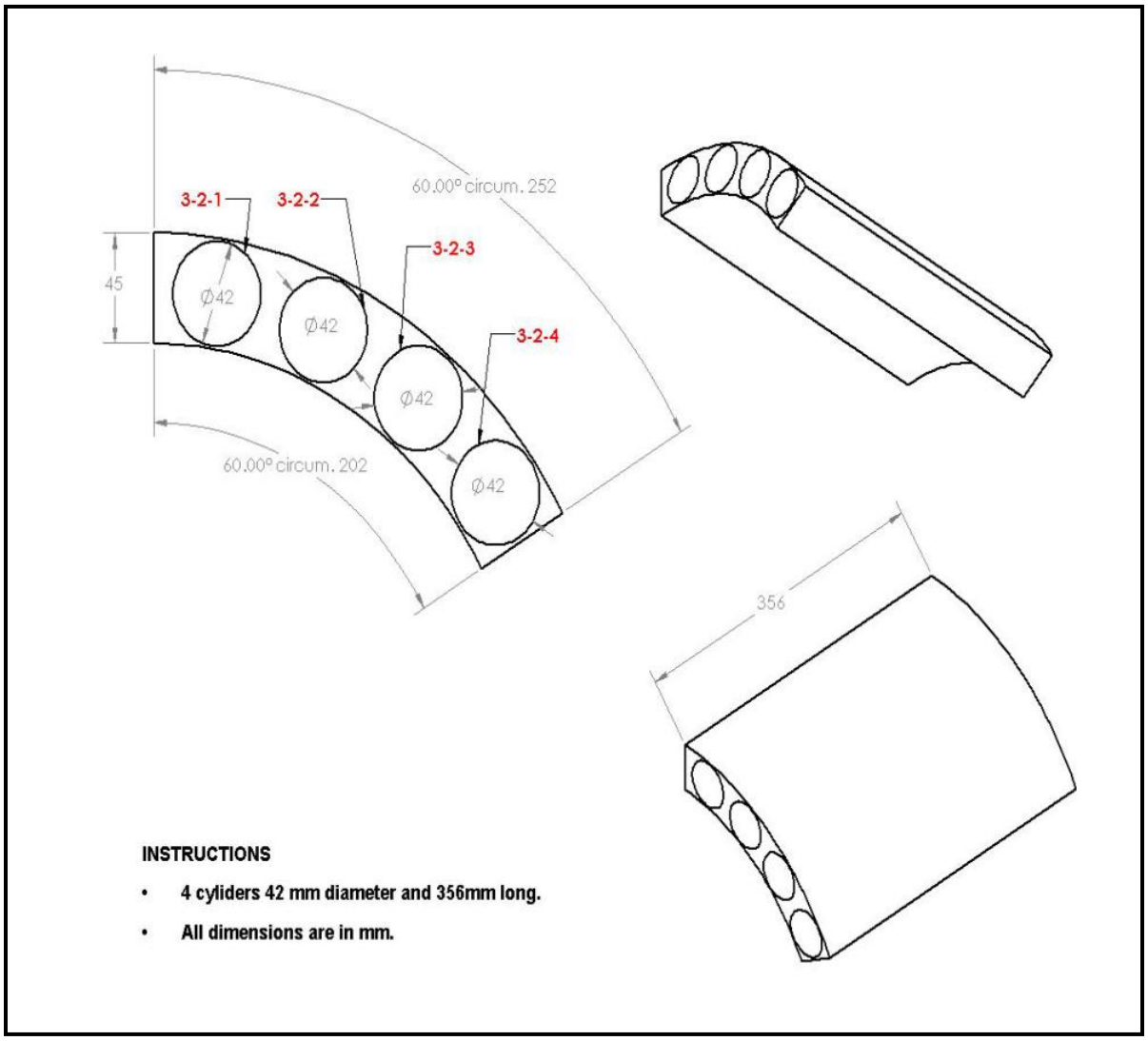

Figure 5.6. Machining layout for DEN(T-C) specimen blanks.

5.3 Specimen Configuration

5.3.1 Tensile and Creep Rupture Testing

Smooth round specimens with a gage length and diameter of 25.4 mm and 5.08 mm, respectively, that were designed as per ASTM E-139 standard (see figure 5.7) were used to conduct creep tests [84]. Uniaxial monotonic tensile tests were conducted (on-site at BiSS, India)

on cylindrically threaded dogbone specimens with a gage length and diameter of 12.7 mm and 5.08 mm, respectively as per ASTM E-8 standard [85].

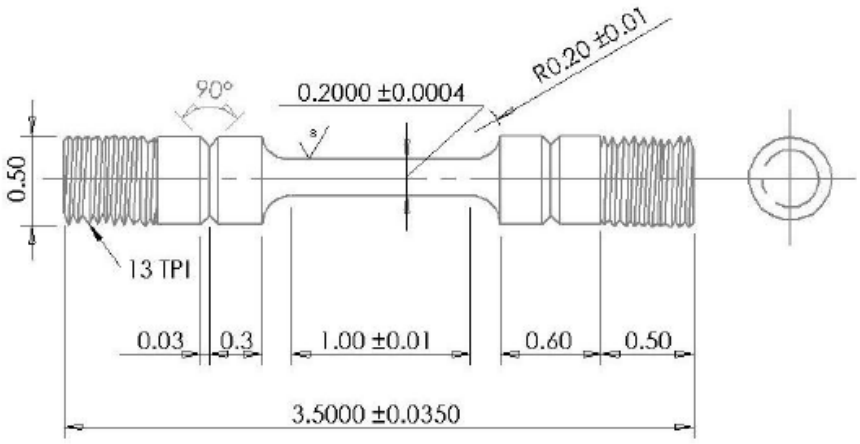

Figure 5.7. Specimen drawing used for the creep deformation and rupture testing of grade P91 steel (all dimensions in inches).

5.3.2 Crack Growth Testing

The standard C(T) specimen chosen for the test program has a width, W = 50 mm, thickness, B = 12.5 mm and initial notch, a_0 = 13.5 mm. The dimensions chosen are in accordance with ASTM E2760 [8]. The DEN (T-C) specimens had half Width, W, of 19.05 mm, thickness, B, of 6.35 mm.The initial crack-starter notch length, a_0, was about 10% of the width. In the case of creep-fatigue crack growth testing, the specimens were side-grooved after pre-cracking (10% thickness on each side, 60 degree V-notch) to prevent tunneling at elevated temperature for both C(T) and DEN(T-C) specimens. Figures 5.8 and 5.9 elucidate the notch, side grove and other details.

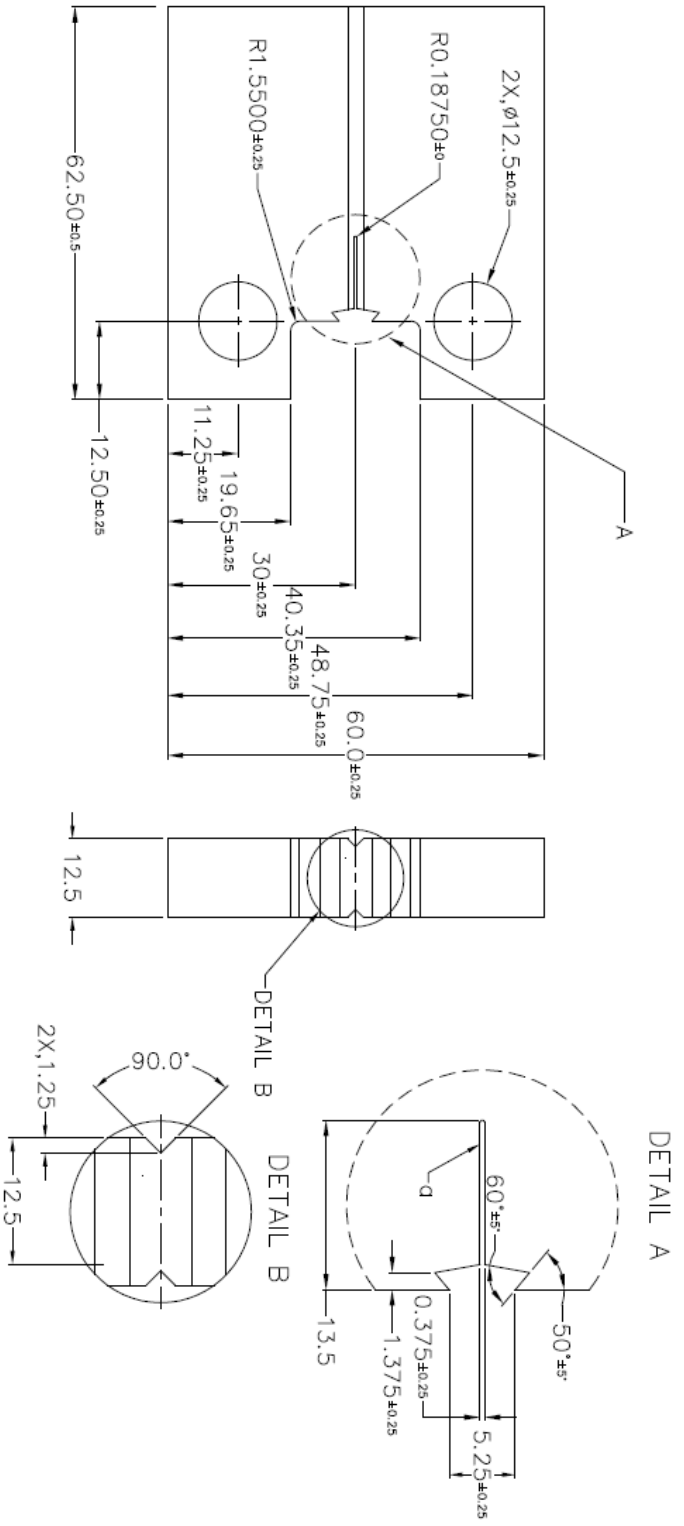

Figure 5.8. Specimen drawing for C(T) (all dimensions in millimeters).

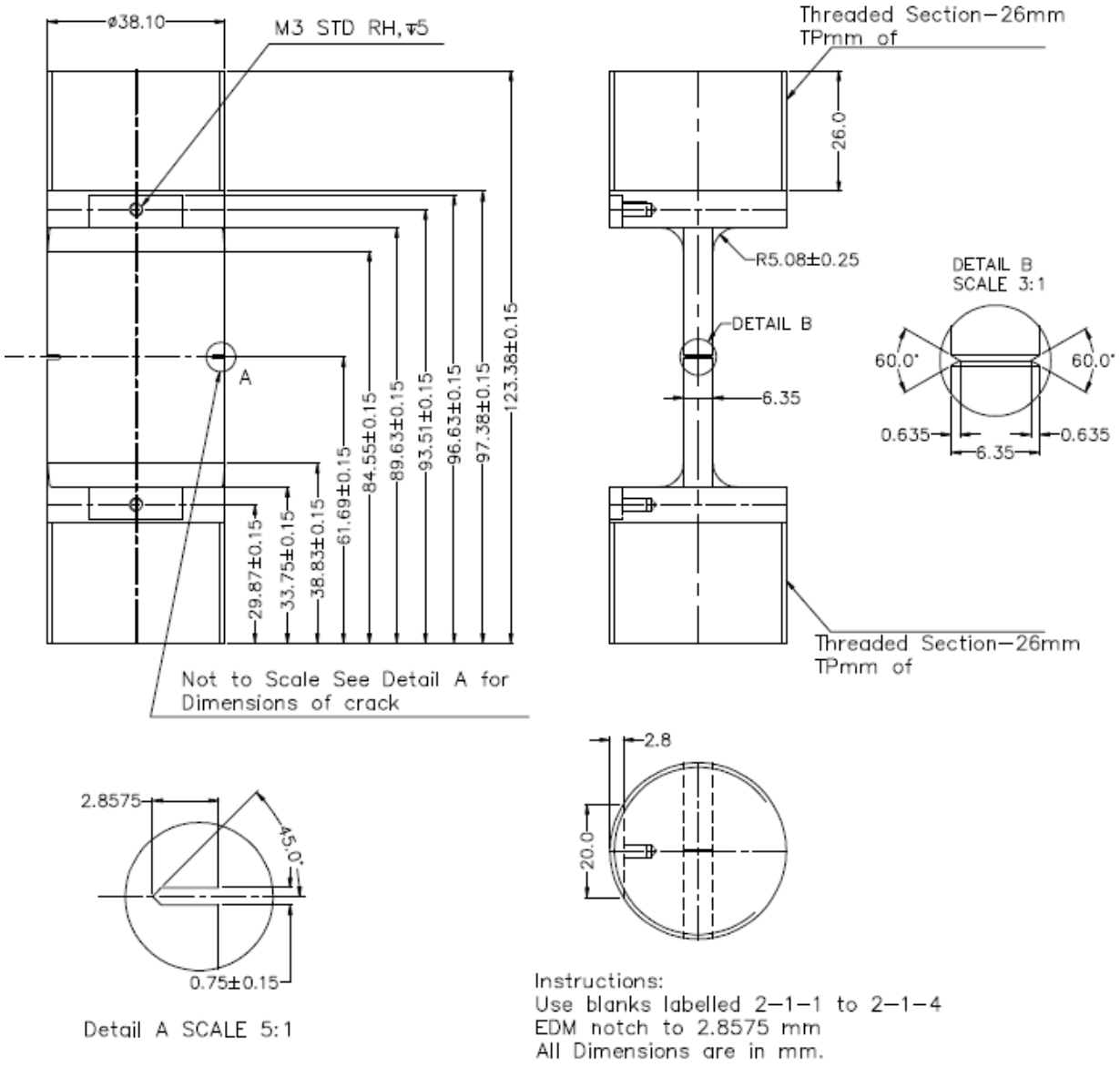

Figure 5.9. Specimen drawing for DEN(T-C) (all dimensions in millimeters).

Chapter 6

Tensile and Creep Rupture Experiments

6.1 Monotonic Tensile Experiments

6.1.1 Experimental Procedure

Uniaxial monotonic tensile tests were performed both at room temperature (24^{o} C) and at elevated temperature of 625^{o} C at a static strain-rate of 0.00192 s^{-1} in a lab controlled atmosphere (20 ± 2^{o}C and 50% relative humidity). A high temperature ceramic extensometer was used to measure the specimen elongation during testing. These tests were performed on-site at BiSS, Bangalore, India.

6.1.2 Results

Table 6.1 summarizes the uniaxial monotonic tensile response of Grade P91 steel both at room (24°C) and elevated temperature (625°C). These results agree well the published literature for this grade of steels.

Table 6.1. Uniaxial monotonic tensile test results of Grade P91 steel.

Material Properties	24^{o} C	625^{o} C
0.2 % Yield Strength, MPa	532.6	325.1
Tensile Strength, MPa	708.4	343.7
Young's modulus, MPa	220,000	125,000
% elongation	26	33

6.2 Creep Rupture Experiments

6.2.1 Experimental Procedure

Tests were performed at 625^{o}C (898 K) under uniaxial static (constant stress and temperature) loading conditions in a lab-controlled atmosphere (20 ± 2^{o}C and 50% relative humidity) using dead weights. A calibrated LVDT (linear variable differential transformer) transducer with a repeatability of 0.1 μm was used to measure specimen elongation during the tests. K-type thermocouples attached to top and bottom ends of the specimen gage length monitored the test temperature (see figure 6.1). The temperature fluctuations were found to be within ± 2^{o}C of the test temperature during the tests.

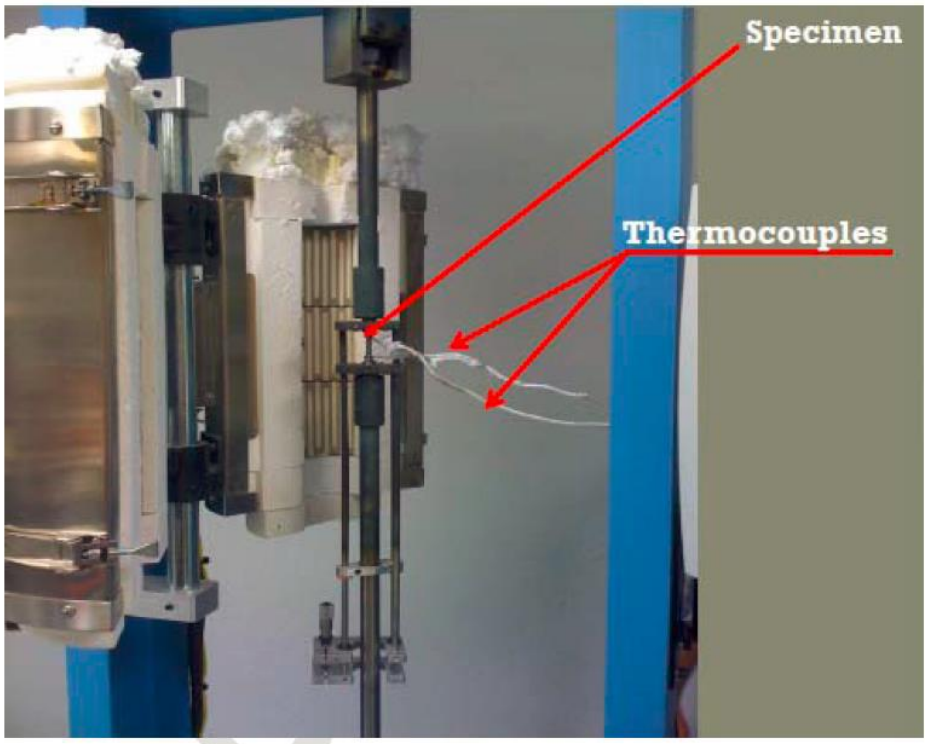

Figure 6.1. A picture of creep testing set-up with a specimen loaded for creep deformation and rupture testing in a 3 control zone conventional resistance furnace based heating system. Courtesy of MPRL, University of Arkansas.

A summary of test conditions are given in Table 6.2. A model based on Larson-Miller parameter was used to finalize the test conditions. LMP provides an analytical relation between the absolute temperature (T) and expected rupture time (t_r) in hours. Figure 6.2 shows stress versus LMP for Grade P91 steel, where the constant, C is equal to 30 [86].

Table 6.2. Test parameter matrix for the creep deformation and rupture testing.

Type of Testing	Test Temperature, °C	Expected Life, hours	Stress Required, MPa
Creep deformation and rupture	625	5000	101.5
		2000	117.5
		1000	130.0
		750	136.8
		500	138.3
		300	142.7
		150	151.5

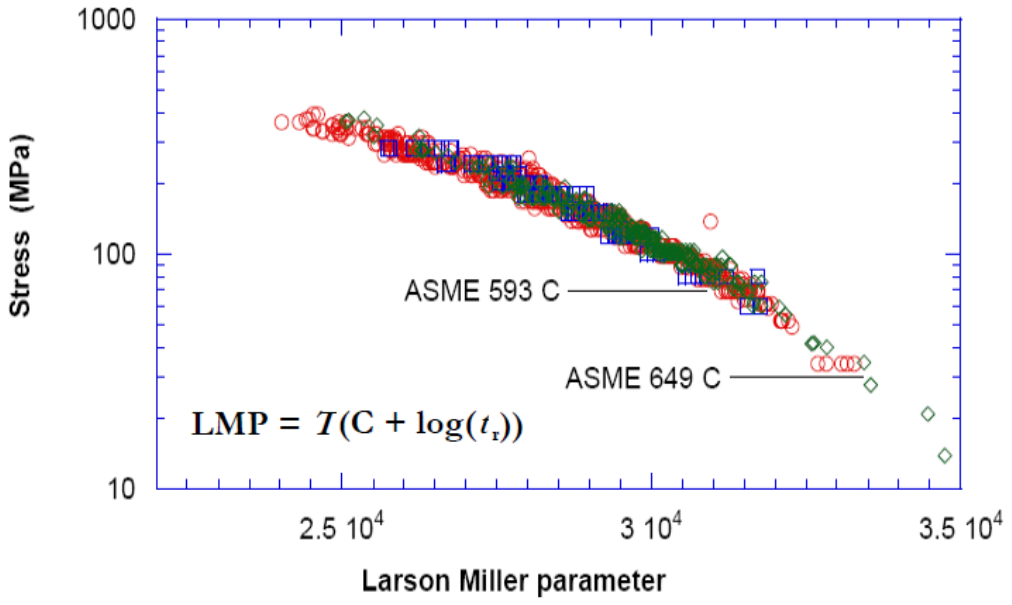

Figure 6.2 A plot of stress versus Larson-Miller Parameter (LMP), for Grade P91 steel [86].

6.2.2 Creep Deformation and Rupture Behavior

Creep deformation and rupture tests were conducted on Grade P91 steel under different stress conditions at 625° C as part of the ASTM RR on creep-fatigue crack formation [83]. Figure 6.3 shows the creep curves obtained from these tests. The results agree well with published literature under comparable loading conditions for this material [87,88,89]. Figure 6.4 shows the results from the RR tests for P91 steel overlaid in the LMP Plot [86]. It can be observed from the plot that the creep characteristics of Grade P91 compare favorably with data from the literature.

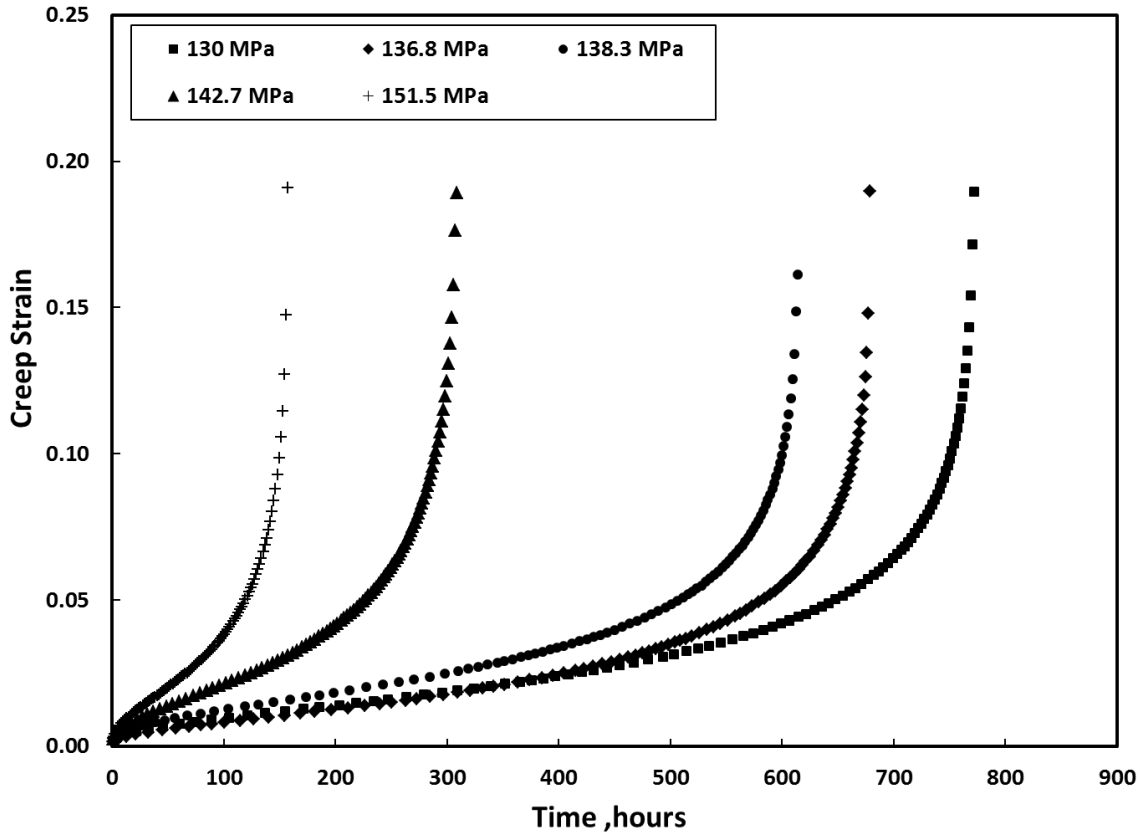

Figure 6.3. Creep deformation properties for 9Cr-1Mo steel.

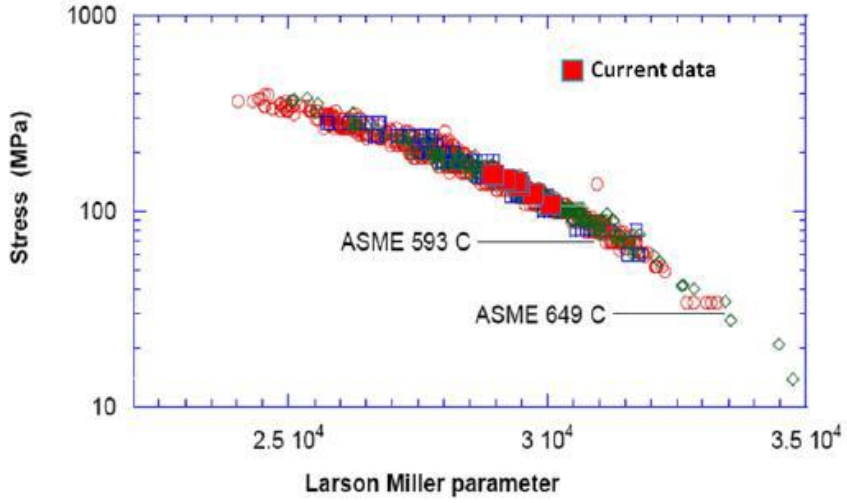

Figure 6.4. LMP plot overlaid with data from the RR tests.

The deformation mechanism for P91 steel in a creep test can be dominated by cross-slip or dislocation climb (> 70 MPa) and grain boundary diffusion (< 70 MPa) [87]. Metallurgical changes play a vital role in the creep resistance properties of martensitic steels, leading to loss in creep rupture strength [90]. Depending on the external stress, creep strain versus time curves typically exhibit very short primary (~ 10% of t), relatively substantial secondary or steady-state and tertiary creep regimes (see figure 6.3). The minimum creep rate $\dot{\varepsilon}_{ss}$ as observed in the secondary creep regime is linearly fit using Norton's power law, $\dot{\varepsilon}_{ss} = A\sigma^n$, where A and n are material constants.

Table 6.3. Steady-state creep rate as a function of stress for P91 steel at 625°C.

Applied stress (MPa)	Steady-state creep rate (h^{-1})	Norton's power-law constants
101.5	0.00035	
130.0	0.00166	$A = 9.53 \times 10^{-21}$
136.8	0.00381	
138.3	0.00523	$n = 8.24$
142.7	0.00779	
151.5	0.00748	

Chapter 7

Fatigue and Creep-Fatigue Crack Growth Experiments using C(T) Specimens

7.1 Experimental Procedure

The crack growth experiments were conducted in both electric-actuator and servo-hydraulic closed loop test machines. Figure 7.1 shows a setup of the test machine for creep-fatigue crack growth testing of C(T) specimens.

7.1.1 Pre-Cracking

The C(T) specimens were pre-cracked to an initial crack length to width ratio, a/W, of about 0.4, under cyclic loading at room temperature. The specimens were then side-grooved to prevent tunneling at elevated temperature. The loads chosen for pre-cracking were generally well below the tests loads.

7.1.2 Crack Length Measurement

An electric potential system consisting of a constant current supply and a multiple gain amplifier was used to monitor the physical crack length (a) on each specimen. Electric potential probes were attached to the front face of each specimen on either side of the specimen notch. Current leads were attached to the top and the bottom of each specimen in order to provide a uniform current flux in the specimen gage section. This is schematically depicted in the figure 7.2. In addition, an extensometer having a starting gage length of 0.5 in. (12.7 mm) was used to monitor the crack length and load-line displacement. This extensometer had pointed ceramic arms which contacted small holes on the load-line of the specimen. These small holes were spaced 12.7 mm apart.

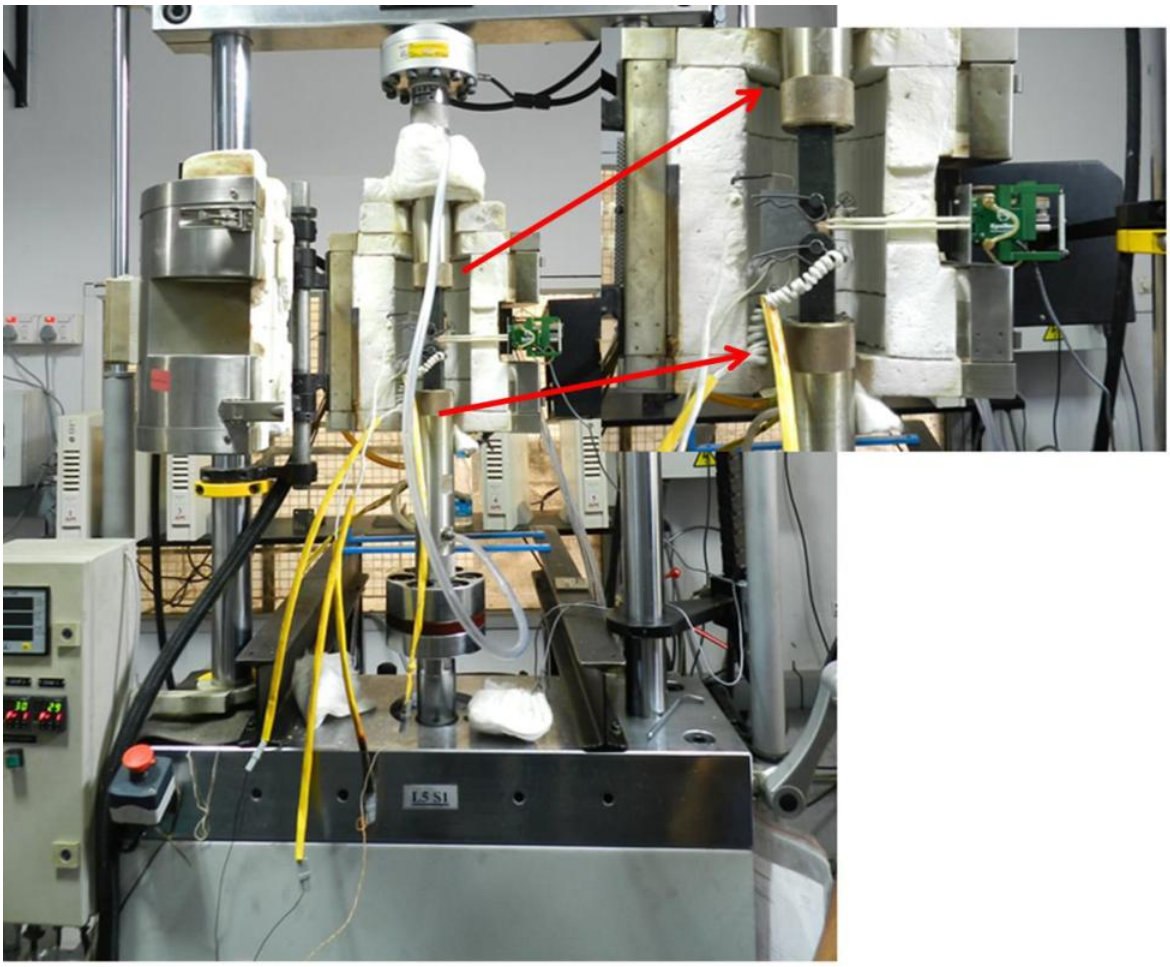

Figure 7.1. A picture of C-FCG testing set-up with a C(T) specimen loaded for testing in a 3 control zone conventional resistance furnace based heating system. Courtesy of BiSS Bangalore, India.

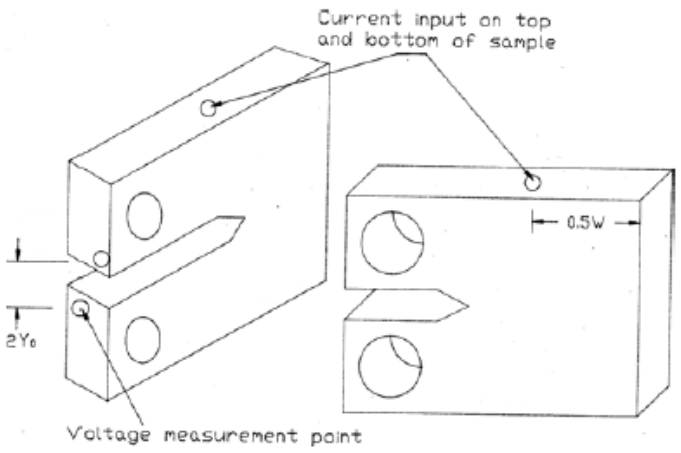

Figure 7.2. Location of the input current and output voltage leads for C(T) specimen [8].

The crack length during the test was determined by passing a constant current through the specimens and measuring the potential drop between the two potential probes. The crack length is related to the change in potential drop by [8]:

$$\frac{a}{W} = \frac{2}{\pi}\cos^{-1}\left[\frac{\cosh\left(\frac{\pi Y_o}{2W}\right)}{\cosh\left(\frac{U}{U_0}\right)\cosh^{-1}\left\{\frac{\cosh\left(\frac{\pi Y_o}{2W}\right)}{\cos\left(\frac{\pi a_o}{2W}\right)}\right\}}\right] \tag{7.1}$$

where, a_0 = initial crack length, U_0 = initial voltage, Y_o = half the distance between the probes (see figure 7.2) and W = specimen width.

The tests were normally stopped prior to fracture and cooled to room temperature and subsequently subjected to cyclic loading at room temperature to break open the specimen. This practice helps in accurately determining the crack extension during the creep-fatigue loading. The crack size at five equally spaced points centered on the specimen mid-thickness line was

measured at the end of the pre-crack and at the end creep-fatigue portion of the test, as shown in the figure 7.3. The initial crack size, a_0, and the final crack size, a_f, were then calculated by averaging the five measurements along the crack front. Having measured the initial and the final crack size, the crack size at any instant was then calculated using equation 7.2. [8, 11]:

$$a = a_0 + (a_f - a_0) \times \frac{V - V_0}{V_f - V_0} \tag{7.2}$$

Where a_f, a_0, a are the final, initial and instantaneous crack lengths, respectively and V_f, V_0 and V are the corresponding final, initial and instantaneous value of the PD voltage.

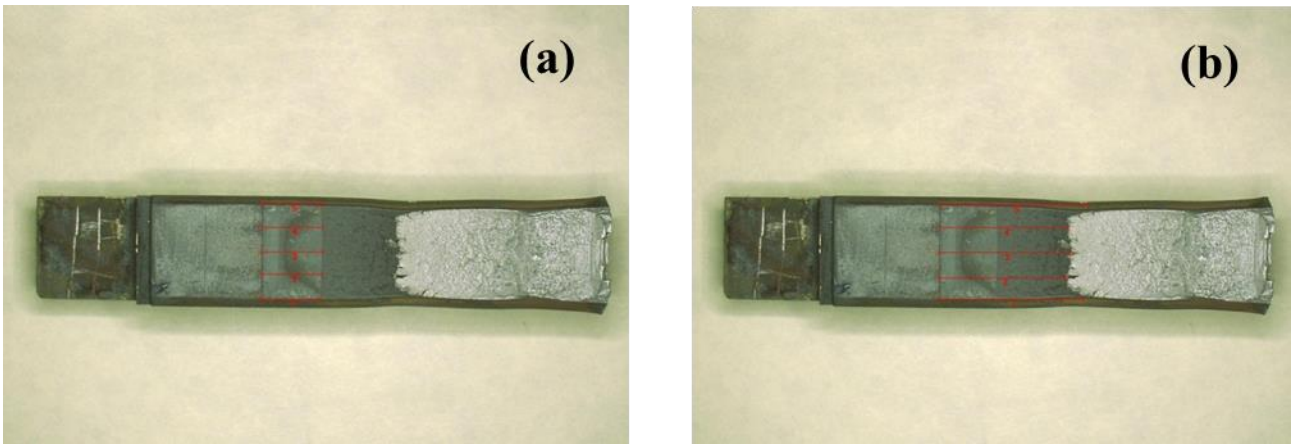

Figure 7.3. (a) Initial crack length measurement, (b) Final Crack length measurement. Courtesy of WMTR, Youngstown, PA.

The crack length was also measured using the unloading compliance technique in some cases for comparison with the crack length measured by potential drop. The crack length can be measured using the following elastic compliance expression for C(T) specimen [12]:

$$\frac{a}{W} = C_0 + C_1(U_x) + C_2(U_x)^2 + C_3(U_x)^3 + C_4(U_x)^4 + C_5(U_x)^5 \quad (7.3)$$

where $$U_x = \frac{1}{\left(\frac{BEV}{P}\right)^{1/2}+1}$$

The regression coefficients for the load-line location are given by:

C_0 = 1.0002, C_1 = -4.0632, C_2 = 11.242, C_3 = -106.04, C_4= 464.33, C_5 = -650.68

7.1.3 Test Procedure

The waveforms for loading and unloading portions were triangular and the loading/unloading times were held constant (2 seconds rise and decay times). Hold times of predetermined duration (0, 60 and 600 seconds) were superimposed on the triangular waveforms at maximum load as shown in the figure 7.4. All the tests were carried out at 625°C and at a load ratio, R, of 0.1. The minimum and maximum load, load-line displacements at minimum, maximum and hold time positions, unloading compliance, PD voltage, test temperature were continuously monitored and recorded during the tests. Figures (7.4-7.7) show the load versus displacement, force-line displacement during the hold time and the maximum and minimum displacement recorded for one of the tests conducted.

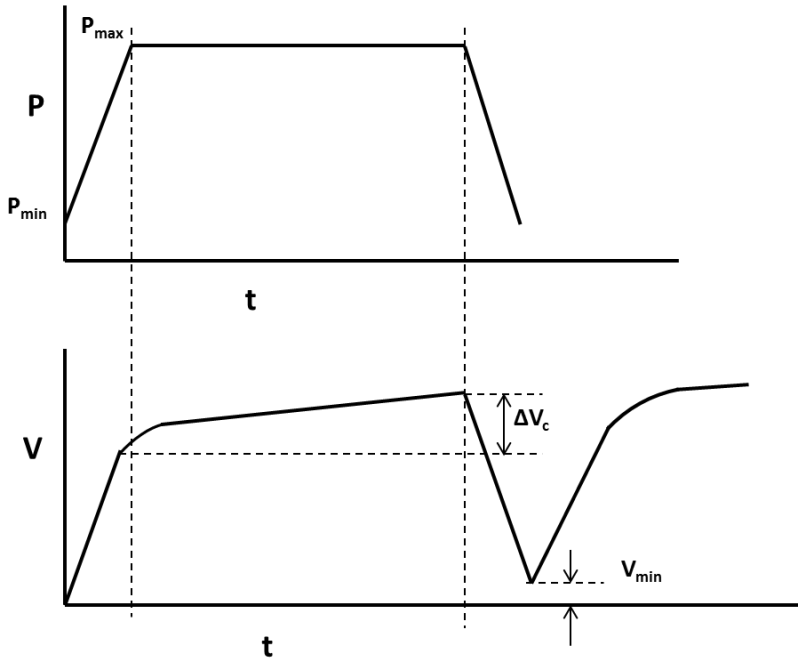

Figure 7.4. Cyclic loading and measurements made during testing for standard compact specimens, C(T), under constant load amplitude.

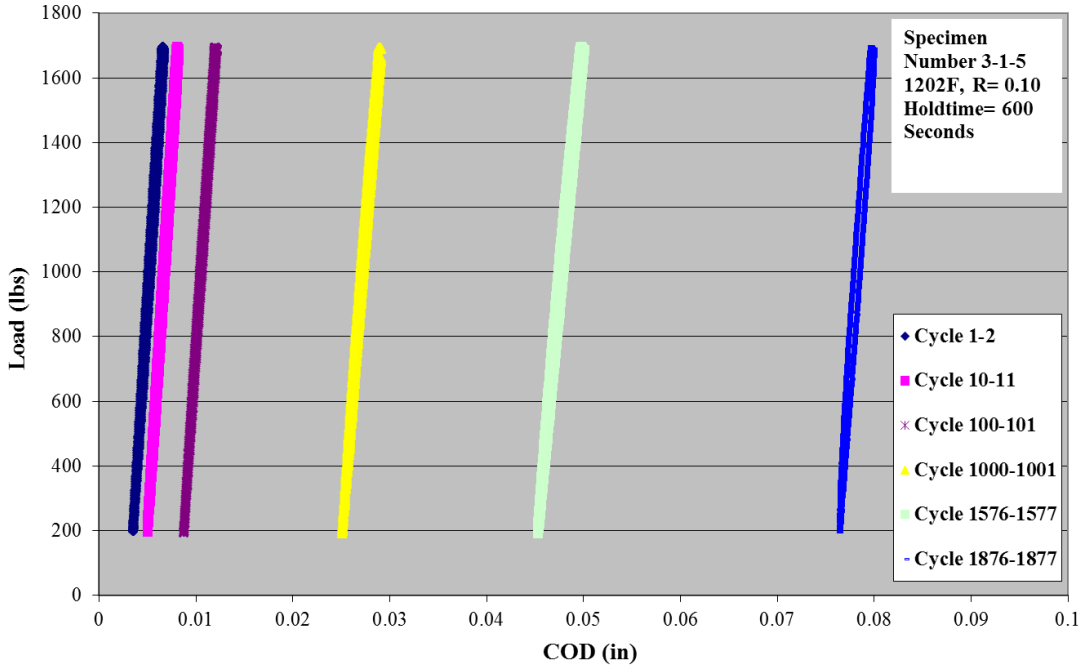

Figure 7.5. Load versus displacement record for one of the C-FCG tests conducted using C(T) specimen.

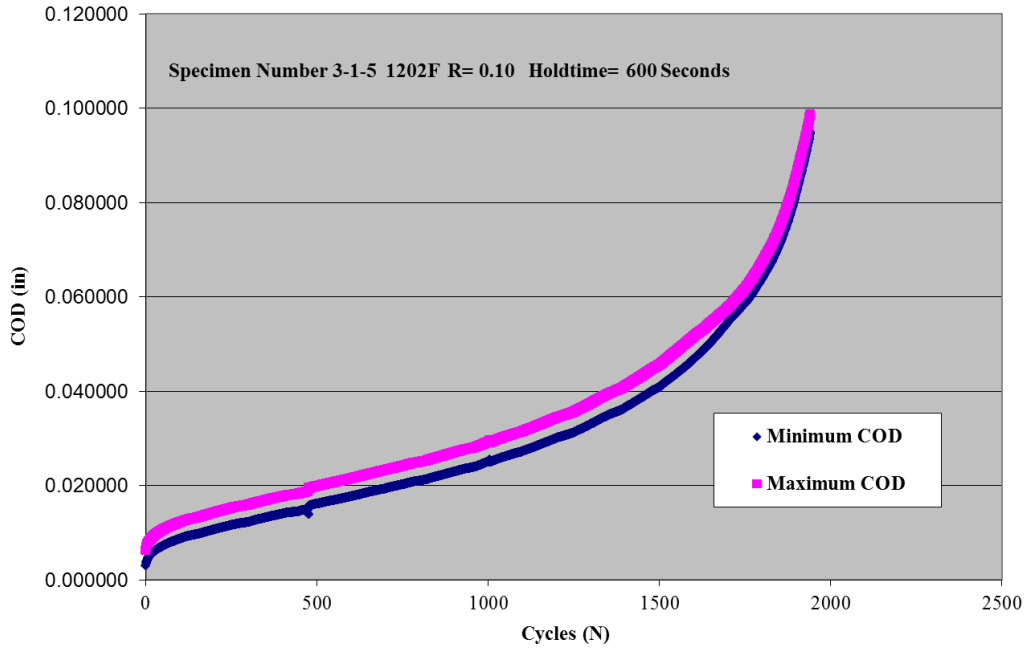

Figure 7.6. Recordings of the maximum and minimum displacements as a function of elapsed cycles.

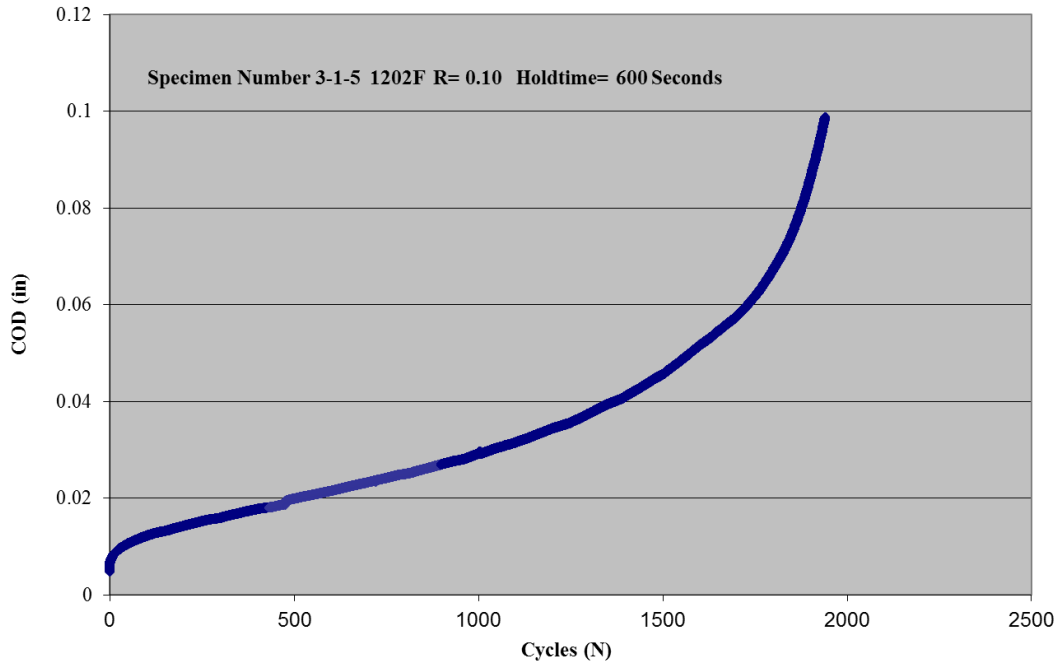

Figure 7.7. Load-line displacement measurement during the hold-time as a function of elapsed cycles.

7.2 Overview of the Test Conditions

Table 7.1 summarizes the fatigue and creep-fatigue crack growth test conditions. The starting ΔK levels varied from 23.0 to 29.1 MPa√m for the zero hold time or continuous cycling tests. The first set of 60 and 600 seconds hold time tests had starting ΔK levels of 23.6 MPa√m and 23.9 MPa√m, respectively. In order to have overlapping crack growth data, the second set of 60 and 600 seconds hold time tests had a lower starting ΔK level of 19.6 MPa√m. These load levels ensured that each test yielded sufficient crack growth data. Data reduction techniques are essential to analyze the crack growth data as per ASTM standards [8, 11, 12]. The data are considered valid if it met the following criteria:

1. The specimen was predominantly elastic, that is: $W - a \geq \frac{4}{\pi}\left(\frac{K_{max}}{\sigma_{ys}}\right)^2$
2. The crack deviated less than 20 degrees from the plane of symmetry.
3. The difference between the front and back crack lengths was less than 0.25 B.
4. The accumulated minimum displacement was less than 0.05 W.

Table 7.1. Summary of fatigue and creep-fatigue crack growth test conditions.

Specimen ID	Hold time, seconds	Max Load, KN	Initial ΔK, MPa√m	Final ΔK, MPa√m	Initial Crack length, mm	Final Crack length, mm	N_f Cycles
3-1-1(W)	0	9.0	23.9	57.5	20.25	33.06	15790
3-1-2(W)	60	9.0	23.6	39.51	19.90	28.50	3470
3-1-3(W)	600	9.0	23.9	35.6	20.27	27.00	763
3-1-4(W)	60	7.5	19.6	38.9	19.92	30.70	8018
3-1-5(W)	600	7.5	19.6	29.5	19.95	26.90	1915
3-1-8(B)	0	9.0	23.0	53.0	19.54	32.17	16298
3-1-9(B)	0	11.0	29.1	56.7	20.17	30.59	8800

7.3 Results and Discussions

The results from this section are published in Narasimhachary et al., A Crack growth behavior of 9Cr-1Mo Steel under creep-fatigue conditions, International Journal of Fatigue 56 (2013) 106-113.

7.3.1 Crack Growth Behavior

Two types of creep behavior generally observed in materials during creep crack growth and creep-fatigue crack growth tests are creep-ductile and creep-brittle [16]. The total measured change in the load -line displacement rate, ΔV, can be separated into an instantaneous elastic part, ΔV_e, and a time-dependent part that is associated with the accumulation of creep strains, ΔV_c to determine if the creep-fatigue crack growth rates should be expressed as da/dN versus ΔK for a fixed hold time in the case of creep-brittle materials or if they should be expressed as $(da/dt)_{avg}$ versus $(C_t)_{avg}$,. ΔV_e is estimated using the following equation [91]:

$$\Delta V_e = \frac{t_h \left(\frac{da}{dt}\right)_{avg}}{P} B \left[\frac{2\Delta K^2}{E'}\right] \tag{7.4}$$

A determination can be made about creep-ductile versus creep-brittle material by estimating, ΔV_e, from equation 7.4 and by comparing it to a measured load-line displacement during the hold-time, ΔV_c,. The material can be classified as creep-brittle if, $\Delta V_e \geq 0.5\ \Delta V$ and the crack growth behavior may be characterized by the stress-intensity factor. On the other hand, if $\Delta V_e \leq 0.5\ \Delta V$, creep-ductile conditions are said to prevail and the crack growth behavior should be characterized by $(C_t)_{avg}$.

The change in displacement for the instantaneous elastic part and the measured change in load-line displacement during the hold-time are compared in figure 7.8. The closed symbols

represent the results of 60 and 600 seconds hold time tests for the measured change in load-line displacement during the hold period. The open symbols are the results of 60 and 600 seconds hold time tests estimated from the equation 7.4. The change in displacement during the hold-time are two to three orders in magnitude higher when compared to their elastic counterparts. Thus, creep effects dominate the crack tip behavior and the average time rates of crack growth during a loading cycle, $(da/dt)_{avg}$, should be expressed as a function of the average magnitude of the (C_t) parameter, $(C_t)_{avg}$ for creep-ductile materials such as 9Cr-1Mo steels.

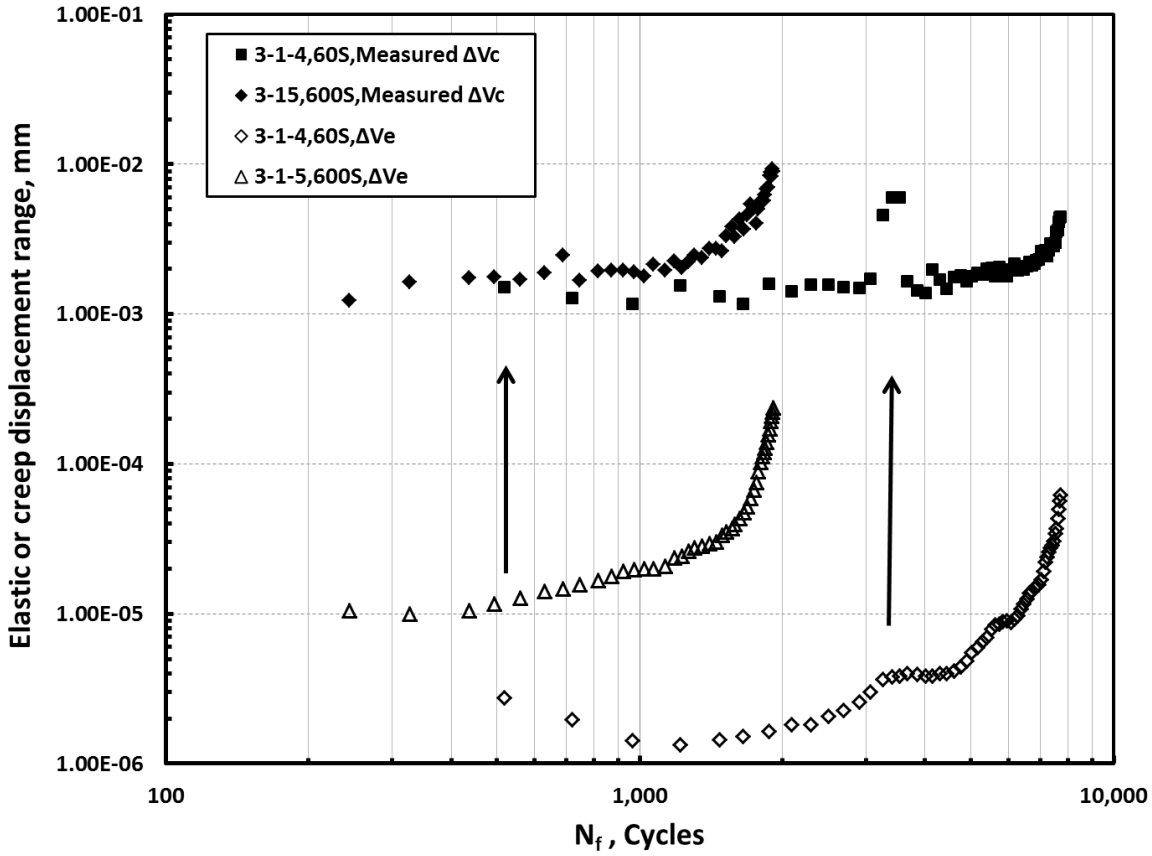

Figure 7.8. Estimated load-line elastic and measured total displacements during hold time as a function of the elapsed cycles.

7.3.2 Relationship between Creep-Fatigue Crack Growth Rate and ΔK

The crack growth rate behavior of 9Cr-1Mo steel at 625°C as a function of stress-intensity factor range for the hold times of 0, 60 and 600 seconds is plotted in figure 7.9. The average time rate of crack growth rate, $(da/dt)_{avg}$, as a function of ΔK for hold times of 60 and 600 seconds tests, is shown in Figure 7.10. This is same data as in figure 7.9, except plotted as $(da/dt)_{avg}$, where $(da/dt)_{avg} = \frac{1}{t_h}(da/dN)_{time}$. The solid symbols shows results for the zero hold time tests while the open symbols are results for the 60 and 600 seconds hold time tests, respectively.

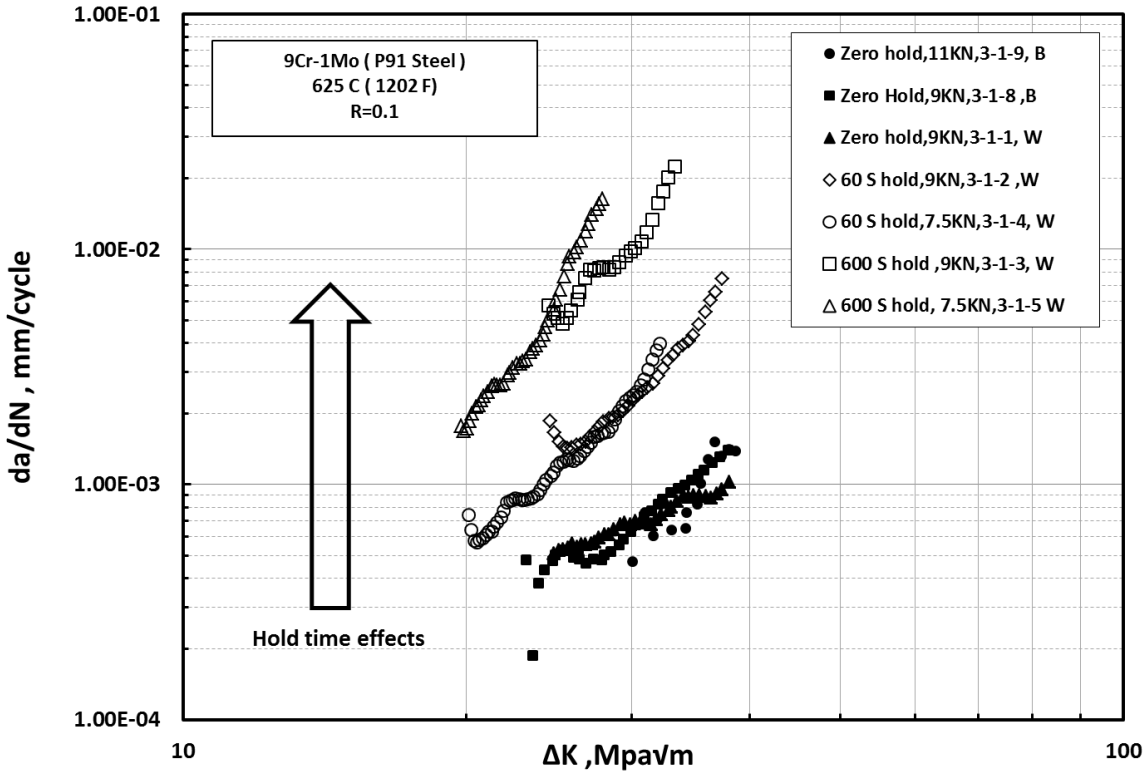

Figure 7.9. Fatigue crack growth rate behavior of 9Cr-1Mo steel at 625°C as a function of ΔK

The crack growth rate increases with increase in hold time and stress-intensity factor range, ΔK, as expected. Linear elastic conditions were maintained in the various test specimens throughout the tests as can be seen from overall reasonable correlation between crack growth rate and ΔK . However, there are other concerns about the use of ΔK at elevated temperature as discussed in the next section.

Crack growth behavior is affected by creep deformation at the crack tip causing transients in the crack growth behavior [39]. A characteristic hook develops in the plot of crack growth rate and ΔK in the early stage of crack growth. During the early stages of crack growth period, the crack growth rates seem to first decrease with increase in ΔK and subsequently increase developing the hook pattern. Such trends have been reported in several previous studies [7,46,51,92] and are clearly observed in figures 7.9 and 7.10 in the data from the majority of the tests. Even though linear elastic conditions dominate in the specimen, the transient behavior implies that even for constant loading frequency and waveform, da/dN or da/dt does not uniquely correlate with ΔK . The transient trend can be important in service life predictions because this region typically occupies 30-40 % of total creep fracture life [2,93]. An explanation for the presence of hooks is given herein.

Initially, creep-deformation occurs rapidly due to high elastic stress fields in the crack tip region, but slows down with accumulated time as the crack tip stresses relax due to redistribution. With time, the rate of stress relaxation decreases continuously. Concurrently, the applied ΔK level rises due to increase in crack size. Thus, there exists competing forces of stress relaxation at a decreasing rate and increase in ΔK resulting in a tendency for the crack growth rate to first decrease, and then subsequently increase resulting in the “hook” pattern. This is the

motivation to seek other parameters that are able to establish better correlations such as the the $(C_t)_{avg}$ parameter.

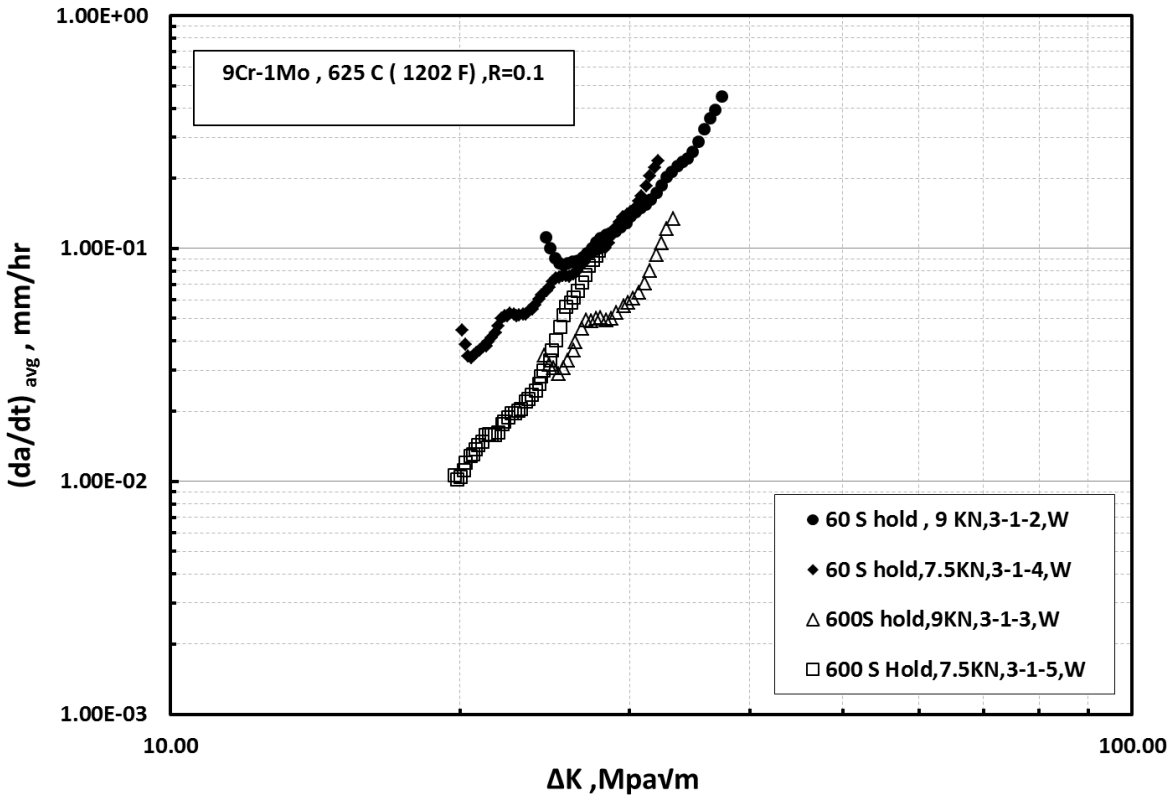

Figure 7.10. Average time rate of crack growth rate during hold time as a function of ΔK for hold times of 60 and 600 seconds for 9Cr-1Mo steel at 625°C.

7.3.3 Correlation Between $(da/dt)_{avg}$ and $(C_t)_{avg}$

The hooks are expected to disappear when the same data in figures 7.9 and 7.10 are plotted with $(C_t)_{avg}$, because the value of $(C_t)_{avg}$ directly captures the stress relaxation trend. A closer examination of equation 4.22 reveals that this also depends on the magnitude of ΔK which increases with crack size. Equation 4.10 can be used to determine the value of $(C_t)_{avg}$ provided ΔV_c is directly recorded during the tests. ΔV_c accounts for contributions to the creep

deflection during the hold time from both the small-scale and the extensive creep terms in equation 4.22. When ΔV_c measurements are not available because of resolution or other issues with extensometers, equation 4.22 must be used to estimate the value of $(C_t)_{avg}$. The creep deflections during the hold time could be reliably measured for some tests conducted in this study, These results will be used to verify the accuracy of equation 4.22 using the measured values of $(C_t)_{avg}$ obtained from equation 4.10.

The calculated values of $C^*(t)$ and $(C_t)_{avg}$ and the measured $(C_t)_{avg}$ are compared in figure 7.11. The fine dashed lines and the solid lines are the estimated values of $(C_t)_{avg}$ and $C^*(t)$ for the hold time of 60 seconds from equation 4.22. The open triangle symbols are the measured $(C_t)_{avg}$ values for the 60 second hold time tests. The $(C_t)_{avg}$ value is dominated by the small-scale creep term on the right hand side of the equation 4.22 for the 60 second hold time tests. For short hold times the crack tip creep zone is expected to be small in comparison to the relevant specimen dimension. The creep zone growth is constrained by the surrounding elastic stress fields characterized by K and time. In general, for short hold time tests, the contribution of the C^* term is expected to be much less than the $(C_t)_{ssc}$. The calculated values of $(C_t)_{avg}$ are consistently higher than the measured values by as much as a factor of 5. The reasons for this discrepancy are several. The analytical estimates were derived under the assumption that the specimen is under pure plane strain conditions, neglecting any contribution from the instantaneous plasticity and primary creep at the crack tip. All these factors contributes to uncertainty in the $(C_t)_{avg}$ value.

The dashed-dotted lines and the medium dashed lines are the numerically estimated values of $(C_t)_{avg}$ and $C^*(t)$ for the hold time of 600 seconds from equation 4.22. The open diamond symbols are the measured $(C_t)_{avg}$ values for the 600 second hold time tests. The

measured value of $(C_t)_{avg}$ was much closer to the estimated value compared to the case of 60 second hold time for the 600 seconds hold time tests. Never-the-less, even in this case, the small-scale creep contributions to $(C_t)_{avg}$ seem to dominate the extensive creep contributions. Thus, for the majority of the test dominantly elastic conditions were preserved.

The importance of measuring load-line deflection during the hold time when conducting creep-fatigue crack growth testing can be seen in figure 7.11, which shows the differences between the measured and calculated values of $(C_t)_{avg}$ for both hold times. t ASTM standard E-2760-10 does not require the measurement of force-line deflections and allows for estimated values of $(C_t)_{avg}$ to be used for correlating crack growth data. This need to be investigated further and perhaps appropriate changes should be made to the standard.

Figure 7.12 shows the results of the 60 and 600 seconds hold time tests for the dominant damage and the damage summation, represented by filled and open symbols, respectively. Creep-fatigue crack growth data exhibit scatter that might be attributed to the measurement of load-line displacement during the hold time. Outliers in the figure 7.12 are due to measurement issues. These random errors in measurement are due to the displacements values being a small quantity. The change in load-line displacement values during hold-time have been averaged over five successive cycles to reduce scatter. The seven point incremental polynomial methods was used to compute crack growth rate.

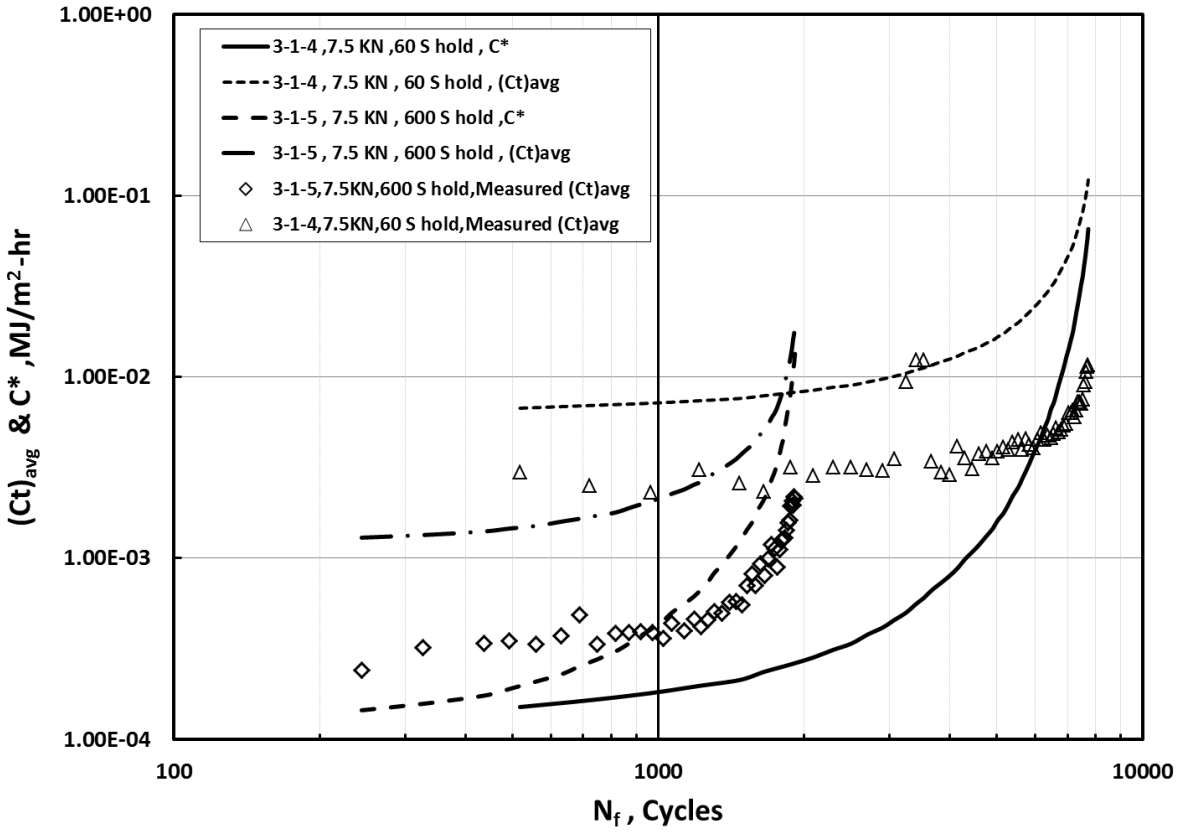

Figure 7.11. Comparison of experimental (measured) $(C_t)_{avg}$ and analytical $C^*(t)$, $(C_t)_{avg}$

Several other trends can be noted from figure 7.12. First, the differences between the dominant-damage hypothesis and the damage-summation hypothesis are minimal. The minimal difference between the models is due to the domination of the time-dependent contribution to the crack growth rate compared to the cycle-dependent part for both the hold time test of 60 seconds and 600 seconds. Second, the hooks that were observed in the da/dN or da/dt versus ΔK plots are no longer present strongly supporting the ability of the $(C_t)_{avg}$ parameter to correlate the data. Recall that the value of $(C_t)_{avg}$ depends both on the value of ΔK and the hold time. Third, the difference in the crack growth rates for 60 s and 600 s hold times are much smaller in

comparison with the plots of ΔK. Although there are some differences between the time-rate of crack growth between the conditions of 60s and 600s hold times, all data appear to lie in a narrow scatter band. An almost linear correlation between $(da/dt)_{avg}$ and $(C_t)_{avg}$ is observed, disregarding the small differences. Earlier studies of creep-fatigue crack growth behavior of several Cr-Mo steels using the $(C_t)_{avg}$ parameter [2] have observed similar correlations. Such correlations are very useful in life-predictions because temperature and hold times in components can vary from temperatures and hold times used in obtaining the data.

The time rates of crack growth for the longer hold time tests of 600 seconds are lower than the crack growth rates from the 60 seconds hold time test; this difference is attributed to the time-dependent damage mechanisms at the crack tip. Saxena and co-workers [4] have shown microscopically at the crack tip that, creep deformation and cavitation plays an important role in the damage mechanisms for a long hold time test such as 600 seconds compared to shorter hold times. Under such conditions, creep effects dominate and the crack grows by cavity coalescence resulting in inter-granular cracking. The average crack tip stresses during the hold period in a short hold time tests are larger because of a shorter duration available for stress relaxation. Thus, there is less chance for creep cavitation and generally the mode of fracture is trans-granular in nature. It would be interesting to conduct creep crack growth testing of this material and compare the data to the 600 second hold time test.

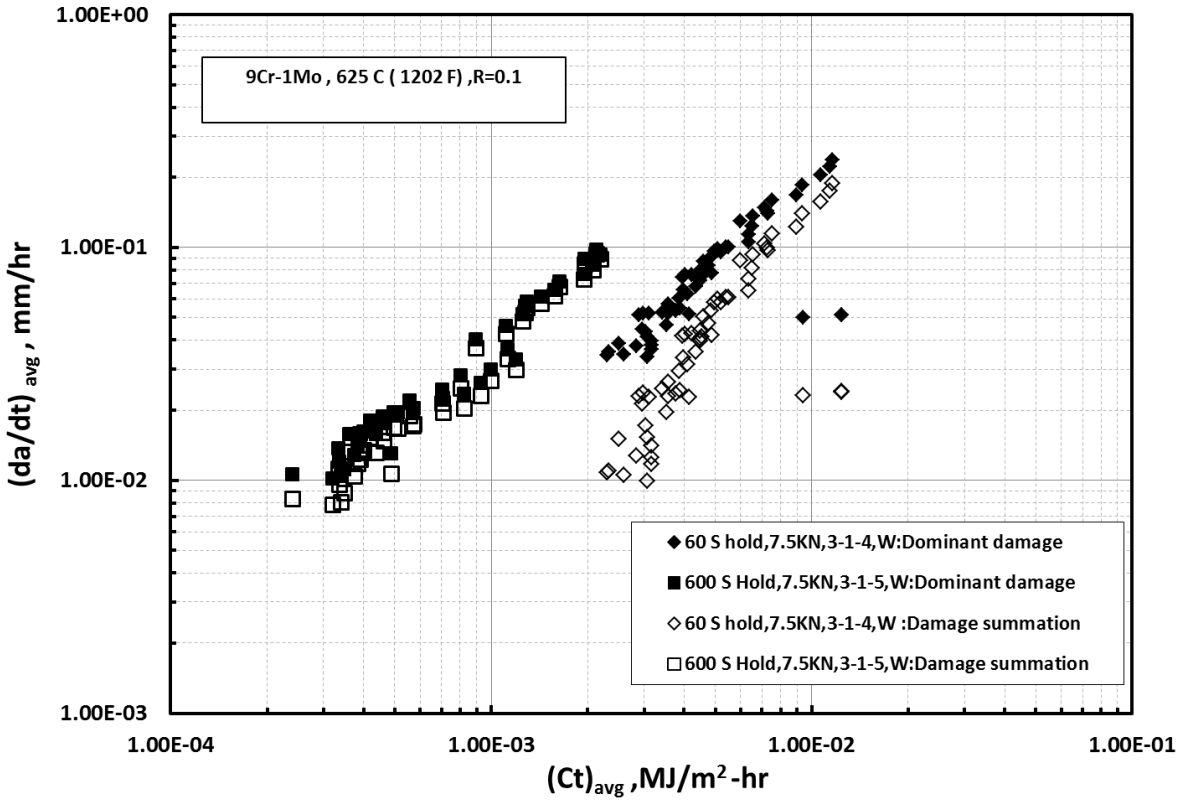

Figure 7.12. Average time rate of crack growth during hold-time as a function of $(C_t)_{avg}$ for hold times of 60 and 600 seconds for 9Cr-1Mo steel at 625°C.

We note that at the very end of the tests, the value of the minimum force-line displacement or the residual deflection starts to increase rapidly as shown in the figures 7.13 and 7.14 for 60 and 600 seconds respectively. This indicates rapid accumulation of inelastic deformation, which may be due to ratcheting or also due to rapid crack growth. Hence, the data collected after the minimum force-line displacement exceeded $0.05W$ were considered invalid in accordance with the ASTM Standard E2760-10. In load-control testing, if there is significant creep deformation during the hold time, there will be a residual creep component accumulated after each cycle. Thus, there is risk that if the accumulated creep deformation becomes large as

cycles accumulate, failure due to ratcheting can occur. The standard mandates stopping the test after the accumulated displacement reaches $0.05W$.

Creep-fatigue crack growth properties are widely used in the power generation industry to establish inspection intervals and to predict full or remaining lifetimes in the defect assessment of components. Thus, from a component application standpoint, it would be desirable to study long term crack growth behavior under creep-fatigue conditions. This requires conducting tests at hold times greater than 600 seconds that was currently used for our tests. Figures 7.15, 7.16 and 7.17 show the crack length measurements for zero, 60 and 600 seconds hold time tests, respectively. The crack extensions measured are about 18 mm, 11 mm and 6 mm for zero, 60 and 600 tests seconds, respectively. With increase in hold time it can be seen that the capability of the specimen to yield valid data is quickly diminishing.

Therefore, there is a high risk of only obtaining invalid data during longer hold time tests under load-control conditions. The answer to this is the development of a displacement range controlled test or a test in which the accumulated (residual) displacement can be reversed suitably. As discussed in the earlier chapters, displacement range control will require the minimum loads to go into compression and therefore C(T) specimen becomes unsuitable for these type of test. The DEN(T-C) specimen with rigid connections on the two ends was specifically developed for this purpose. Under these conditions, ratcheting will no longer be an issue and longer hold times will be possible. The next chapter will exclusively focus on the validation and testing of the DEN(T-C) specimen design under fatigue and creep-fatigue conditions.

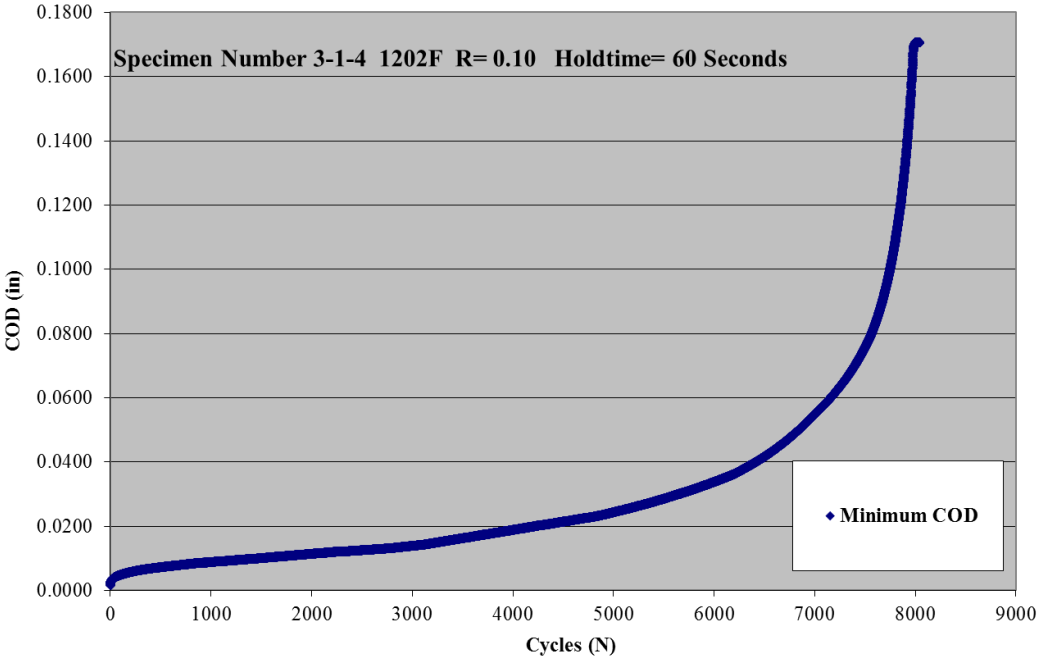

Figure 7.13. Residual displacement versus elapsed cycles for 60 seconds hold time test.

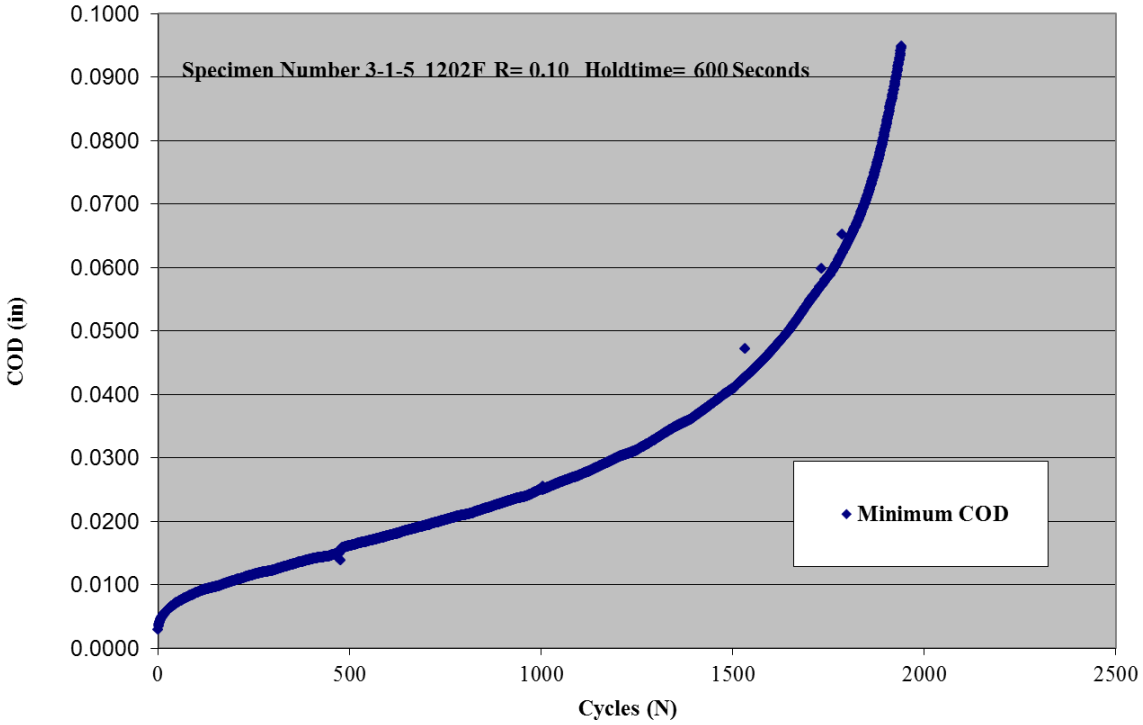

Figure 7.14. Residual displacement versus elapsed cycles for 600 seconds hold time test.

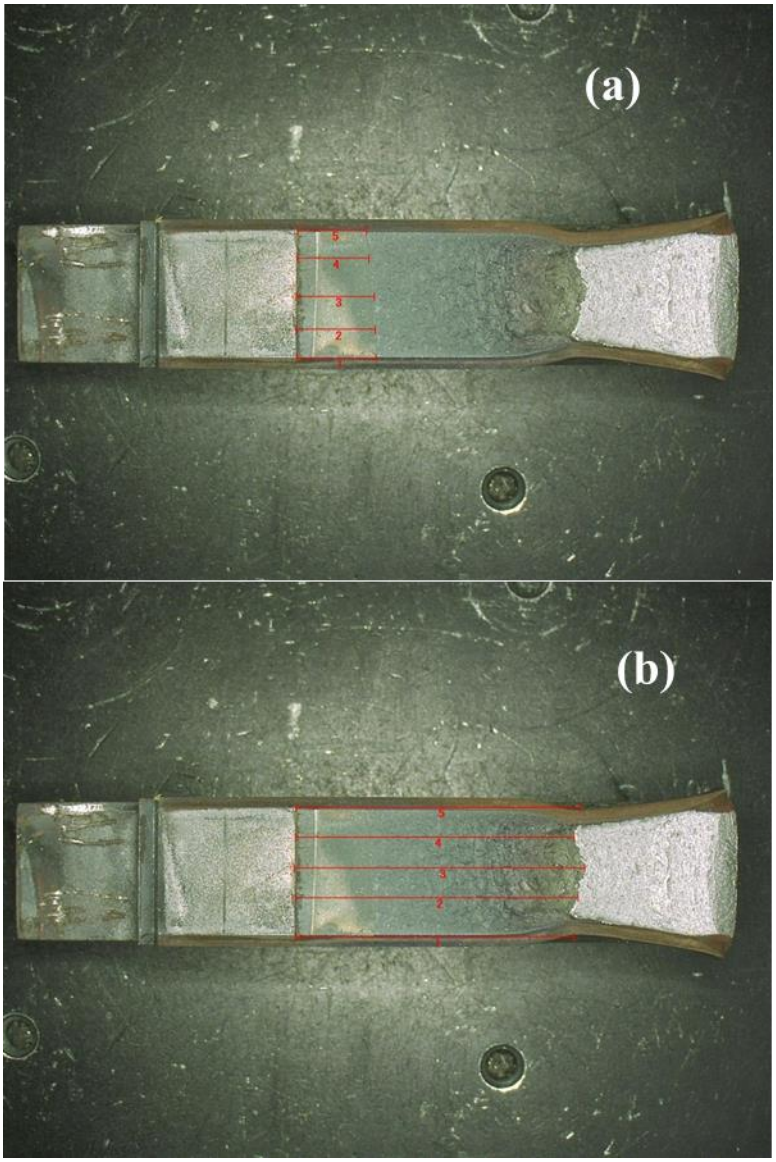

Figure 7.15. Crack extension (≈ 18 mm) in a zero hold time test. (a) pre-crack, (b) final crack length. Courtesy of WMTR, Youngstown, PA.

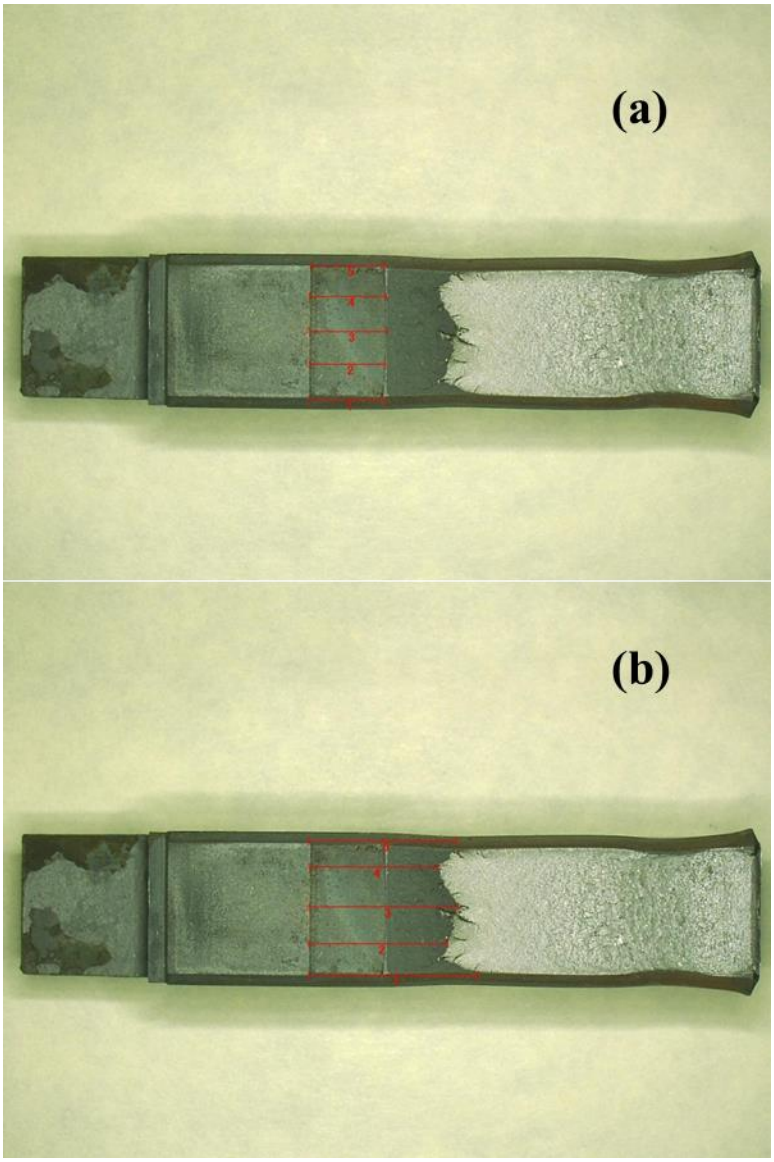

Figure 7.16. Crack extension (≈ 11 mm) in a 60 seconds hold time test. (a) pre-crack, (b) final crack length. Courtesy of WMTR, Youngstown, PA.

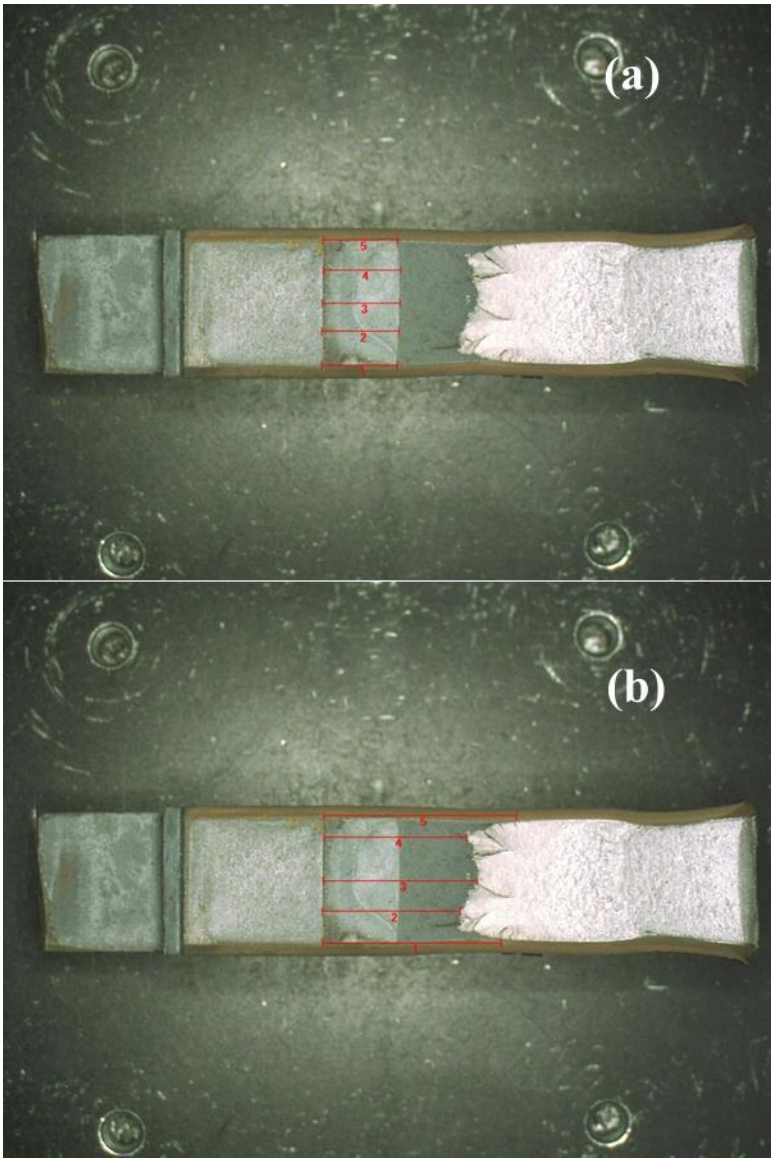

Figure 7.17. Crack extension (≈ 6 mm) in a 600 seconds hold time test. (a) pre-crack, (b) final crack length. Courtesy of WMTR, Youngstown, PA.

CHAPTER 8

Fatigue and Creep-Fatigue Crack Growth Experiments using DEN(T-C) specimens

8.1 Experimental Procedure

Preliminary fatigue crack growth tests were conducted in laboratory air conditions and creep-fatigue crack growth tests were conducted at elevated temperature of 625°C. These tests were performed at BiSS Research and Westmoreland Testing and Research using servo-hydraulic test machines. Figure 8.1 shows a setup of one of the test machine used for creep-fatigue crack growth testing of DEN(T-C) specimen.

Alignment was achieved by the use of self-aligning and self-locking low cycle fatigue grips. These grips were specifically machined for elevated temperature testing. The specimens were mounted using specially designed cups made from an Inconel alloy intended for use in elevated temperature applications. The holding cups were then hand tightened to the actuator. A tensile preload was applied to self-align the specimen using spherical seats that are provided in the grip assembly. This process ensured that there was no backlash during tension-compression testing. At the start of each test, the specimens were cycled at loads below the test loads to ensure that all systems were operational.

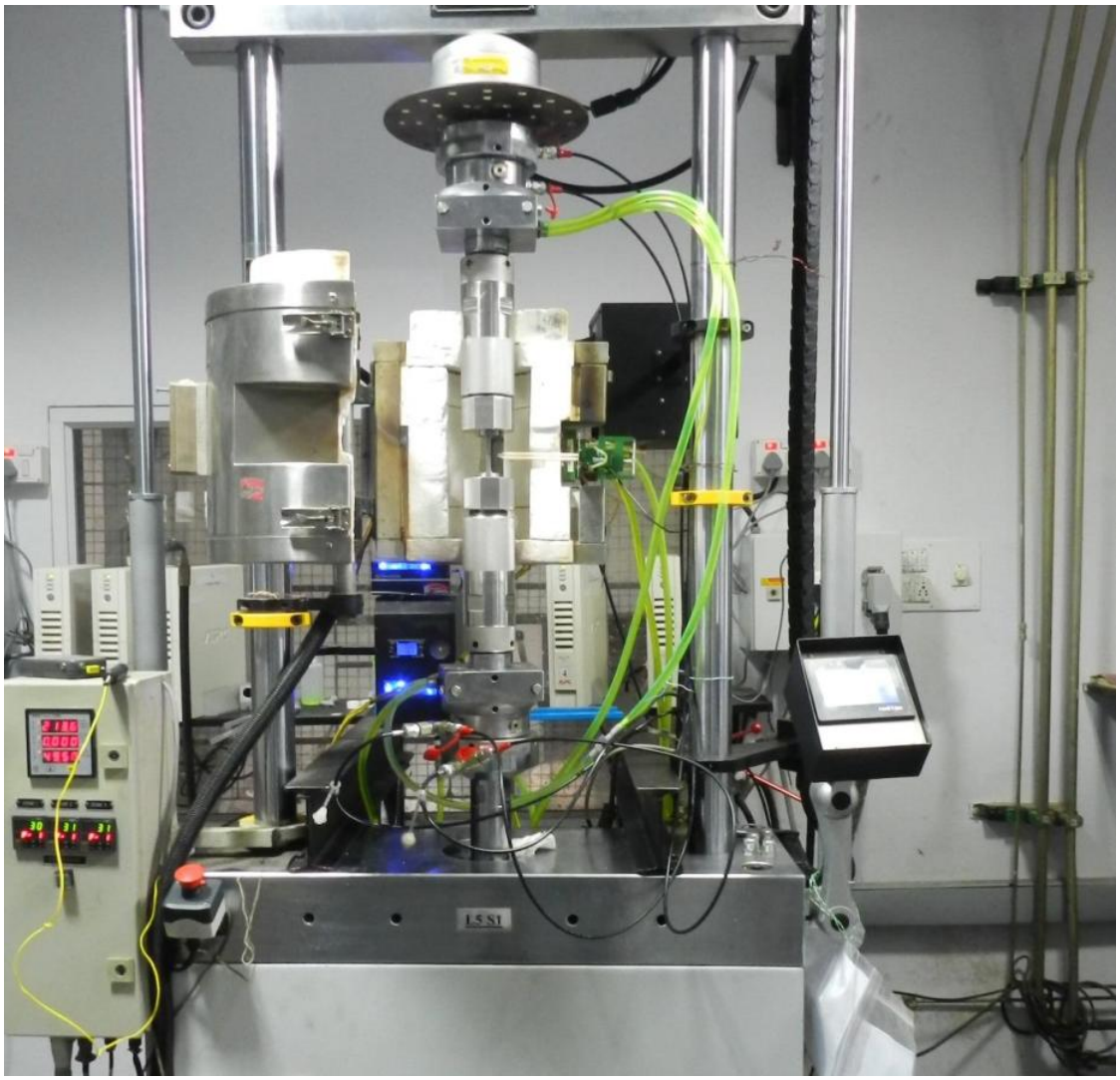

Figure 8.1. A picture of C-FCG testing set-up with a DEN(T-C) specimen loaded for testing in a 3 control zone conventional resistance furnace based heating system. Courtesy of BiSS, Bangalore.

8.1.1 Pre-Cracking

Fatigue pre-cracking is significant in a specimen such as DEN(T-C). It provides a sharpened fatigue crack of satisfactory size, straightness, symmetry and also ensures that the effect of the machined starter notch is removed from the specimen response. It also ensures that there are no load history effects that can affect the subsequent crack growth data [12]. Since crack asymmetry is a potential problem with DEN specimens, it was chosen to pre-crack the specimens by "compression-compression" loading. This pre-cracking procedure is commonly referred to as Compression Pre-cracking Constant Amplitude (CPCA) loading [94].

In the CPCA method, a small fatigue crack is produced at the crack tip which naturally stops growing. A tensile residual-stress field instead of the typical compressive residual stresses from tension-tension cycling envelopes the crack tip. A crack grown by this method is fully open before the start of the constant amplitude loading indicating that the crack has reached a threshold under compression-compression loading. Typical crack length from compression-compression pre-cracking were about 0.4mm (±0.2 mm) in length resulting from compression cycling at load ratio, R, of 0.3 at a nominal frequency of 10 HZ and 100,000 cycles. Compressive load levels required to produce fatigue cracks were estimated from the following relationship:

$$\frac{|K_{cp}|}{E} = 0.000091\sqrt{m}$$

where K_{cp} is the maximum compressive stress-intensity factor during compression pre-cracking and E is the elastic modulus. It was suggested by Newman that, $|K_{cp}|/E$ required to produce a starter pre-crack for steels is about $0.00015\sqrt{m}$ [95]. It was found from trial and error during pre-cracking, $|K_{cp}|/E$ of $0.000091\sqrt{m}$, which corresponds to maximum compressive load of 50 KN was satisfactory enough to produce a pre-crack.

Following compression pre-cracking, the specimen was pre-cracked using constant-amplitude loading at loads below the actual tests loads. Once crack-growth was detected, the fatigue crack was extended several compressive plastic-zone sizes from the notch tip to avoid potential transient effects resulting from the compressive loading and the resulting tensile residual stresses. It was observed during the several runs of the compression pre-cracking that the specimen did not exhibit any signs of buckling under such high compressive loads. It is noted that the pre-cracking procedure employed in this research served as one of the validation criteria of the specimen design. Because, the specimen was essentially optimized such that the chances of buckling are minimal and also the stress intensity factor is not highly sensitive to the chosen H/W value of 1.2.

8.1.2 Crack Length Measurements

An electric potential system consisting of a constant current supply and a multiple gain amplifier was used to monitor the physical crack length (a) on each specimen. Electric potential probes were attached to the front face of each specimen on either side of the specimen notch. Current leads were attached to the top and the bottom of each specimen in order to provide a uniform current flux in the specimen gage section. In addition, a room temperature crack opening displacement gage and high temperature extensometer were mounted to the knife edge fixtures to monitor the crack length and load-line displacement (see figure 8.3). Deflections at the load-line were measured experimentally with the help of knife edges mounted at H/W ≈1.87. The schematics of this arrangement are shown in the figure 8.2**.** This is the location where deflections were predicted using FEA.

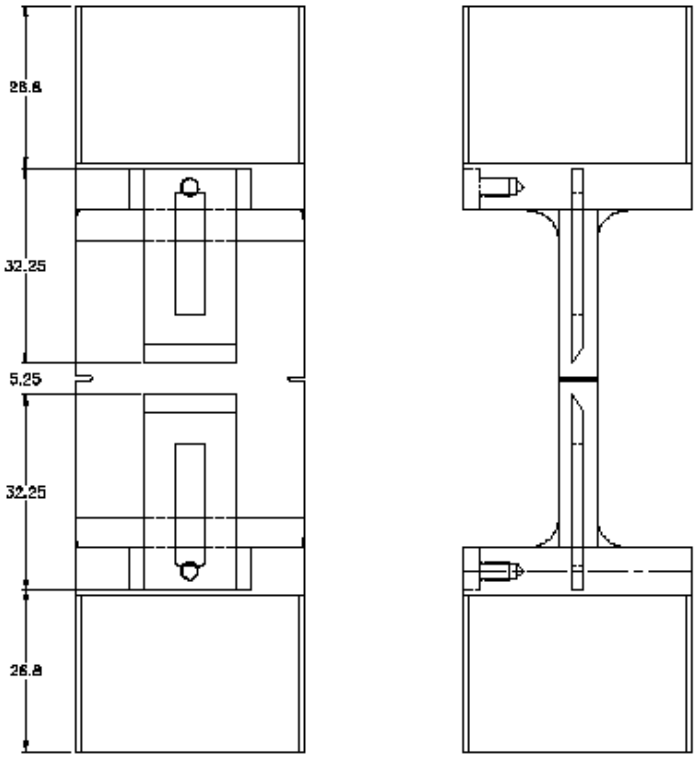

Figure 8.2. Schematic of measuring load-line deflections in DEN(T-C) specimens.

Figure 8.3. (a) Crack opening displacement gage and (b) High temperature extensometer. Courtesy of BiSS, Bangalore, India.

The tests were normally stopped prior to fracture and cooled to room temperature and, subsequently subjected to cyclic loading at room temperature to break open the specimen. This practice helps in accurately determining the crack extension during the creep-fatigue loading. The crack size at five equally spaced points centered on the specimen mid-thickness line was measured at the end of the pre-crack and at the end creep-fatigue portion of the test as shown in the figure 8.4. The initial crack size, a_0, and the final crack size, a_f, were then calculated by averaging the five measurements along the crack front. Crack asymmetry is a problem with the DEN(T-C) specimen. In general, the crack lengths for the two notches are averaged. The criteria for data validity with respect to the maximum difference between the two cracks is discussed in Section 8.3. Having measured the initial and the final crack size, the crack size at any instant was then calculated using the following equation [8,11]:

$$a = a_0 + \left(a_f - a_0\right) \times \frac{V - V_0}{V_f - V_0} \tag{8.1}$$

where a_f , a_0 , a are the final, initial and instantaneous crack lengths, respectively and V_f , V_0 and V are the corresponding final, initial and instantaneous value of the PD voltage. The crack length was also measured using the unloading compliance technique in some cases for comparison with the crack length measured by potential drop. The crack length can be measured using the developed elastic compliance expression for DEN(T-C) specimen:

$$\frac{a}{W} = C_0 + C_1(U_x) + C_2(U_x)^2 + C_3(U_x)^3 + C_4(U_x)^4 + C_5(U_x)^5 \tag{8.2}$$

Where $$U_x = \frac{1}{\left(\frac{BEV}{P}\right)^{1/2} + 1}$$

The regression coefficients for the load-line location given by:

C_0 = 8.90, C_1 = -36.20, C_2 = 11.77, C_3 = 0.02, C_4= 520.89, C_5 = -881.3

Note that B is replaced by effective thickness, B_e in equation 8.2 to account for side-grooving and this is used for the elastic unloading compliance measurement of crack length. The equation for B_e in ASTM E1820 is:

$$B_e = B - {(B - B_N)^2}/{B} \tag{8.3}$$

where B is thickness, B_N is net thickness - distance between the roots of the side grooves in side-grooved specimens, B_e is effective thickness - for side-grooved specimens.

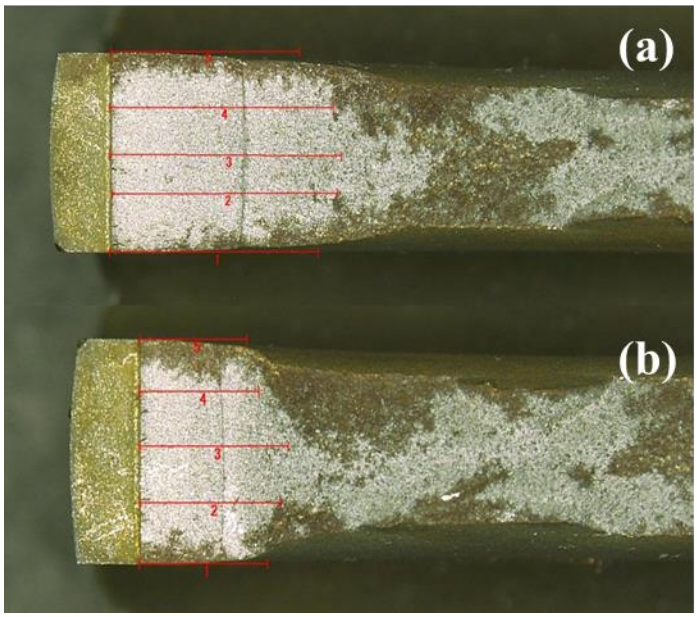

Figure 8.4. Pre-crack and final crack length measurement for (a) Notch 1 (b) Notch 2. Courtesy of WMTR, Youngstown, PA.

8.1.3 Test Procedure

Preliminary fatigue crack growth rate tests were conducted on the low strength steel – C15 or AISI 1015 using the conventional sinusoidal waveform. These tests were conducted in ambient laboratory air conditions. Figures 8.5 and 8.6 shows the load versus displacement record and compliance measured from one of the tests conducted.

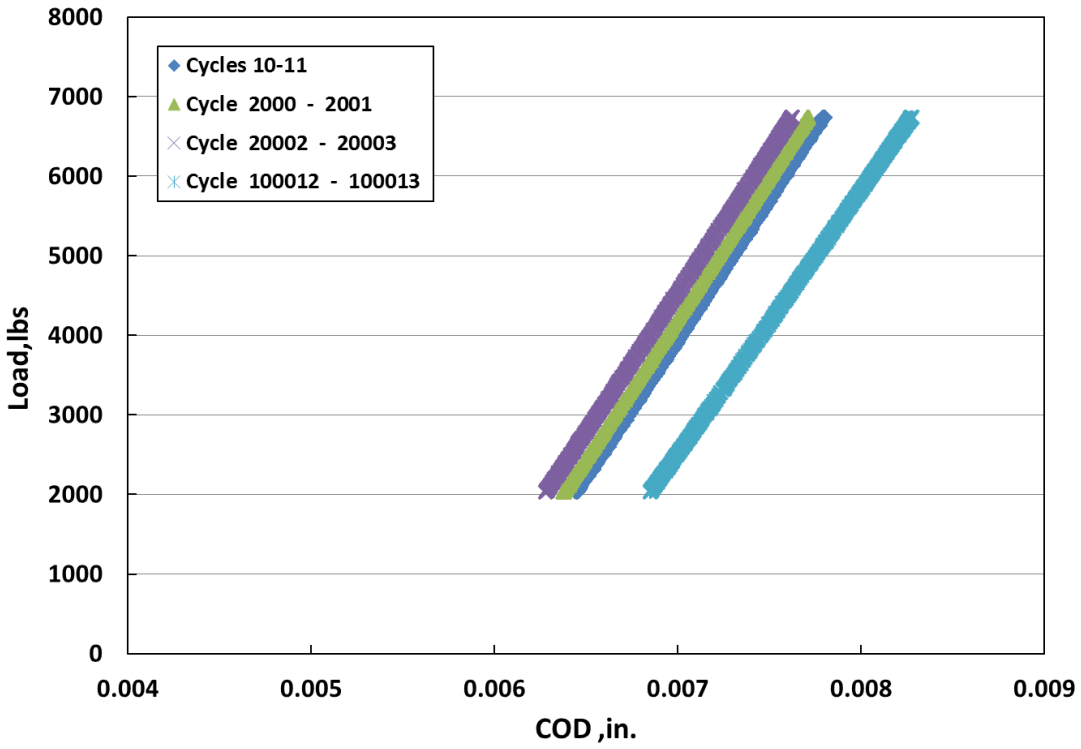

Figure 8.5. Load versus displacement record for fatigue crack growth rate test conducted at ambient air conditions.

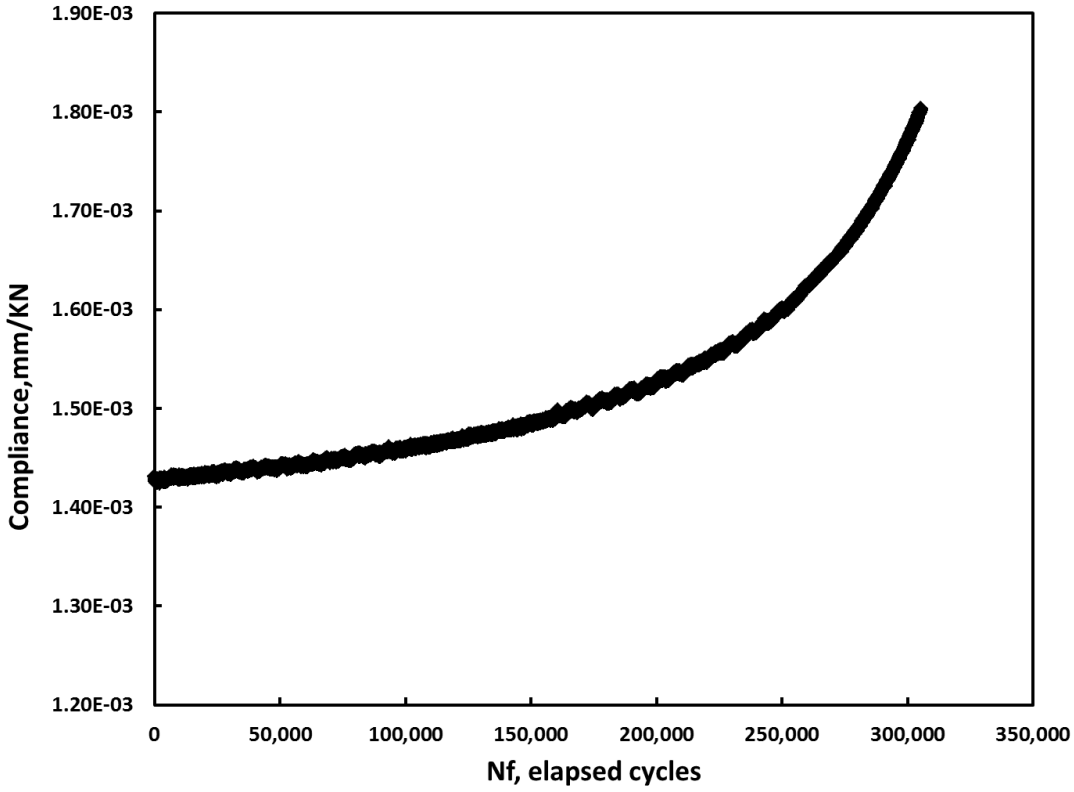

Figure 8.6. Measured compliance for DEN(T-C) specimen using COD gage.

Creep-fatigue crack growth tests were conducted for hold times of predetermined duration (0, 60 seconds) that were superimposed on the triangular waveforms at maximum load as shown in the figure 8.7. These tests were carried out at 625°C using 9Cr-1Mo steels. In the hold time tests, the specimen was first cycled for 10 cycles under load-controlled conditions at R = 0.1 with ramp-up and ramp-down time of 2 seconds to establish the baseline data. The subsequent cycles were then run under load controlled conditions for the loading and the hold time portion of the waveform. At the end of the hold time, the specimen was unloaded to a displacement value that is equal to 0.1 (maximum displacement). In other words, the mode was switched to displacement control during unloading. Thus, the specimen displacement at the load-line due to plastic and/or creep strains are reversed by switching the mode to displacement

control during unloading. It is noted that the loading and hold time portion of the waveform are identical to waveform used in testing of C(T) specimen. The unloading time (ramp down) was marginally higher than the 2 seconds. This ensured that the extensometer had sufficient time to reverse the displacement to 0.1 (maximum displacement). The tests were stopped when the compressive load reached its fully reversed state (R = -1) or when the minimum displacement reached....05 mm, whichever occurred first.

The minimum and maximum load, load-line displacements at minimum, maximum and hold time positions, unloading compliance, PD voltage, test temperature were continuously monitored and recorded during the tests. Figure 8.8 shows the compliance measured from one the tests conducted. It can be observed from the figure**,** there was considerable scatter in the measured compliance using the set-up illustrated in figure 8.3 (b). Some possible explanations are:

The HT extensometers with the ceramic rods have flat ends that are seated freely on the knife edge fixtures, unlike the COD gage which has a small knife edge machined onto its steel plates and are firmly secured to the fixtures as shown in figure 8.3 (a). Hence, the quality of the measured compliance using COD gage is much better as seen in figure 8.6**.** As the displacement changes during the loading/unloading/ dwell process in a given cycle, the friction between the flat ends of the ceramic rods and the knife edge fixtures can produce inherent scatter in the data. Presumably, this contact will affect the quality of the measured compliance data. This is further amplified by switching back and forth between load and displacement control in a given cycle.

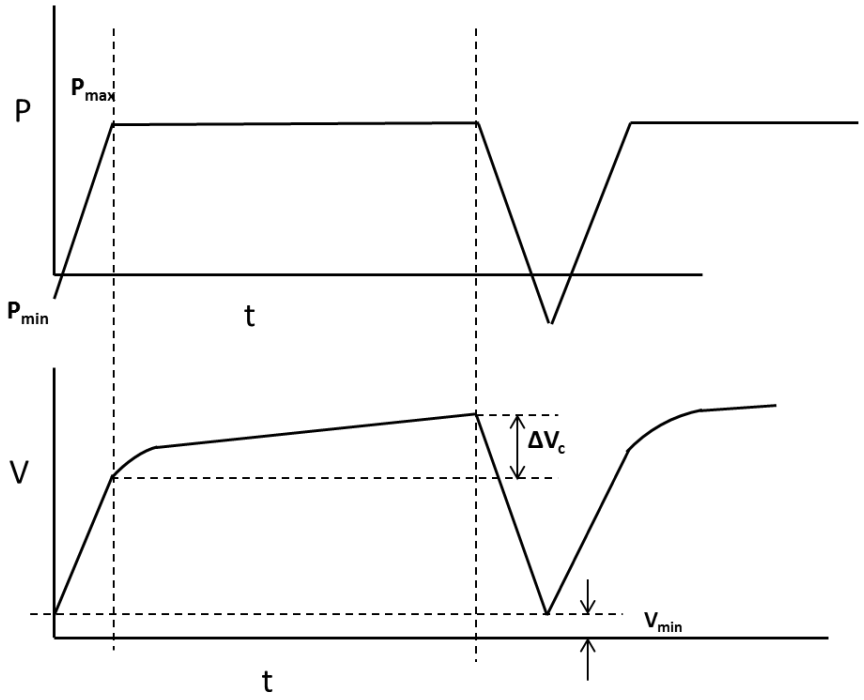

Figure 8.7. Cyclic loading and measurements made during testing for double- edge-notch tension-compression, DEN(T-C), specimen.

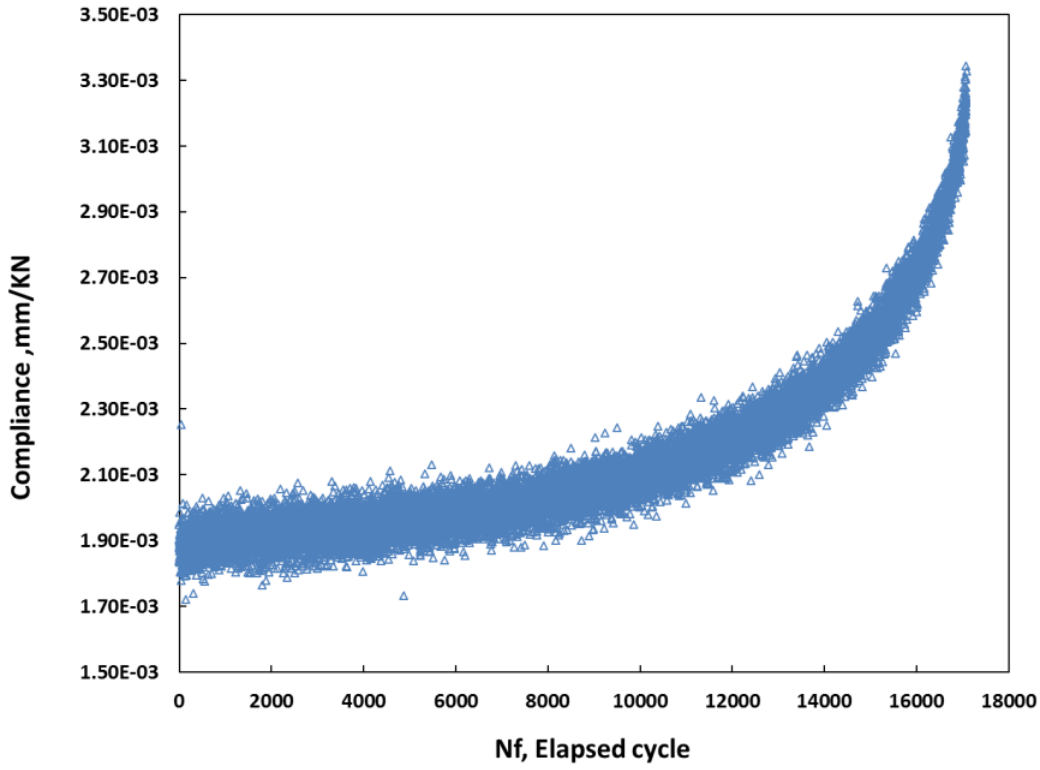

Figure 8.8. Measured compliance for DEN(T-C) specimen using HT extensometer.

8.2 Overview of the Tests Conditions

Table 8.1 and 8.2 summarize the fatigue and creep-fatigue crack growth test conditions. For the room temperature fatigue crack growth tests on the C15 steel, the starting ΔK levels varied from 10 to 18.3 MPa√m. The zero hold time or continuous cycling tests had a starting ΔK of 16.0 MPa√m. The 60 seconds hold time tests were started with ΔK level of 25.2 MPa√m for which the corresponding load level was 54 KN. This load was deemed too high as the tests lasted only for about 100 cycles. Thus the second 60 seconds hold time test had a lower starting ΔK level of 11.8 MPa√m. These load levels ensured that each test yielded sufficient crack growth data. Data reduction techniques described in section 7.2 are applied for DEN(T-C) specimens as well.

Table 8.1. Summary of fatigue crack growth test conditions.

Specimen ID	Max Load, KN	Initial ΔK MPa√m	Final ΔK MPa√m	Initial Crack length, mm	Final Crack length, mm	Nf, Cycle
W-DEN(T-C)1	30	10	17.2	3.7	9.6	305180
W-DEN(T-C)2	45	15	27	3.5	8.9	153715
BD-DEN(T-C)3	65	18.30	30.39	2.3	8.1	67427
CT-1	16	19.2	68	12	32.6	121648

Table 8.2. Summary of creep-fatigue crack growth test conditions.

Specimen ID	Hold time Seconds	Max Load, KN	Initial ΔK, MPa√m	Final ΔK, MPa√m	Initial Crack length, mm	Final Crack length, mm	Nf Cycles
BSP-DEN1	60	54	25.2	60.4	3.5	5	107
BSP-DEN2	60	30	11.8	35.1	2.5	4.6	1068
BK-DEN3	0	35	16.20	37.37	3.5	12.66	17084

8.3 Results and Discussions

8.3.1 Experimental Validation of Compliance Equation

A crack opening displacement gage suitable for use at room temperature only and a high temperature extensometer were used in fatigue crack growth tests to monitor the crack length. Deflections at the load line were measured experimentally with the help of knife edges mounted at $H/W \approx 1.87$. The schematics of this arrangement were shown in the figure 8.2. The figure 8.6 shows the compliance measured from one of the tests conducted. Overall, the compliance response was found to be satisfactory. The crack length was also monitored by the EPD probes attached to the two notches, which provided an independent measurement of the crack length.

It was observed from the tests that the crack length calculated from the measured compliance was very close to an average of the crack length measured by the potential drop at the two notches. This is because the deflections at the load-line are uniform in nature due to the heavier cylindrical sections. We also note here that the experimental observations are consistent with the numerical analyses where uniform displacement boundary condition was used for stress analysis for this specimen.

Since crack asymmetry is a problem with the DEN(T-C) specimen, the crack growth data was analyzed such that the maximum difference between the two cracks were 2 mm out of an overall crack length of about 11 mm (Notch 1+ Notch 2). This 2 mm difference is approximately 5 % of the specimen width of 38.1 mm indicating crack asymmetry is not a severe problem for the data from this test. These results are consistent with the recent work of Wire and Mills [63] for similar type of specimen geometry.

During the tests on C15 steel (AISI 1015) for deep cracks, experimentally measured compliance was found to be in good agreement with the current equation as shown in the figure 8.9. Here the measured crack length to width ratio of the specimen is compared with the computed compliance (CBE). Some slight discrepancies occurred in the range of a/W from 0.1-0.15. This is because the percent error in the current compliance equation is greater than 2 % at lower a/W values (0.1-0.2). Never the less, the overall agreement between the measured and calculated crack length to width ratios from the compliance was very satisfactory.

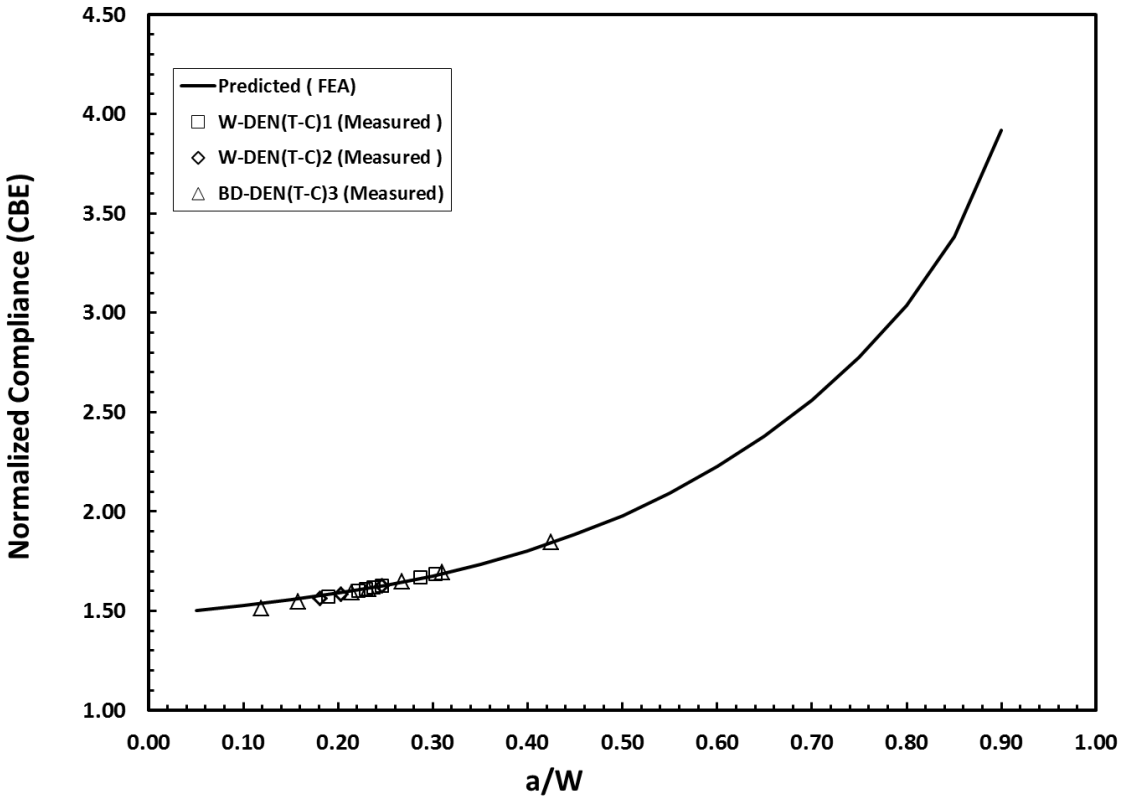

Figure 8.9. Comparison of measured and calculated normalized compliance against crack-length-to-width (a/W) ratio.

In the tests conducted, it was observed that the difference in crack length between the two notches starts to increase rapidly after $a/W \approx 0.45$. If we include the data such that the difference between the two cracks are greater than 2 mm, the compliance value measured from the current equation at the end of the test still corresponded to an average of crack length of the two notches. If we plot the measured crack length to width ratio of the specimen with the computed compliance (CBE), the agreement between the measured and the predicted would still agree with each other (figure 8.10), thus, validating the developed compliance equation for the DEN(T-C) specimen.

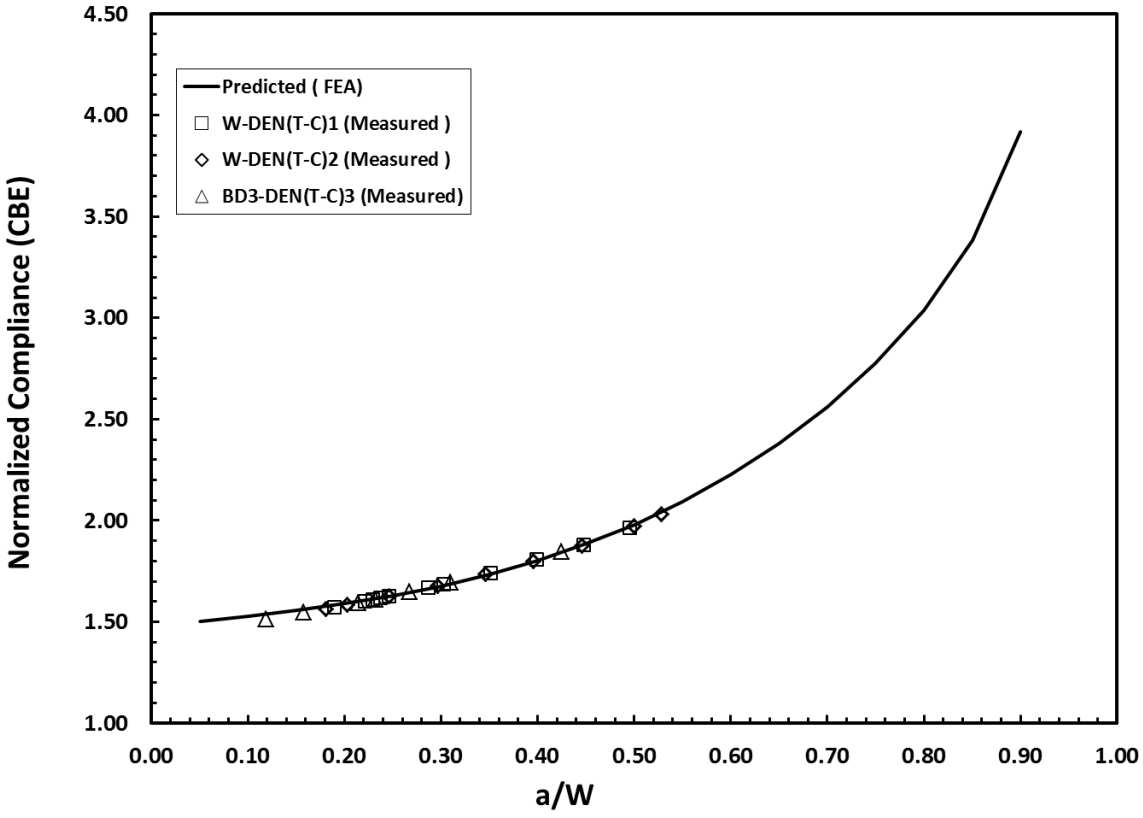

Figure 8.10. Comparison of measured and calculated normalized compliance against crack-length-to-width (a/W) ratio. This plot includes compliance data for the DEN(T-C) specimen where the difference in crack length between the two cracks are greater than 2 mm.

8.3.2 Experimental Validation of Stress-Intensity Factor Equation

Preliminary fatigue crack growth tests were conducted on DEN(T-C) specimen at a load ratio, R = 0.3 using C15 steel (AISI 1015). Under the same load ratio, a C(T) specimen was used to generate fatigue crack growth rate data on the C15 steel. All tests were conducted in ambient laboratory air conditions. Constant load amplitude loading was selected to run these tests with frequencies ranging from 10 Hz to 1 Hz. The lower frequencies were chosen for some of the tests to make optical measurements. In order to have overlapping crack growth data, the starting ΔK levels varied from 10 MPa√m to 19 MPa√m for the tests conducted. These load levels ensured that each test yielded sufficient crack growth data.

A comparison of crack growth rate trends from DEN(T-C) tests and the selected C(T) specimens are shown in figure 8.11. In this case, the crack growth data was analyzed such that the maximum difference between the two cracks were 2 mm out of an overall crack length of about 11 mm (Notch 1+Notch 2). The open symbols are the results for the DEN(T-C) specimens and the closed symbols are the results from a C(T) specimens. It can be observed from the plot of da/dN versus ΔK that the DEN(T-C) and C(T) data are in good agreement in the intermediate crack growth rate regime. The differences in the crack growth data are due to using the secant method to reduce the scatter in the data, instead of the seven point incremental polynomial method (smoothing). Studies have shown that the secant method is more sensitive to metallurgical features than the polynomial smoothing method [94].

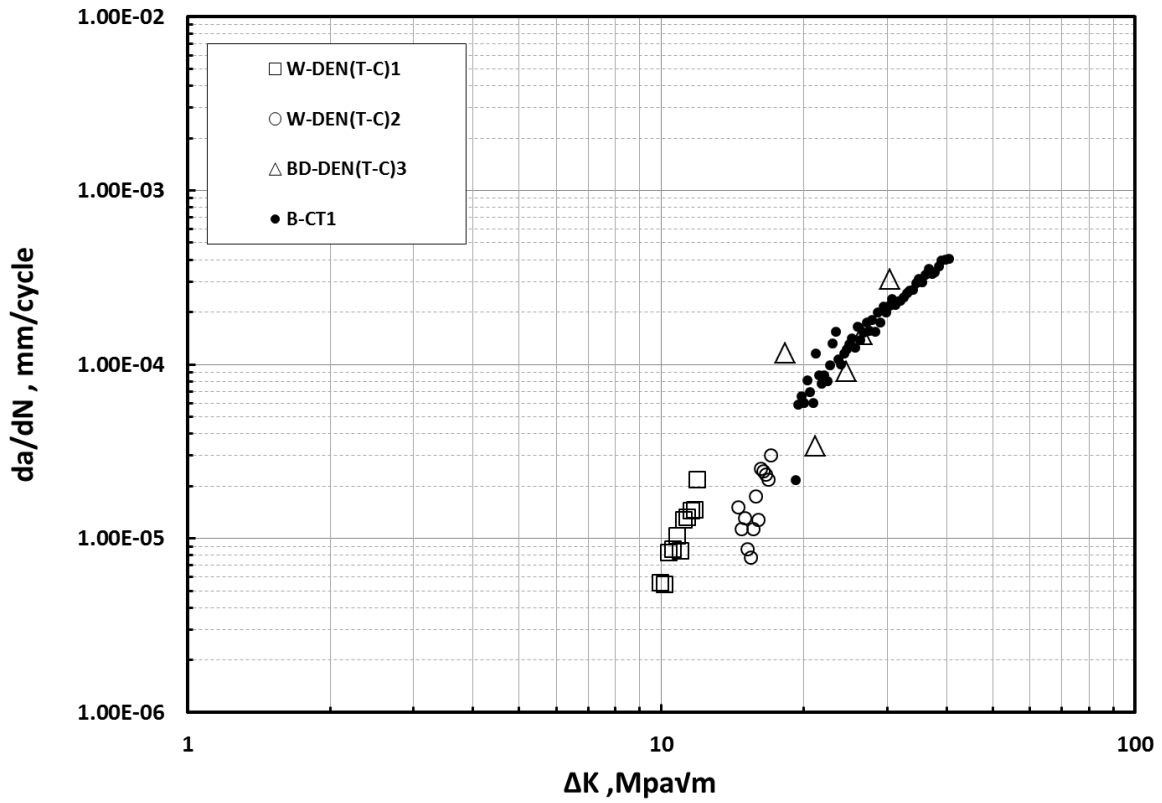

Figure 8.11. Comparison of fatigue crack growth rate behavior of C15 steel using DEN(T-C) and C(T) specimens.

If the data were analyzed such that the difference between the two cracks are greater than 2 mm, the crack growth data for DEN(T-C) and C(T) data would still fall within a narrow scatter band as shown in the figure 8.12. Thus, validating the stress-intensity factor equation for DEN(T-C) specimen.

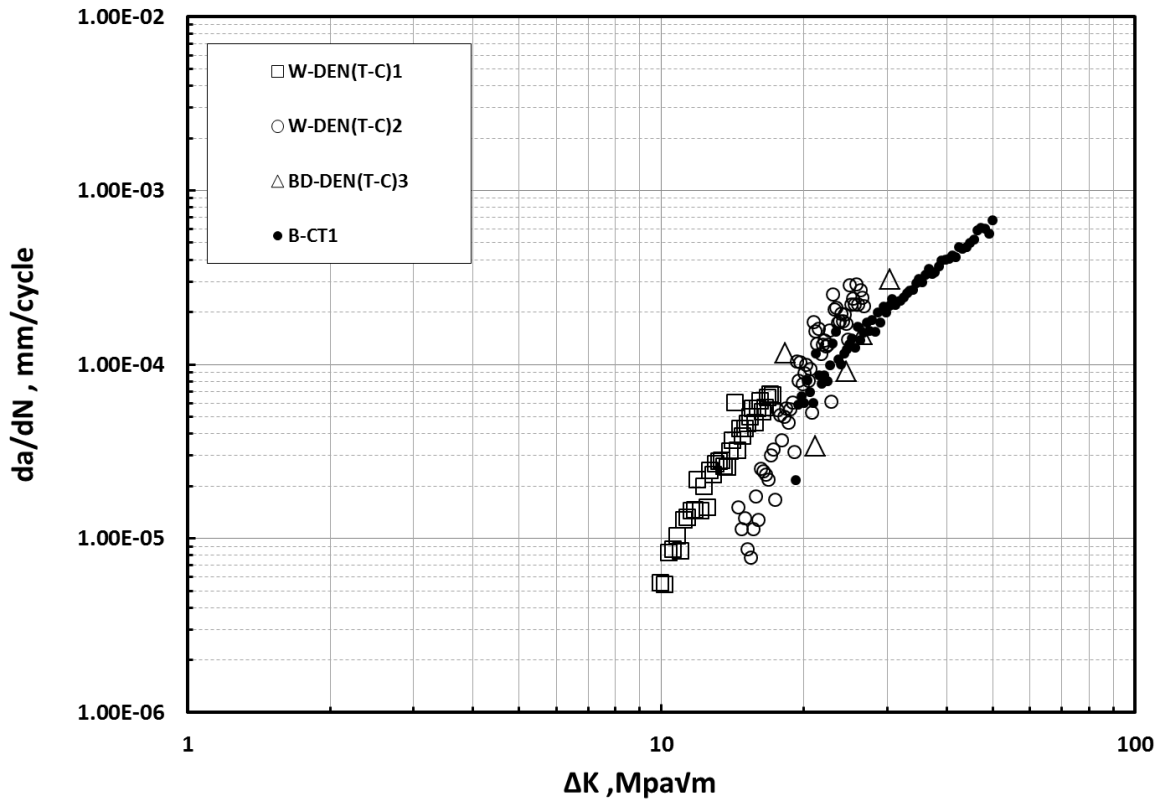

Figure 8.12. Comparison of fatigue crack growth rate behavior of C15 steel using DEN(T-C) and C(T) specimens. This plot includes crack growth data for the DEN(T-C) specimen where the difference in crack length between the two cracks are greater than 2 mm.

8.3.3 Creep-Fatigue Crack Growth Behavior

Zero hold time tests were conducted on the 9Cr-1Mo steels at 625°C using the DEN(T-C) specimens under constant-amplitude load controlled conditions ($R = 0.1$). This enables to establish the baseline data and for comparison with the zero hold time tests conducted using the C(T) specimens. The 60 seconds hold time tests were conducted by reversing the accumulated displacement at the load line during unloading. For this case, the minimum loads are compressive. The compressive load increases with every cycle. As creep deformation

accumulates with every cycle, the maximum displacement in a given cycle increases. Thus, to reverse the displacement back to its initial state, the load required will be increasingly compressive in nature.

Figure 8.12 shows the crack growth rate behavior of 9Cr-1Mo steel at 625°C as a function of stress-intensity factor range for the hold times of 0 and 60 seconds for the tested C(T) and DEN(T-C) specimens. The open symbols are the results for the DEN (T-C) specimens, while the solid symbols shows the results for the C(T) specimen discussed in chapter 7. In general, creep-fatigue crack growth data exhibit scatter. There are a couple of outliers in the data trends in figure 8.12 that are due to compliance measurement issues discussed in section 8.1.3.

It can be noted from the figure 8.12 that the crack growth data generated under creep-fatigue conditions for DEN(T-C) specimen correlated well with the crack growth rate data generated using C(T) specimens. In general, as expected, the crack growth rate increases with increase in hold time and stress-intensity factor range, ΔK. An overall reasonable correlation between crack growth rate and ΔK is an indication that dominantly linear elastic conditions were maintained in the various test specimens throughout the testing. For the tests conducted in this study using DEN(T-C) specimens, the creep deflections during the hold time could not be reliably measured. This is not unexpected considering that the displacements during one cycle are very small in a short hold time tests making the measurement not as reliable. Thus, it remains a problem to be solved in the future.

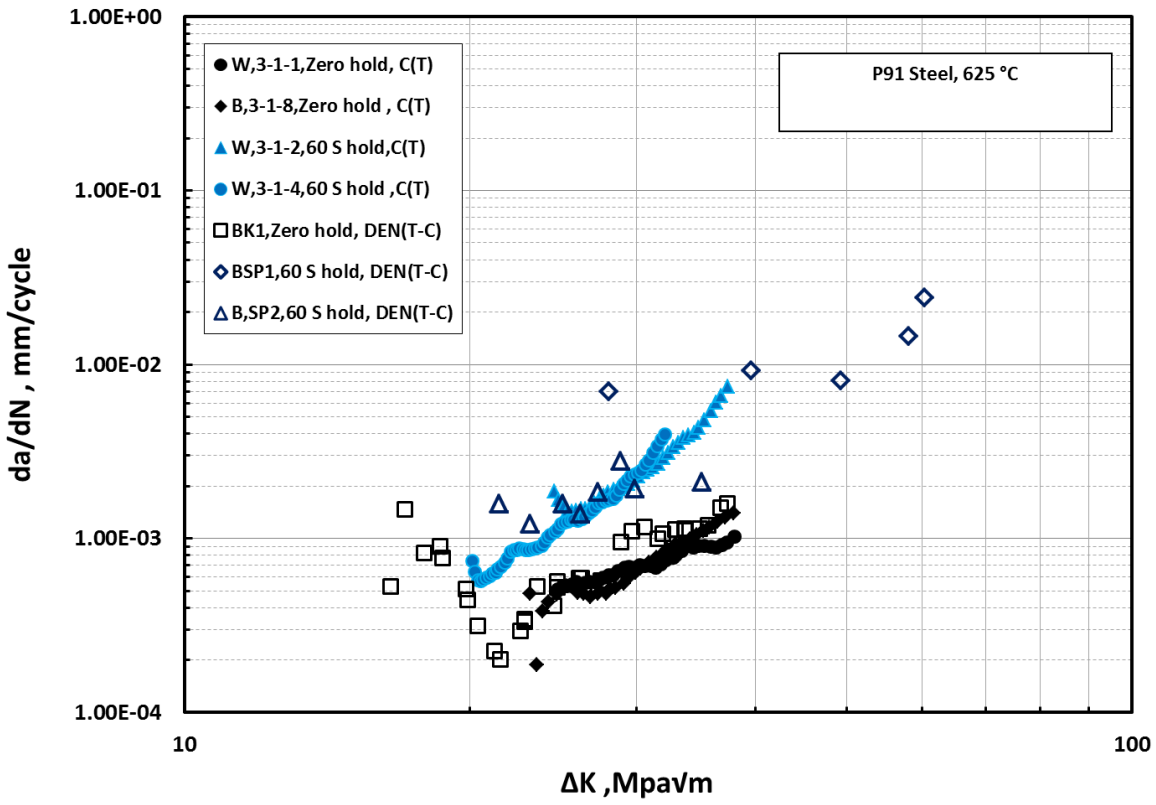

Figure 8.13. Comparison of Creep-fatigue crack growth rate behavior (P91 steel) for DEN(T-C) and C(T) specimens using ΔK parameter.

CHAPTER 9

Scientific and Technological Contributions

In summary, this research should have broad impact and will serve as a guide for creep-fatigue testing performed in support of activities such as materials research and development, mechanical design, process and quality control, product performance, and failure analysis. Structural components are typically operated under a variety of loading conditions at elevated temperatures leading to complex start up and shut down events. Crack growth properties are often required to evaluate the structural integrity under the presence of detected or postulated flaws. Therefore, for sound design considerations, a good understanding and predictive capability for the creep-fatigue crack growth behavior under various loading conditions is required.

The present work focuses on evaluating the creep-fatigue crack growth behavior under various loading conditions such as tension-tension and tension-compression. The scientific contributions of the study include the development and validation of double-edge-notch specimen design for use in tension-compression fatigue and creep-fatigue crack growth testing for the first time to the best of our knowledge. For example, techniques to measure crack growth using unloading compliance for DEN(T-C) specimen have been developed as a part of the work and the results have been compared with those from the electric potential technique. Also, expressions have been developed to estimate the values of crack tip parameters such as stress intensity parameter,K, the J-Integral and the cyclic J-Integral ΔJ, the C^* -Integral, the C_t – Parameter and the $(C_t)_{avg}$ parameter for the DEN (T-C) specimen.

Fatigue crack growth experiments were carried out to validate crack growth results obtained from DEN(T-C) specimens using the C(T) specimen data as the benchmark. There were

some issues with regard to uneven crack growth in the DEN(T-C) specimens but notwithstanding those, the usefulness of DEN(T-C) specimens for crack growth studies under displacement controlled conditions to combat ratcheting problems in tests conducted under load conditions has been established. Perhaps implementing better alignment control procedure will address the issue of uneven crack growth.

The overall C-FCG RR program led by the University of Arkansas was designed to meet several objectives that range from studying crack growth behavior in grade P91 steel to contributing to C-FCG test standard development. As a part of this effort, constant load-amplitude creep-fatigue crack growth testing were successfully performed using C(T) specimen using procedures specified in ASTM E-2760. For example, the importance of directly measuring the change in deflection during hold time for all creep-fatigue testing were demonstrated by comparing the differences between the calculated values of $(C_t)_{avg}$ and those based on measured values of load-line deflection. A major contribution also included the optimization of test temperature, loading conditions, and the hold-time durations, for use in the future round-robin tests. The results of this work and the future round-robin exercise will be used to primarily formulate a definitive precision and bias statement for supporting the test standard ASTM E-2760.

The acquired knowledge could immeasurably assist the future researchers and engineers pursuing creep-fatigue crack growth studies using various test specimens and loading conditions. Knowledge of the crack growth behavior will also aid in the selection of appropriate inspection intervals and remaining- life assessment procedures, thus minimizing the risk of catastrophic structural failures.

CHAPTER 10

Conclusion and Recommendation for Future Work

10.1 Conclusions

DEN(T-C) Specimens:

A Double-Edge-Notch Tension-Compression, DEN(T-C), specimen is designed and optimized using linear elastic fracture mechanics analysis. This specimen geometry allows the user to efficiently obtain fatigue crack growth data under displacement controlled test with least load misalignment. Two-dimensional (2-D) Finite Element and boundary element analysis were used to obtain stress-intensity factors and displacements over a wide range in crack-length-to-width (a/W) ratios. These investigations reveal that there exist strong influence between the gage length and stress-intensity factor and displacement values. A height-to-width, H/W of at least 1.2 was required to ensure that the stress-intensity and displacements are not highly dependent of gage length. It was also shown that the boundary correction factor, $F(a/W)$, does not approach 1.12 in the limit as the crack length approaches zero for the boundary condition of uniform remote displacement with u = 0 along the loading section for DEN(T-C) specimen. Expressions for calculating the stress intensity factor, elastic deflections at the load line and crack mouth, and compliance equation are provided for a wide range in crack-length to width (a/W) ratios for the DEN(T-C) specimen geometry.

The DEN(T-C) specimens were pre-cracked by compression-compression loading during which the specimen was subjected to high compressive loads. The specimen did not exhibit any signs of buckling, suggesting that the chosen height to width ratio, $H/W = 1.2$, and the specimen design provides sufficient buckling resistance under compressive loading.

Experimentally determined compliance values generated on fatigue crack growth tests on two metallic materials compared well with the calculated values. The fatigue crack growth data generated on the two metallic materials (C15 Steel and P91 Steel) suggest that the crack growth data are in good agreement in the intermediate crack growth regime for C(T) and DEN(T) specimens. The crack growth behavior of 9Cr-1Mo steel was investigated under creep-fatigue conditions at 625°C using C(T) and DEN(T-C) specimens. Crack growth data generated under creep-fatigue conditions using DEN(T-C) specimens correlated well with crack growth data generated using standard C(T) specimens when characterized with ΔK parameter.

C(T) Specimens:

Creep-fatigue crack growth behavior of 9Cr-1Mo steel was investigated at 625°C using C(T) specimens. ΔK and $(C_t)_{avg}$ parameters were used to characterize creep-fatigue crack growth data for the cycle-dependent crack growth and time-dependent crack growth rates, respectively. $(C_t)_{avg}$ was determined from experimentally measured load-line displacement rates during the hold time for the C(T) specimens. The load-line displacement rate was dominated by creep deformation making $(C_t)_{avg}$ the more appropriate parameter for characterizing time rates of crack growth for P91 Steels at 625°C. Following other observations and conclusions can be drawn from the experimental data:

- The crack growth rates increased substantially with hold time, when plotted with ΔK. However, the rates during the 60s hold time tests were higher compared to the rates during 600s hold time tests, when the time rates of crack growth were plotted with ΔK. Also, a transient behavior "hook" was observed in the crack growth rates at the beginning of each hold time test.

- The hooks disappeared from the data trends when the data was plotted with $(C_t)_{avg}$indicating that the correlation between crack growth rates and $(C_t)_{avg}$ was significantly better and unique. The average time rate of crack growth during hold-time was lower for the 600s hold time test than for the 60s hold time test. This is indicative of creep-fatigue interactions during crack growth and acceleration in crack growth due to fatigue cycling.
- Dominant- damage and the damage-summation models showed minimal differences for the crack growth data analyzed.
- Significant differences (factors of 2 to 5) were observed between the calculated values of $(C_t)_{avg}$ and those based on measured values of load-line deflection. This underscores the importance of directly measuring the change in deflection during hold time for all creep-fatigue testing.

10.2 Future Work

C(T) Specimens

A test program (round-robin) under the auspices of the American Society for Testing and Materials (ASTM) involving various participants from North America, Europe and Asia, is to commence in the latter half of 2013. The primary objective of the round-robin is to conduct testing to further validate the ASTM Standard E-2760 and to assess precision and bias in the data generated while using the procedures specified in this ASTM standard. The round-robin will be conducted using standard C(T) specimens using test material P91 steel**.** The following test conditions and procedure are recommended for conducting the creep-fatigue crack growth tests as part of the round-robin:

- Each Laboratory should follow the current version of ASTM standard E2760-10 to conduct at least two tests as part of their contribution to the round-robin and it is necessary that for tests with hold-time, load-line deflections be measured during the hold period.
- The test temperature of 625°C and the loading conditions and the hold-time durations of 60s and 600s used in the pilot tests are appropriate for conducting the tests.
- The specimen blanks are machined and ready to be shipped out as soon as the list of participants is finalized.

DEN(T-C) Specimens:

This research has opened up avenues for very exciting research in the future. The following recommendations for future explorations are presented:

- In order to reduce the scatter in the measured displacement/compliance data, the set-up shown in the figure 10.1 can be tried for future testing of specimens like DEN(T-C). The extensometer can be mounted directly on the specimen across the notch at a gauge length, say for example 0.5 in. (12.7 mm). We believe this configuration will provide more stability when we switch back and forth between load and displacement control. The extensometer needs to have pointed ceramic arms which will contact small holes on the load-line of the specimen. It is important to note here that this location of the deflection measurement is different from the ones used in this FEA work to derive the compliance expression and hence new expressions will be needed to monitor the crack length.

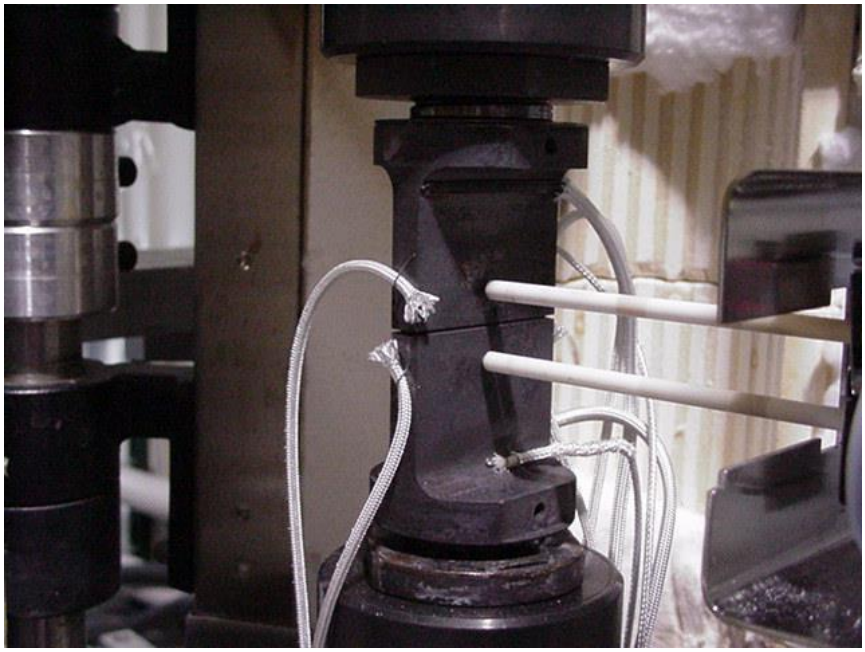

Figure 10.1. HT extensometer mounted directly on the load-line of DEN(T-C) specimen. Courtesy of WMTR, Youngstown, PA.

- Creep-fatigue crack growth tests were conducted by reversing the accumulated displacement at the load-line by switching the mode to displacement control during unloading. Although the current technique appears to work, it is recommended that future test using DEN(T-C) specimen be conducted under incremental displacement controlled conditions. This would eliminate the inherent scatter in the measured compliance data due to switching the control mode and also more crack extension can be obtained for a over a wide range in crack-length to width ratios (a/W).
- Special attention should be paid to alignment in the test fixtures to avoid uneven crack growth at the tips of the two notches.
- The current V-notch configuration in the DEN(T-C) specimen can be modified to have a blunt notch or notches of different radii. Thereby the user can conduct both crack initiation and crack growth tests out of the same specimen.

REFERENCES

[1] Grover, P.S., Saxena, A., Developments in Creep-Fatigue Crack Growth Testing and Data Analysis, In:ECF-10, Structural Integrity: Experiments, Models Applications Vol.1, 1-21 (1994).

[2] Saxena, A., Fracture Mechanics Approaches for Characterizing Creep-Fatigue Crack Growth, JSME International Journal, Series I (Solid Mechanics, Strength of Materials) 36(1), 1-20 (1993).

[3] Yoon, K.B., Saxena, A., McDowell D.L., Effect of Cyclic Overload on the Crack Growth Behavior during Hold Period at Elevated Temperature, International Journal of Fracture Vol.59, 199-211 (1993).

[4] Yoon, K.B., Characterization of Creep-Fatigue Crack Growth Behavior using C_t Parameter, Ph.D. Thesis, Georgia Institute of Technology , Atlanta , GA (1990).

[5] Adefris, N., Saxena A., McDowell D.L., Creep-Fatigue Crack Growth Behavior in 1Cr-1Mo-0.25V Steels. Part I: Estimation of Crack Tip Parameters, Fatigue Fracture Engineering Materials Structure 19(4), 387-99 (1996).

[6] Grover, P.S., Saxena, A., Characterization of Creep Crack Growth Behavior in 2.25Cr-1Mo Steel using $(C_t)_{avg}$, International Journal of Fracture 73, 273-286 (1995).

[7] Yoon, K.B., Saxena, A. Liaw, P.K., Characterization of Creep-Fatigue Crack Growth Behavior under Trapezoidal Waveshape using C_t-Parameter, International Journal of Fracture 59(2), 95-114 (1993)..

[8] ASTM E2760 -10e1: Standard Test Method for Creep-Fatigue Crack Growth Testing, (2010).

[9] Shibli A., Starr F., Some Aspects of Plant and Research Experience in the use of New High Strength Martensitic Steel P91 ,International Journal of Pressure Vessels and Piping 84, 114-122 (2007).

[10] Swindeman, R. W., Santella M. L., Maziasz, P. J., Roberts, B. W. and Coleman, K., Issues in Replacing Cr-Mo Steels and Stainless Steels with 9Cr-1Mo-V Steel, International Journal of Pressure Vessels and Piping 81, 507-512 (2004).

[11] ASTM E1457 - 07e4: Standard Test Method for Measurement of Creep Crack Growth Times in Metals (2007).

[12] ASTM E647-08e1: Standard Test Methods for Measurements of Fatigue Crack Growth rates (2008).

[13] Davies, C.M., Kourmpetis, M., O'Dowd, N. P., Nikbin, K. M, Experimental Evaluation of the J or C* Parameter for a Range of Cracked Geometries, ASTM STP 1480, 321-340. (2007).

[14] Dogan, B.,Ceyhan, U., Nikbin, K.M., Petrovski, B., Dean, D.W., European Code of Practice for Creep Crack Initiation and Growth Testing of Industrially Relevant Specimens, ASTM STP 1480 , 23-42 (2007).

[15] Scholz, A., Berger, C., Mueller, F., Klenk, A., Long-term Crack Behavior under Creep and Creep-Fatigue Conditions of Heat Resistant Steels, 5th International Conference on Advances in Materials Technology for Fossil Power Plants, October 3, - October 5, 718-732. (2008)

[16] Saxena, A., Nonlinear Fracture Mechanics for Engineers, Boca Raton, FL, CRC Press (1998).

[17] James, L. A., Effect of Frequency Upon the Fatigue-Crack Growth of Type 304 Stainless Steel at 1000 F, ASTM STP , 218-229 (1972).

[18] Plumtree, A., Yu, M., Influence of Waveform on the Fatigue Crack Propagation Rate of Stainless Steel at 570 C. Thermal and Environmental Effects in Fatigue: Research - Design Interface. Presented at the 4th National Congress on Pressure Vessel and Piping Technology, American Society of Mechanical Engineers 71, 13-19 (1983).

[19] Pelloux, R. M., Huang, J. S., Creep-Fatigue-Environment Interactions in Astroloy, AGARD Conference Proceedings 151-164 (1980).

[20] Floreen, S., Kane, R. H., An Investigation of the Creep-Fatigue-Environment Interaction in a Ni-base Superalloy, Fatigue of Engineering Materials and Structures 2(4), 401-12 (1979).

[21] Saxena, A., Model for Predicting the Environment Enhanced Fatigue Crack Growth Behavior at High Temperature. Thermal and Environmental Effects in Fatigue: Research - Design Interface. Presented at the 4th National Congress on Pressure Vessel and Piping Technology, American Society of Mechanical Engineers 71,171-184 (1983).

[22] Saxena, A., Williams, R. S., Shih, T. T., Model for Representing and Predicting the Influence of Hold Time on Fatigue Crack Growth Behavior at Elevated Temperature. Fracture Mechanics 86-99 (1981).

[23] Weerasooriya, T., Nicholas, T., Overload Effects in Sustained Load Crack Growths in Inconel 718, in Fracture Mechanics, ASTM STP 905, 81 (1988).

[24] Nicholas, T., Weerasooriya, T., Hold time effects in Elevated Temperature Fatigue Crack Propagation, in Fracture Mechanics, ASTM STP 905, 155 (1986).

[25] Dowling, N. E., Begley, J.A., Fatigue Crack Growth during Gross Plasticity and the J-Integral, in Mechanics of Crack growth , ASTM STP 590, 82 (1976).

[26] Lamba, H. S., The J-integral Applied to Cyclic Loading. Life prediction for Fatigue Crack Initiation, Engineering Fracture Mechanics 7(4), 693-701 (1975).

[27] Rice, J. R., Path Independent Integral and Approximate Analysis of Strain Concentration by Notches and Cracks, ASME Meeting APM-31, 8 (1968).

[28] Ohtani, R., Kitamura, T., Nitta, A., Kuwabara, K., High-Temperature Low cycle Fatigue Crack Propagation and Life Laws of Smooth Specimens Derived from the Crack Propagation Laws, ASTM STP 942, 1163-1180 (1987).

[29] Kubo, S., Yafuso, T., Nohara, M., Ishimaru, T., Ohji, K., Investigation on Path-Integral Expression of the J-integral Range using Numerical Simulations of Fatigue crack Growth, JSME International Journal, Series 1: Solid Mechanics, Strength of Materials, 32(2), 237-244 (1989).

[30] Ohji, K., Fracture Mechanics Approach to Creep-Fatigue Crack Growth. Proceedings of the International Conference, 131-44 (1987)..

[31] Kumar, V., German, M. D., Shih, C. F., Engineering Approach for Elastic-Plastic Fracture Analysis. Electric Power Research Institute (Report) , EPRI (1981).

[32] Saxena, A., For the Characterization of Creep-Crack-Growth Behavior in 304 Stainless Steel. Fracture Mechanics: Proceedings of the 12th National Symposium on Fracture Mechanics, 131-151 (1980).

[33] Landes, J. D., Begley, J. A., A Fracture Mechanics Approach to Creep Crack Growth, in Mechanics of Crack Growth, ASTM STP 590, 128 (1976).

[34] Nikbin, K. M.,Webster, G.A., Turner,C.E., Relevance of Nonlinear Fracture Mechanics to Creep Cracking in Cracks and Fracture, ASTM STP 601, 47 (1976).

[35] Taira,S., Ohtani, R., Kitamura,T., Application of J-integral to High Temperature Crack Propagation, Transactions of ASME-Journal of Engineering Materials and Technology 101,154 (1979).

[36] Ohji,K., Ogura,K., Kubo,S., Stress-Strain Field and Modified J-Integral in the Vicinity of a Crack Tip under Transient Creep Conditions. Japan Society of Mechanical Engineers 790-13,18 (1979).

[37] Riedel, H., Rice, J. R., Tensile Cracks in Creeping Solids, Fracture Mechanics: Proceedings of the 12th National Symposium on Fracture Mechanics, 112-130 (1980).

[38] Bassani, J. L., McClintock, F. A., Creep Relaxation of Stress around a Crack Tip, International Journal of Solids and Structures 17(5), 479-92 (1981).

[39] Saxena, A., Creep Crack Growth under Non steady-State Conditions ,Fracture mechanics: ASTM STP 905, 17, 185-201 (1986).

[40] Bassani, J. L., Hawk, D. E., Saxena, A., Evaluation of the C_t Parameter for Characterizing Creep Crack Growth Rate in the Transient Regime, Nonlinear Fracture Mechanics: Time Dependent Fracture , ASTM STP 993,7 (1986).

[41] Leung, C., McDowell, D. L., and Saxena, A., Consideration of Primary Creep at a Stationary Crack Tip: Implications for the C_t Parameter , International Journal of Fracture 36(4), 275-289 (1988).

[42] Saxena, A., Creep Crack Growth in High Temperature Ductile Materials, Engineering Fracture Mechanics 40(4-5), 721-736 (1991).

[43] Gibbons, T. B., The VAMAS Initiative on Advanced Materials and Standards: A Unified Approach to creep crack growth measurement, Materials at High Temperatures 10(2), 66-8 (1992).

[44] Riedel, H., Detampel, V., Creep Crack Growth in Ductile, Creep-Resistant Steels, International Journal of Fracture 33(4), 239-262 (1987).

[45] Grover, P. S., Saxena, A., Characterization of Creep Crack Growth Behavior in 2.25Cr-1Mo Steel using $(C_t)_{avg}$, International Journal of Fracture 73, 273-286 (1995).

[46] Saxena, A., Gieseke, B., Transients in Elevated Temperature Crack Growth. Proceedings of the MECAMAT International Seminar on High Temperature Fracture Mechanisms and Mechanics, 291-291 (1990).

[47] Nikbin, K. M., Webster. G. A. , Prediction of Crack Growth under Creep-Fatigue Conditions, in Low-cycle Fatigue, ASTM STP 942 , 281-292 (1987).

[48] Ohji, K., Kubo, S., Fracture mechanics Evaluation of Crack Growth Behavior under Creep and Creep Fatigue Conditions, in High Temperature Fracture and Fatigue, Japanese Materials Research Vol.3, 91-113 (1988).

[49] Saxena, A., Application of C_t in Characterizing Elevated Temperature Crack Growth during Hold Time , American Society of Mechanical Engineers Vol. 18, 113-121 (1990).

[50] Ohji, K., Kubo, S., Crack Growth Behavior and Fractographs under Creep-Fatigue Conditions Including the near Threshold Regime, in Fractography, Publication of the Society of the Material Science , Japan, Elsevier Applied Sciences 105 (1990).

[51] Gieseke, B., Mechanics of Creep fatigue Crack Growth in Cu-1Wt% Sb, Ph.D. Thesis , Georgia Institute of Technology, Atlanta , GA (1990).

[52] ECCC Recommendations, Testing practices for Creep Crack Initiation Vol. 3 Part 4 Issue 2 (2005).

[53] Neate, G.J., Creep Crack Growth in 1/2 Cr-Mo-V Steel at 838K II: Behavior under Displacement Controlled Loading , Material Science and Engineering Vol. 82 , 77-84 (1986).

[54] Gladwin, D.N., Miller, D.A., Priest, R.H., Examination of Fatigue and Creep-Fatigue Crack Growth Behavior of Aged Type 367 Stainless Steel Weld Metal at 659 C , Materials and Technology Vol. 5, 40-51 (1989).

[55] Kuwabara, K., Nitta, A., Kitamura, T.,Ogala, T., Effect of Small Scale Creep on Crack Initiation and Propagation Under Cyclic Loading , ASTM STP 924, 41 (1988).

[56] Laiarinandrasana, L., Kabiri, M. R., Reytier, M., Effect of Specimen Geometries on the C^* versus da/dt Master Curve for Type 316L Stainless Steel , Engineering Fracture Mechanics 73(6), 726-37 (2006).

[57] Mueller, F., Scholz, A., Berger, C., Klenk, A., Maile, K., Roos, E., Crack Behavior of 10 Cr-Steels under Creep and Creep-Fatigue Conditions, Materials at High Temperatures 25(3), 169-78 (2008).

[58] Kussmaul, K., Maile, K., Bareiss, J., Kloos, K.H., Granacher, J. and Tscheushner, R., Creep Crack Investigation of Turbine Steels with Specimens of Different Size, Creep , Fatigue Evaluation and Leak-before-break Assessment ,ASME Vol. 266 (1993).

[59] Gengenback,T., Kelnk, A., Creep, Creep-Fatigue Crack Initiation and Growth in 9-12% Chromium steels , OMNI Vol. 3 Issue 2 (2004).

[60] Yokobori, T., Yokobori, A. T., High Temperature Creep, Fatigue and Creep-Fatigue Interaction in Engineering Materials, Advances in Defect Assessment in High Temperature Plant Based on the Papers Presented at the Second International `HIDA' Conference 78 (11-12), 903-908 (2001).

[61] Allen, P.A., Aggarwal, P. K., Swanson, G. R., Development of a Fatigue Crack Growth Coupon for Highly Plastic Stress Conditions , 45th AIAA/ASME/ASCE/AHS/ASC Structures, Structural Dynamics and Materials Conference , Palm Springs, California (19 - 22 April 2004).

[62] Dowling, N. E., Iyyer, N. S., Fatigue Crack Growth and Closure at High Cyclic Strains, Material Science and Engineering Vol. 96, 99-107 (1987).

[63] Wire, G. L., Mills, W. J., Fatigue Crack Propagation Rates for Notched 304 Stainless Steel Specimens in Elevated Temperature Water , Transactions of the ASME. Journal of Pressure Vessel Technology Vol.126, n 3, 318-326 (2004).

[64] Ansys, Inc., Theory Reference, Release 12.1 (2009).

[65] Anderson, T. L., Fracture Mechanics: Fundamentals and Applications, Boca Raton, FL, CRC Press. (2005).

[66] Shih, C. F., Moran, B. and Nakamura, T., Energy Release Rate Along a Three-Dimensional Crack Front in a Thermally Stressed Body, International Journal of Fracture 30(2), 79-102 (1986).

[67] Hutchinson, J. W., Singular Behavior at the End of a Tensile Crack in a Hardening Material, Journal of the Mechanics and Physics of Solids 16(1), 13-31 (1968).

[68] Rice, J. R., and Rosengren, G. F., Plane Strain Deformation Near a Crack Tip in a Power-Law Hardening Material , Journal of the Mechanics and Physics of Solids 16, 1-12 (1968).

[69] Chang, C. C., Mear, M. E., A boundary Element Method for Two-Dimensional Linear Elastic Fracture Analysis, International Journal of Fracture 74 ,219-51 (1996).

[70] Newman, J.C., Jr., Chang, C. C., Mear, M. E., Xiao, L., Kale, V. J., FADD2D: Fracture Analysis by Distributed Dislocations Version 1.0 ,User Guide for Personal Computers with Demonstration Example (October 2006).

[71] Tada, H., Paris, P. C., Irwin, G. R., The Stress Analysis of Cracks Handbooks 3rd ed, The American Society of Mechanical Engineers (2000).

[72] Abaqus User's Manual, V 6.3 , Hibbit, Karlsson and Sorensen, HKS Inc. , Pawtucket, USA (2002)..

[73] Irwin, G. R., Kies, J. A., Critical Energy Rate Analysis of Fracture Strength, Welding Journal v. 33, n 4, 193-8 (Apr 1954).

[74] Irwin, G. R., Analysis of Stresses and Strains Near End of Crack Traversing , American Society of Mechanical Engineers, Journal of Applied Mechanics v. 24, n 3, 361-364 (Sept 1957).

[75] Piascik, R. S., Mechanisms of Intrinsic Damage Localization During Corrosion Fatigue: Al-Li-Cu System, Ph.D Dissertation, University of Virginia (1989).

[76] Landes, J. D., McCabe, D. E., Ernst, H. A., Elastic-Plastic Methodology to Establish R Curves and Instability Criteria, Westinghouse R&D Center, Final Report, Pennsylvania (1984).

[77] Sikka, V. K., Ward, C.T., Thomas, K. C., Modified 9Cr-1Mo Steel-An Improved Alloy for Steam Generator Application. Ferritic Steels for High-Temperature Applications, ed. Khare, A. K., American Society of Metals , Metals Park, OH, 65-84 (1983).

[78] Hald, J., Metallurgy and Creep Properties of New 9-12% Cr Steel, Steel Res. 67 , 369-374 (2009).

[79] Parker, J., P91 material offered by Kent K. Coleman, EPRI, private communication to Ashok Saxena (2009).

[80] Hanus, R., Casting, COST Summer School, Lanzarote (2008).

[81] Ennis, P. J. and Czyrska-Filemonowicz, A., Recent Advances in Creep-Resistant Steels for Power Plant Applications, Sadhana - Academy Proceedings in Engineering Sciences 28(3-4), 709-730 (2003).

[82] Fournier, B., Sauzay, M., Barcelo, F., Rauch, E., Renault, A., Cozzika, T., et al, Creep-Fatigue Interactions in a 9 % cr-1 % Mo Martensitic Steel: Part II.Mmicrostructural evolutions, Metallurgical and Materials Transactions A (Physical Metallurgy and Materials Science) 40(2), 330-41 (2009).

[83] Kalyanasundaram, V., Saxena,A., Narasimhachary, S., Dogan, B., ASTM Round-robin on Creep-Fatigue and Creep Behavior of P91 Steel, ASTM STP 1539 , 23-40 (2011).

[84] ASTM E139 – 11, Standard Test Methods for Conducting Creep, Creep-Rupture, and Stress-Rupture Tests of Metallic Materials (2011)..

[85] ASTM E8-06, Standard Test Methods for Tension Testing of Metallic Materials, Annual Book of ASTM Standards, ASTM International, West Conshohocken, PA (2006).

[86] Gold, M., Tanzosh, J., Swindeman, R. W., Maziasz, P. J., Santella, M. L., Safe Use Limits for Advanced Ferritic Steels in Ultra-Supercritical Power Boilers, CRADA Final Report Report No. ORNL00-0598.

[87] Gaffard, V., Besson, J., Gourgues-Lorenzon, A. F., Creep Failure Model of a Tempered Martensitic Stainless Steel Integraiting Multiple Deformation and Damage Mechanisms, International Journal of Fracture 133, 139-166 (2005).

[88] Kloc, L., Fiala, J., On Creep Behaviour of Several Metallic Materials at Low Stresses and Elevated Temperatures, Chemical Papers 53 (3), 155-164 (1999).

[89] Kloc, L., Sklenicka, V., Transition from Power-law to Viscous Creep Behaviour of P91 Type Heat-resistant Steel, Materials Science and Engineering A 234-A236, 962-965 (1997).

[90] Sikka, V. K., Advanced Alloy Technology Program - Semiannual Progress Report for period ending March 1983 pp. 1-49 Report No. ORNL/MSP/1.7-83/2 (1983).

[91] Saxena, A., Ernst, H. A., Landes, J. D., Creep Crack Growth Behavior in 316 Stainless Steel at 594°C, International Journal of Fracture 23, 245-257 (1983).

[92] Ohji, K., Kubo, S., Crack Growth Behavior and Fractographs under Creep-Fatigue Conditions Including the near threshold regime, in Fractography, Publication of the society of the Material Science , Japan, Elsevier Applied Science 105 (1990).

[93] Yokobori, A.T., Jr., Differences in the Creep and Creep Crack Growth Behavior Between Creep Ductile and Brittle Materials, Engineering Fracture Mechanics 62 , 61-78 (1999).

[94] Newman, J.C., Jr., Yamada, Y., Compression Precracking Methods to Generate Near-Threshold Fatigue-Crack-Growth-Rate Data, International Journal of Fatigue v 32, n 6, 879-885 (2010).

[95] Private communication with J.C. Newman, Jr., Mississippi State University (June 2012).